LIVING MATTER:

GENERIC MECHANISMS IN EMBRYONIC TISSUE MORPHOGENESIS

Wei Zeng, M.S.

Submitted to the faculty of the University Graduate School

in partial fulfillment of the requirements

for the degree

Doctor of Philosophy

in the Department of Physics

Indiana University

May 2005

Accepted by the Graduate Faculty, Indiana University, in partial fulfillment of the requirements for the degree of Doctor of Philosophy.

Doctoral Committee

James A. Glazier, Ph. D.

John M. Beggs, Ph. D.

Joseph B. Duffy, Ph. D.

Filippo Menczer, Ph. D.

Rob de Ruyter, Ph. D.

Dec, 15, 2004

ACKOWLEDGEMENT

First and foremost, I would like to thank my advisor, Dr. James A. Glazier, for his advice, support, understanding, open mind and patience which allowed me to explore my own potential and make my own choices, even when my choices did not further his own agenda.

I would like to thank Dr. Stuart A. Newman, whose knowledge and patience opened the door of biology to a physics student like me. Besides teaching me experimental embryology, his interest in evolution, bioethics and art have had a great impact on me.

I would like to thank Dr. Cornelis J. Weijer for hosting me in his laboratory at the Wellcome Trust Biocentre in Dundee, Scotland. His curiosity towards nature and ability to observe are the true treasures I discovered. Our daily discussions and his stylish experiments were rare luxuries.

I would like to thank Dr. Thomas L. Gilberto for long-time and long-distance collaboration. His expertise in simulation and tips about life have been of great help. He also taught me to explore different cultures.

I would like to thank Dr. Mark Alber, Dr. Yuji Sawada, Dr. Yoshinori Hayakawa, Dr. Gemunu Gunaratne, Dr. Charles Little, Dr. Claudio Stern, Dr. Cathy Krull, Dr. Olivier

Pourquie, Dr. Fernando Giraldez, Dr. Berta Alsina, Dr. Jordi Villà i Freixa and Dr. Rusty Lansford for discussions, inspiration, correspondence, encouragement and opinions. Special thanks to Dr. John Holland who kept talking to me when I was isolated and struggling in a mental cave, trying to produce the following chapters.

I would like to thank my committee members, Dr. Fillipo Menzer, Dr. Joseph Duffy, Dr. Rob de Ruyter and Dr. John Beggs for their reading, comments and contributions.

I would like to thank the members of all the groups I have worked in for their help and support: Cheng, Kun, Wendy, Yana, Dragos, Gabriel, Ariel, Julio, Lenilson, Veronica, Debasis, Ning, Soma, Mike, Roeland, Stan, Bruce, Sengkai, Marius, Igor, Arpita, Gerti, Jun, Manli, Veronika, Holly, Xuesong, Dirk, Hideshi, Tanya, Natalie, Nadya, Downie, Tsuchiya, Sawai and others.

I would like to thank all my friends especially the other pilgrims on this road for sharing happiness, strength, stress, problems and growing pains.

The work received financial support from NSF-IBN-008365, CAPES-BRAZIL, the Welcome Trust and NASA.

I dedicate this thesis to my parents and sisters: Guoqing Liu, Qinglin Zeng, Li Zeng and Sha Zeng, for the haven they created for me with their patience, understanding

and support.

Special thanks to my grandma for a happy childhood which gives me endless strength to color every moment of life, difficult or not.

ABSTRACT

Wei Zeng, M.S.

LIVING MATTER: GENERIC MECHANISMS IN EMBRYONIC TISSUE MORPHOGENESIS

Embryonic tissue morphogenesis is the establishment of the complex organization of tissues and organs during embryonic development, which involves the development of spatial pattern and structure via the growth & death, differentiation and migration of individual cells. Generic mechanisms are physical processes that are broadly applicable to both living and non-living systems, contrasted with ‘genetic’ mechanisms—highly evolved, biomolecular processes. The striking resemblance between patterns generated by some known generic physical mechanisms and patterns observed in morphogenesis tempts us to explain biological development in terms of generic mechanisms. By studying two specific developmental events, chick limb development and early chick gastrulation theoretically, computationally and experimentally, I will discuss possible scenarios of how generic mechanisms especially cell adhesion, under genetic regulation, give rise to the shape and pattern observed in embryonic tissue morphogenesis.

_____

_____

_____

_____

_____

CONTENTS

CHAPTER ONE

INTRODUCTION

1.1 Morphogenesis and Generic Mechanisms

Morphogenesis (from the Greek *morphê* shape and *genesis* creation) is a major mystery in biological sciences and encompasses a broad range of biological mechanisms. Morphogenesis includes the generation, maintenance, degeneration, and regeneration of tissues and organs in adult and embryonic tissues. Morphogenesis presents questions at many length scales, from the origin of the structure of individual cells, through the formation of multi-cellular arrays and tissues by cells and the extracellular matrix (*ECM*), to the higher-order assembly of tissues into organs and whole organisms. This thesis primarily deals with three aspects of morphogenesis: the role of cell-cell adhesion and cell-ECM adhesion in biological pattern formation; how a tissue's mechanical properties determine its shape; and large-scale cell movement and its regulation.

Morphogenesis is complex and fascinating, yet poorly understood [1, 2]. Can we ever deduce an organism from its genome alone? Maybe soon,

maybe never [3, 4]. In this post-genome era, people hope that elucidating genomes will provide the key to understanding all of biology. But this hope is overoptimistic: life is more than the “bits and pieces” of information coded in the genome.

Some current views equate genes with functions, but this approach is insufficient since no single gene completely encodes a trait or a disease. Craig Venter remarks: "In everyday language the talk is about a gene for this and a gene for that. We are now finding that that is rarely so. The number of genes that work in that way can almost be counted on your fingers, because we are just not hard-wired in that way. You cannot define the function of genes without defining the influence of the environment. The notion that one gene equals one disease, or that one gene produces one key protein, is flying out of the window." (Craig Venter, 2001). The Human Genome Project revealed that humans have only 10,000 more genes than worms. Making a human being takes only one-third more genes than making a worm. Does this rough equality in genetic information mean that our environment is more important than our genetic make-up? What are the key mechanisms that translate genetic information into organisms?

The striking resemblance between the patterns some generic physical mechanisms generate and the patterns of morphogenesis tempts us to explain morphogenesis by generic mechanisms [5]. Generic mechanisms, such as adhesion [6, 7], surface tension [6, 8], gravitational effects [9]，diffusion [10] and viscosity [5], are chemo-physical processes that apply to a broad range of living and non-living materials. In contrast, the complementary genetic mechanisms are highly-organized interactions between specific co-evolved macromolecules, *e.g.* cytoplasmic 'motors' that affect the shape and motility of individual cells [11] or gene promoter elements sensitive to complexes of DNA-binding proteins with specific spatial structures [12]. We can imagine that 'living matter' builds an organism: Genetic information can guide differential gene expression in a given enviroment, resulting in cells containing different types and numbers of biomolecules and thus having different physical properties, *e.g.* cytoplasmic viscosity or membrane adhesion. Generic mechanisms like gravity and adhesion then drive the formation of patterns and shape during morphogenesis. In chapter three, I study one case where generic factors like cell density can determine the biological pattern. Like non-living matter, living matter, though composed of cells which can differentiate in response

to micro-environmental signals and produce and secrete specific macromolecules, must respect the 'generic' laws of physics, *e.g.* gradients in cell-surface adhesivities create surface-tension forces which lead to cell rearrangement. The morphogenic properties of individual cells, *e.g.* polarity and motility, arise from the physical chemistry of highly-evolved intracellular proteins such as tubulin, actin, myosin and kinesin, in the presence of sources of metabolic energy and appropriate cofactors [5].

Sir D'Arcy Thompson was a pioneer in using physical concepts like surface tension to explain biological pattern formation and other biological processes within a mathematical framework [13]. In his 1917 book *On Growth and Form*, Thompson pointed out morphological similarities and potential correlations between biological forms and mechanical phenomena. For example, he showed the similarity between the internal supporting structures in the hollow bones of birds and well-known engineering truss designs. He said "This book of mine has little need of preface, for indeed it is 'all preface' from beginning to end." Recently Ball published a book, *The Self-Made Tapestry* [14], in which he collected more 'modern' examples and tried to explain similarity of patterns by similarity of mechanisms in a

quantitative and predictive way.

1.2 Embryonic Tissue Morphogenesis

1.2.1 Characteristics and Building Blocks

This thesis focuses on embryonic tissue morphogenesis, which establishes the complex organization of multicellular tissues and organs in a developing embryo. Spatial patterns and structure develop via the growth and death, differentiation, shape change and migration of individual cells and cell groups [15] and changes in the amounts and composition of extracellular environments, for example, non-diffusible ECM and diffusible signaling molecules: *morphogens*.

The eukaryotic cell is the functional unit of embryonic tissue morphogenesis (Figure 1). Each cell has a membrane, cytoplasm and a nucleus. The membrane encloses the cell, separating it from its environment, and helps the cell to migrate, recognize extracellular signals, and interact with other cells. The membrane is a thin bilayer film of lipid with embedded proteins. Proteins anchored in the bilayer can induce beneath the membrane a

dynamic cytoskeletal network that is rich in actin, microtubules and intermediate filaments. The cytoskeleton provides mechanical support and coordinates and powers cell movement. The cytoplasm contains organelles that synthesize proteins and provide energy to the cell. The nucleus contains the cell's genetic blueprint: DNA.

Embryonic tissue morphogenesis is analogous to, yet more challenging than, a gigantic jigsaw puzzle (Figure 1): First, it is **self-directing** because of the highly nonlinear feedback loops within the complex biomolecular networks whose components derive from the genetic blueprint. Second, it is **emerging**: No single piece sees the whole picture. Each only evolves by interacting with its neighbors. Third, it is **expanding**: The total number of pieces increases and each piece moves and changes shape. Fourth, it is **evolving**: The expression of the genetic blueprint in each piece is not static but responds to environmental changes. This feedback is an essential characteristic of life [16]. Last, it is **self-correcting**: Despite the substantial number of errors that occur at each level, molecule, cell, tissue, organ, organism, *e.g.* DNA misreplication or cell dislocation, the final organization must be functionally correct for the organism to survive. In the simulation

work I present in Chapter Three, I will show how cellular-automaton (*CA*) simulations can elegantly embody these necessary characteristics of morphogenesis and reproduce developmental events.

The similarity in form of vertebrate embryos at comparable developmental stages makes the existence of a common set of underlying mechanisms and principles of embryonic tissue morphogenesis likely, despite the diversity in quality, genes and organization among different species (Figure 2 adapted from [17]).

From now on, I will use 'morphogenesis' to mean 'embryonic tissue morphogenesis' unless I specify otherwise. The following sections discuss a number of the key mechanisms and structures involved in embryogenesis. To accord with the historical order of their discovery, I will first describe morphological behaviors at the tissue level and discuss hypotheses which attempt to explain these behaviors. Then I will describe experiments at the cell level to test these hypotheses and efforts to explore the molecular bases of these observations and theories.

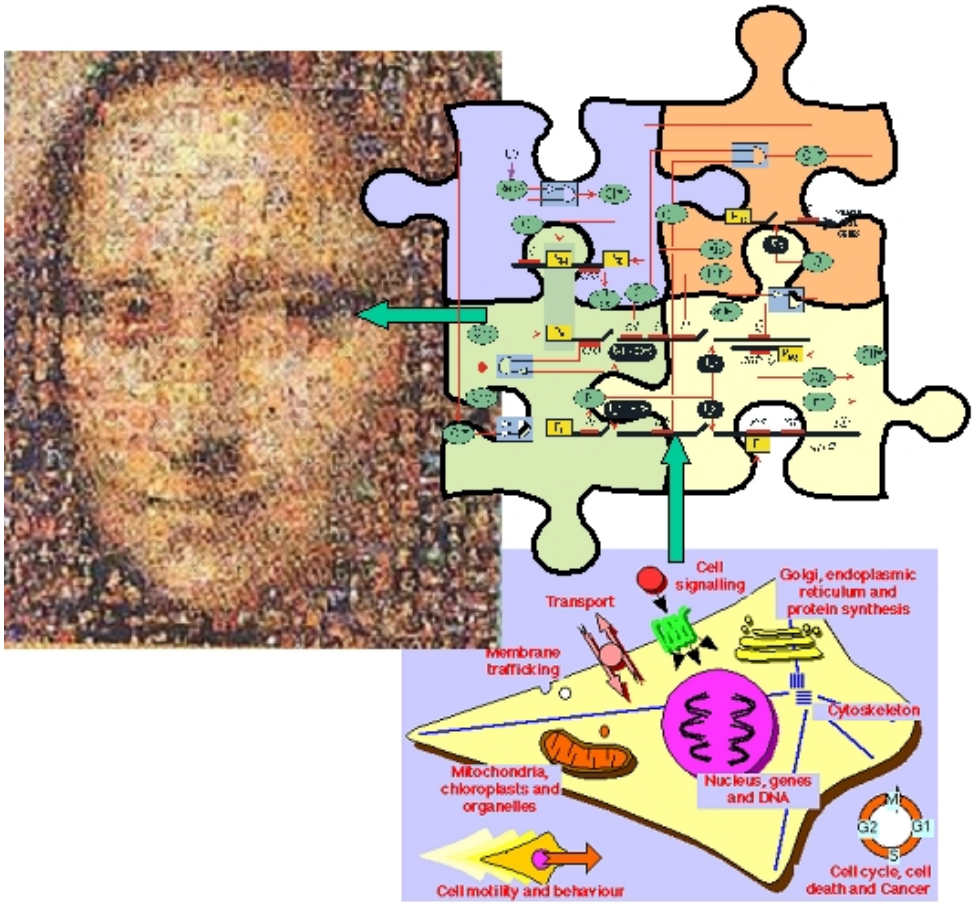

Figure 1. The metaphor of embryonic tissue morphogenesis as a puzzle consisting of populations of cells, where the individual cell is the functional unit.

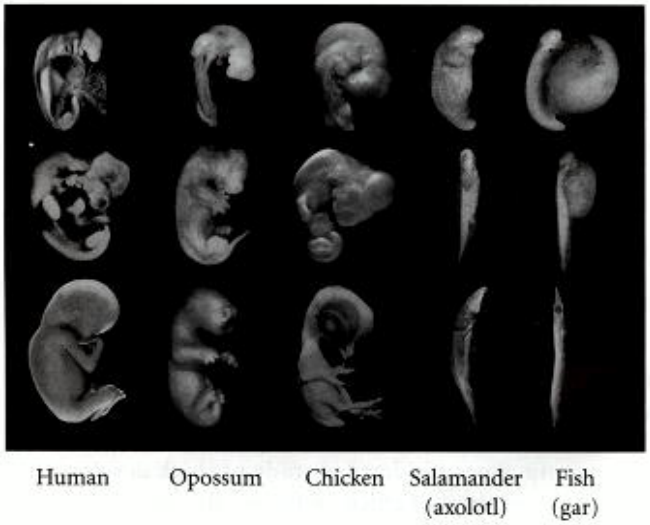

Figure 2. The similarities and differences between the development of different vertebrate embryos. They each begin with a basically similar structure, although they acquire this structure at different ages, when they have different overall sizes. As they develop, they become less like each other. Adapted from [17].

Morphogenesis uses two primary cell types and the typical structures theyproduce to build complex, heterogeneous, three-dimensional organs like hearts, limbs, lungs, and eyes: *epithelial sheets* and *mesenchymal cell masses*. Epithelium and mesenchyme represent two extremes in the organization of groups of cells. In epithelial sheets, cells have a polarity which their apical and basolateral membrane domains determine. Mesenchymal cells, which live surrounded by ECM in a porous environment, lack the distinct apical-basal polarity that characterizes their epithelial counterparts. These cell-level differences affect the tissue level as well. Epithelial cells form tightly-bound flat sheets or rolled tubes, rolled or folded paper, while mesenchymal cells are less internally organized and form fewer and looser connections with other cells. Both types of cells contribute to the body's function in distinct ways, with epithelium being the essential structural and physiological component of organs and tissues such as the kidney and the lining of the gut, and mesenchyme including all migratory cells, including metastatic cancer cells, and providing support for epithelia in various contexts. Despite (or, perhaps, because of) these differences, our bodies contain countless examples of interacting epithelial and mesenchymal cells. Indeed, nearly every one of the body's structures,

from internal organs to limbs to teeth, contains both a mesenchymal and an epithelial component. My work deals with the different morphological behaviors of mesenchymal and epithelial cells.

1.2.2 Fluid-like Properties of Embryonic Tissues

The physical state of embryonic tissues can range from liquid (*e.g.* blood) to solid (*e.g.* bone), while most developmentally-significant morphogenesis takes place in intermediate quasi-liquid tissues [5], which exhibit both elastic and viscous properties. Viscoelasticity allows both the maintenance of tissue shape under external forces and the rearrangement of internal components to change tissue shape.

Embryonic tissues exhibit liquid-like behaviors driven by surface tension and energy minimization. Tissues composed of cells from different sources often behave as distinct fluid phases with a characteristic tension at their common interface. The behaviors of mixtures of liquids reflect the relative cohesion and adhesion of the components. If two immiscible liquids contact one another, the liquid with the lower surface tension will spread over the other. A series of immiscible liquids has a pair-wise, transitive hierarchy of

spreading preferences: if liquid *a* spreads on *b* and liquid *b* spreads on *c*, then liquid *a* spreads on *c*. When different embryonic tissues come into contact, their movements are spontaneous. Tissue fragments can flow in response to external forces, round up in fluid suspension, and coalesce with other fragments [5]. The spreading of one tissue over another is relatively common in morphogenesis.

Cell-sorting experiments demonstrate that the fluid-like properties of embryonic tissues result from generic mechanisms on the cell level, for instance, surface tension, σ (Figure 3 adapted from [18]). In cell sorting, disordered cells of two or more heterogeneous types migrate and rearrange into homogenous domains. In 1744, Trembley performed experiments which showed that an adult *Hydra* could regenerate from aggregates of dissociated cells [19]. Wilson (1907) showed that each minute fragment of a marine sponge could regenerate into a complete individual. He then dissociated sponges into individual cells. Cells clustered, and attached to one another and reconstituted sponges with all the appropriate accoutrements, suggesting that cell sorting might also be important during normal morphogenesis [20]. In 1944 Holtfreter [21] demonstrated that

dissociated cells from amphibian embryos would adhere to form random aggregates that in time would sort according to their germ layer of origin, with ectoderm forming an outer surface layer, endoderm forming a compact central ball and mesoderm producing a loose array of cells in between. These sorting experiments showed that embryonic cells could distinguish between like and unlike cells and establish relative adhesive arrangements with cells of other types. Holtfreter developed the concept of *tissue-specific affinities* and proposed several possible mechanisms: *e.g.*, differences in the degree of cell adhesiveness or "directed movement," now called *chemotaxis* (cells moving in response to a chemical gradient) [22].

Steinberg demonstrated that the movement of cells within aggregates during cell sorting is not oriented as it would be in chemotaxis. Based on the resemblance between tissue and immiscible-liquid arrangements, he hypothesized instead that cell-type-dependent surface adhesivity drives cell sorting, analogously to phase separation in mixed liquids [23]. His *Differential Adhesion Hypothesis* (*DAH*) proposes that cells of a given type have characteristic adhesion strengths to cells of the same or different types; the cells comprising an aggregate are motile and the final organization of

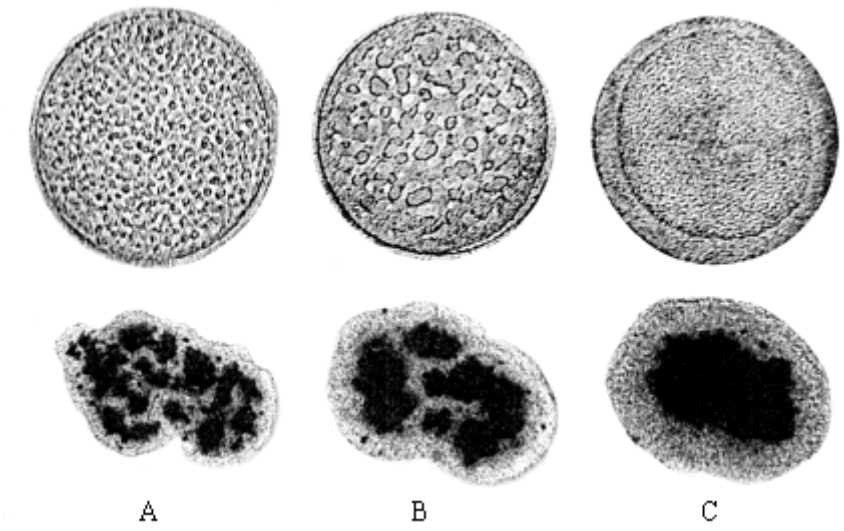

Figure 3. Cell sorting is analogous to liquid phase separation. (Upper) Gas and liquid phase ordering after a thermal quench. The container diameter is 12 mm. Gas and liquid eventually order, with the liquid phase wetting the container wall and surrounding the gas phase, corresponding to $\sigma_l<\sigma_g$. (A) 120 s. (B) 275 s. (C) 3,960 s. (Lower) Sorting of chicken embryonic pigmented epithelial cells (dark) from chicken embryonic neural-retinal cells (light). The average aggregate size is 200 μm. Neural-retinal cells preferentially wet the external tissue culture medium surrounding the aggregates. $\sigma_n<\sigma_p$. (A) 17 h. (B) 42 h. (C) 73 h. Adapted from [18].

cells maximizes the strength of adhesive interactions summed over all the adhesive contacts within the aggregate.

The DAH explains why one cell population spreads over the surface of another during development. When two tissues encounter one another during development, the same tissue always spreads over the surface of the other. Sorting of dissociated cells produces the same configuration as spreading. These cell rearrangements resemble the behavior of immiscible liquids, which separate when co-dispersed, and which, when confronting one another, have the same one always spread over the surface of the other.

The DAH predicts a transitive hierarchy of combined embryonic tissue pairs resembling that of mixed immiscible fluids. In 1970, Steinberg showed that six chick embryonic tissue types spread transitively [24]. The question remained whether spreading was due to differential surface tension. Almost thirty years later, in 1996, Steinberg and his colleagues tested the DAH [25] by correlating the surface tensions of cell aggregates to their spreading tendencies. Tissue surface tensions reflect the ability of the cohesive forces within the tissue to resist forces applied to the aggregate. Of the five tissues,

limb-bud mesenchyme was the most cohesive, and neural retina the least cohesive. In an elegant test of the hypothesis that a cell population that spreads over another must have lower surface tension, Foty *et al.* stained the five tissues with contrasting fluorescent markers, mixed pairwise either cells or cell aggregates from different tissues and monitored the mixtures' behaviors. In every case, the tissues behaved as the hypothesis predicted (Figure 4 adapted from [25]).

To explain "tissue affinities," the DAH predicts that, among the primary germ layers, the cohesiveness of deep ectoderm should be the greatest, that of deep mesoderm should be intermediate, and that of deep endoderm should be the least. Also, the cohesiveness of differentiating neural ectoderm should increase after induction, causing it to internalize and segregate from epidermis. Using a specially-designed tissue surface tensiometer, Davis and colleagues [26] demonstrated that aggregates of *Rana pipiens* deep germ layers: (i) possess liquid-like surface tensions, (ii) have surface-tension values in precisely the sequence necessary to account for germ-layer stratification *in vitro* and *in vivo*, and (iii) the surface tension of deep ectoderm doubles just after it has overlaid the archenteron roof.

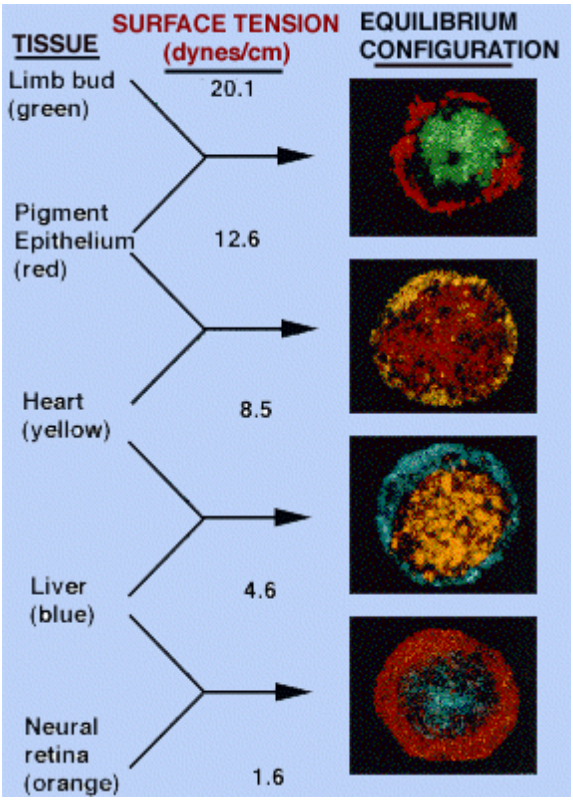

Figure 4. Five chick embryonic tissues in order of decreasing surface tension. At right is the final configuration arising when cells from two of these tissues are mixed. At left is the tissue source and its arbitrary color assignment. Adapted from [25].

These measurements provide direct, quantitative evidence that the "tissue affinities" governing germ-layer flow during early stages of vertebrate morphogenesis reflect tissue surface tensions.

Cell sorting is an important and generic phenomenon in morphogenesis, *e.g.* in the aggregate stage of the development of the cellular slime mold *Dictyostelium discoidium* [27]. Cells from a variety of phylogenetic groups, tissues and developmental stages, even those which normally do not come into contact, sort: invertebrate and vertebrate cells, cells in aggregates and monolayer cultures, and cells from embryonic, postnatal and adult stages [7]. Thus, cell sorting results from generic surface-adhesion mechanisms, not from genetically-programmed behaviors specific to cell types that normally come into contact. The spherical shape of embryonic tissue aggregates is another example of the tissue acting like a fluid to minimize its surface energy.

1.2.3 Cell Adhesion

Embryonic cells' remarkable ability to distinguish between homotypic and heterotypic cells and to establish relative adhesive arrangements results

from the simple mechanism of cell adhesion. What makes cells adhere? Cells adhere because of cell-adhesion molecules on the cell surface. The measurable surface tension is the net result of the various adhesive interactions between cells within a tissue. The functional units of cell adhesion are typically multiprotein complexes of three general classes: cell-adhesion molecules/adhesion receptors, ECM proteins/receptors, and the cytoplasmic-plaque/peripheral-membrane proteins (Figure 5 adapted from [28]). The cell-adhesion receptors are usually transmembrane glycoproteins that mediate binding interactions at the cell surface and determine the specificity of cell–cell recognition. They include members of the integrin, cadherin, immunoglobulin, selectin, and proteoglycan (for example, syndecans) superfamilies [29, 30]. ECM proteins are typically large glycoproteins, including the collagens, fibronectins, laminins, and proteoglycans, that assemble into fibrils or other complex macromolecular arrays. Owing to their binding to adhesion receptors, they can also tightly associate with the cell surface. At the intracellular surface of the plasma membrane, cell-adhesion receptors associate with cytoplasmic-plaque or peripheral-membrane proteins. Cytoplasmic-plaque proteins serve to link the adhesion receptors to the cytoskeleton, to regulate the functions of the

adhesion molecules, and to transduce signals which the adhesion receptors initiate at the cell surface. Adhesion receptors mediate fundamental cellular processes including cell differentiation, cell-cycle control, and programmed cell death. Cells receive their positional information regarding the ECM and surrounding cells through cell-adhesion receptors. The mechanism involves the adhesion-dependent formation of "scaffolds" that allow the efficient assembly and interaction of signaling molecules such as GTPases and kinases [31, 32].

The classic cadherin adhesion molecules mediate one of the most important and ubiquitous types of adhesive interaction. Cadherins are transmembrane, Ca^{2+}- dependent, homophilic adhesion receptors (Figure 6 adapted from [33]) that play important roles in cell recognition and cell sorting during development [34]. However, virtually all solid tissues continue to express them at high levels. Of the many members of the classic cadherin family (a subset of the cadherin superfamily), E-cadherin in epithelial tissues has a cytoplasmic component which associates with various cytoplasmic proteins. β-catenin binds directly to E-cadherin, and other proteins link the E-cadherin/β-catenin complex to actin filaments, thus coupling cell adhesion

to the mechanism that modulates cell shape. Elimination of the genes encoding E-cadherin in either *Drosophila* or mouse, affects cells' adhesive properties and destroys normal development [35]. The role of β-catenin in the *Wnt* pathway allows E-cadherin-mediated adhesion to affect gene expression, as studies on mouse embryonic stem cells that are null for the gene encoding E-cadherin have shown [36]. These cells are defective in cell aggregation (a defect that transfection with cDNA encoding either E-cadherin or N-cadherin driven by a constitutive promoter can correct). The presence or absence of E-cadherin can regulate the expression of the transcription factor T-brachyury. Normal embryonic stem cells can form organized tissues *in vitro*, while cadherin-null cells cannot. However, constitutive expression of E-cadherin restores the cadherin-null cells' ability to form epithelia. In contrast, expression of N-cadherin restores the cells' ability to form neuroepithelium and cartilage, but not epithelia. Thus, specific cadherins appear to stimulate the differentiation of particular tissue types.

The identification of cell-adhesion molecules helps test the DAH further. Differences in both the type and number of adhesion molecules drive cell

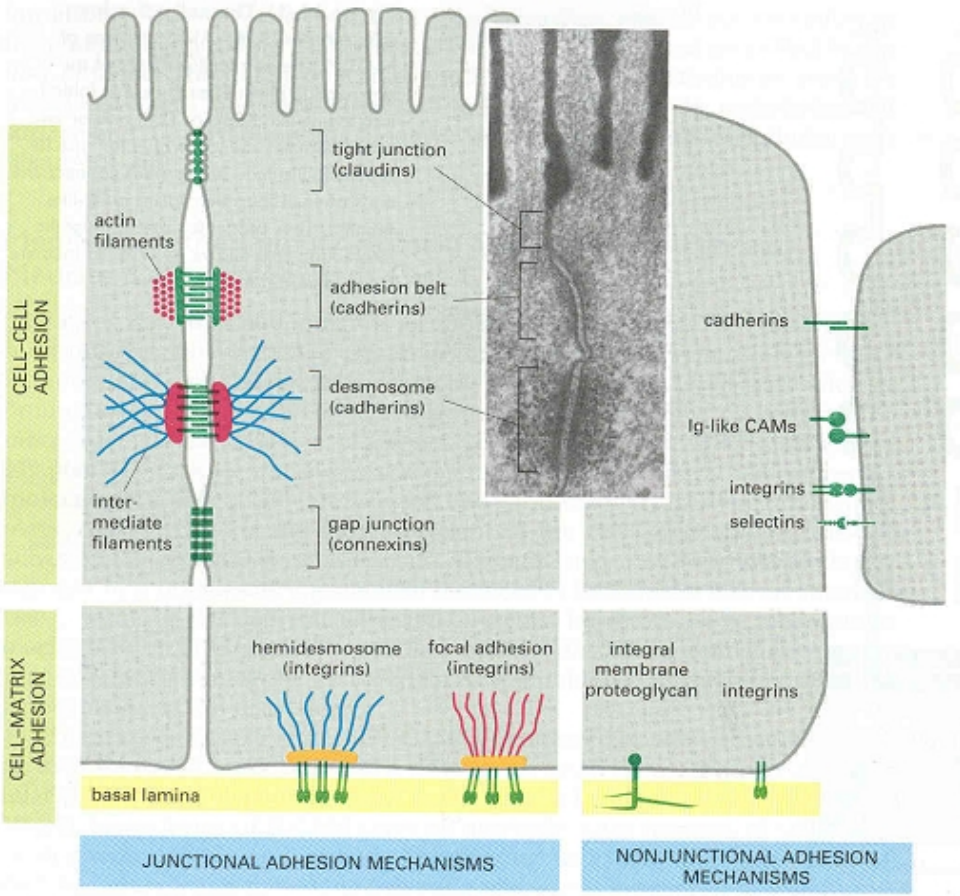

Figure 5. Three classes of adhesion proteins: the cell-adhesion molecules/adhesion receptors (upper right), the ECM proteins (lower), and the cytoplasmic-plaque/peripheral-membrane proteins (upper left). Adapted from [28].

sorting [37]. Godt and Tepass showed that cadherin levels can mediate sorting *in vivo* [38, 39]. By genetically manipulating the E-cadherin expression level of the two germline cell types in follicles of the fruit-fly (*Drosophila*) ovary (Figure 7 adapted from [38]), oocyte and its attendant nurse cells, they concluded that the oocyte and posterior follicle cells express higher levels of E-cadherin than do nurse cells, ensuring that the oocyte moves to the posterior pole. This experiment confirmed the DAH: differences in cell adhesion can drive morphogenic movements *in vivo* and differences in the expression level of a single cell-adhesion molecule suffice to mediate cell sorting in an intact tissue.

Cell adhesion is an important generic mechanism that helps translate genetic information and assemble cells into three-dimensional tissues with diverse and distinctive patterns. Cells do not simply ‘stick’ together: Multiple cell-adhesion mechanisms connect cells, while connections to the internal cytoskeleton regulate the overall architecture of the tissue (Figure 8 adapted from [40]). For example, compaction is a morphogenic outcome of cells’ mesenchymal-to-epithelial transition, which also involves changes in gene expression. Cadherins, catenins, and the actin cytoskeleton mediate

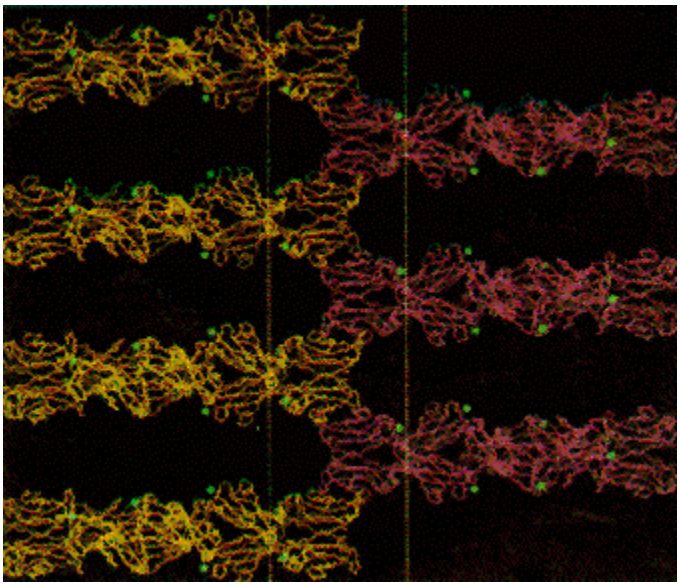

Figure 6. Interactions between two apposing regions of N-cadherin proteins. The purple and yellow proteins represent the cadherins from two apposing cells. The green dots represent the positions of calcium ions. The dashed white line shows the boundaries of the "cell adhesion zipper" these interactions form. Adapted from [33].

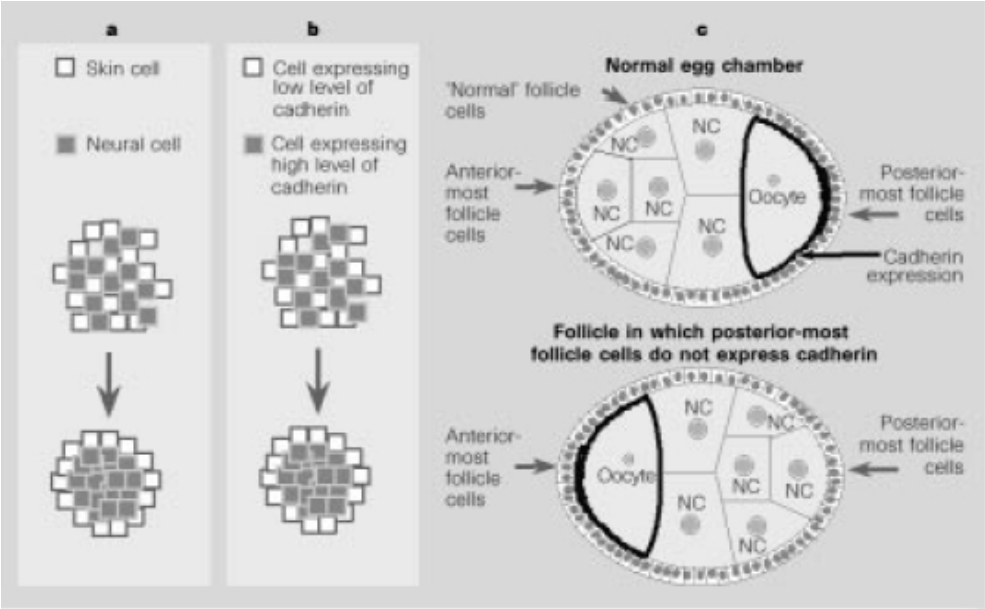

Figure 7. Cell sorting during development: (a) *In vitro*, neural cells preferentially stick to other neural cells. Expression of different cadherins drives this sorting. (b) *In vitro*, cells expressing high levels of cadherin preferentially sort to the center of the aggregate. (c) *In vivo*, the oocyte and posterior follicle cells express higher levels of E-cadherin than do nurse cells (*NC*) and other follicle cells, ensuring that the oocyte sits at the posterior pole. Adapted from [38].

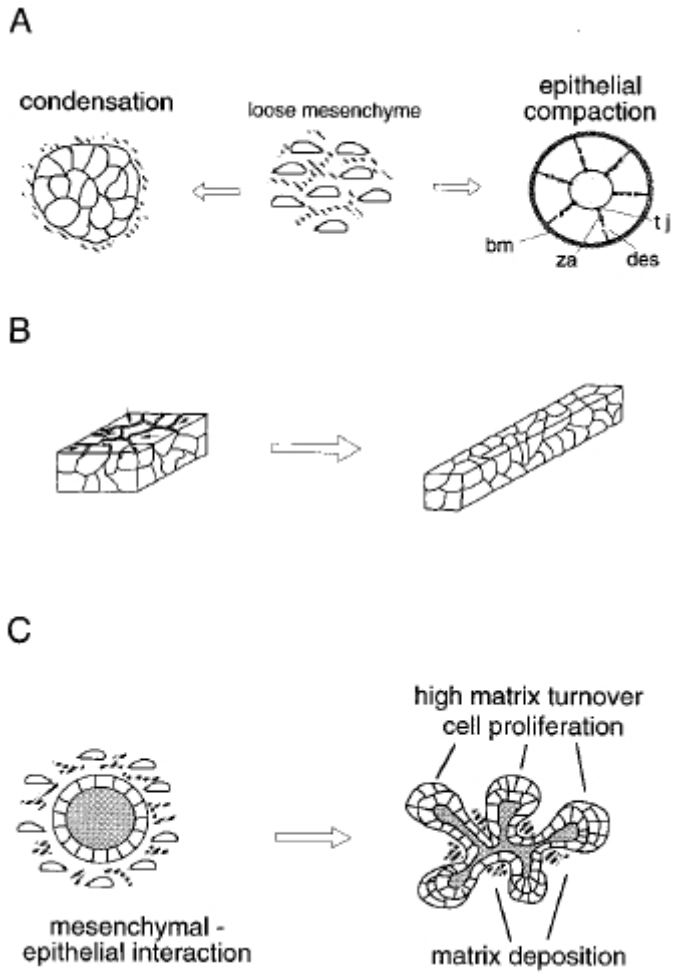

Figure 8. (A) Cadherins, catenins and the actin cytoskeleton mediate condensation and compaction and result in the development of extensive, intimate adhesive contacts between adjacent cell surfaces. Compaction results from cells' mesenchymal-to-epithelial transition. (B) Cellular rearrangements are common in developing embryos. Cells move within the tissue despite adhering tightly to each other. Cadherins participate in the intercellular motility underlying cell rearrangement, but other factors are also likely to be important. (C) Branching morphogenesis depends on complex, dynamic interactions between mesenchymal and epithelial tissues. ECM turnover and cell proliferation occur at the tips of the buds, while ECM accumulates in the clefts, where growth is slow. Adapted from [40].

compaction and result in the development of extensive, intimate adhesive contacts between adjacent cell surfaces. Cadherins also participate in the intercellular motility underlying cell rearrangement, allowing cells to move into a tissue despite adhering tightly to each other.

1.3 Thesis Summary

This thesis uses both experiment and computation to study the role of generic mechanisms, especially cell adhesion, in embryonic tissue morphogenesis. I translate biological knowledge at tissue, cell and subcellular levels into computational language to produce simulations of biological phenomena. Where I lacked data, I designed and executed experiments to obtain it. My simulation results provide insight into the principles of morphogenesis. My work is by no means conclusive; it suggests possible mechanisms of morphogenesis and opens the door to further investigations.

Chapter Two reviews computer modeling of morphogenesis, discussing the Cellular Potts Model (*CPM*) in detail, the computational framework for my

biological simulations. My ultimate goal is to *compute an organism*—to reproduce the most important tissue-level features in a developmental example computationally, using only known cellular and sub-cellular interactions. My modeling strategy is to find known physical mechanisms that quantitatively mimic individual biological observations. I then combine these mechanisms to reproduce observed behaviors. Interacting mechanisms can build complex structures that individual mechanisms cannot.

The fundamental entities in the CPM are individual cells. An *Effective Energy* describes their interaction, motion, differentiation and division. For instance, gradients in cell-surface adhesivities create surface-tension forces, while the migration of a cell in response to a chemical resembles the motion of a molecule in a gradient of chemical potential. The effective energy of the CPM consists of explicit, independent terms describing differentiation, division and other interactions. Cells rearrange diffusively to minimize the total effective energy. The parameters of each cell evolve according to equations I define for its internal state, while reaction-diffusion equations model the variations in the spatio-temporal expression of signaling molecules (Figure 9).

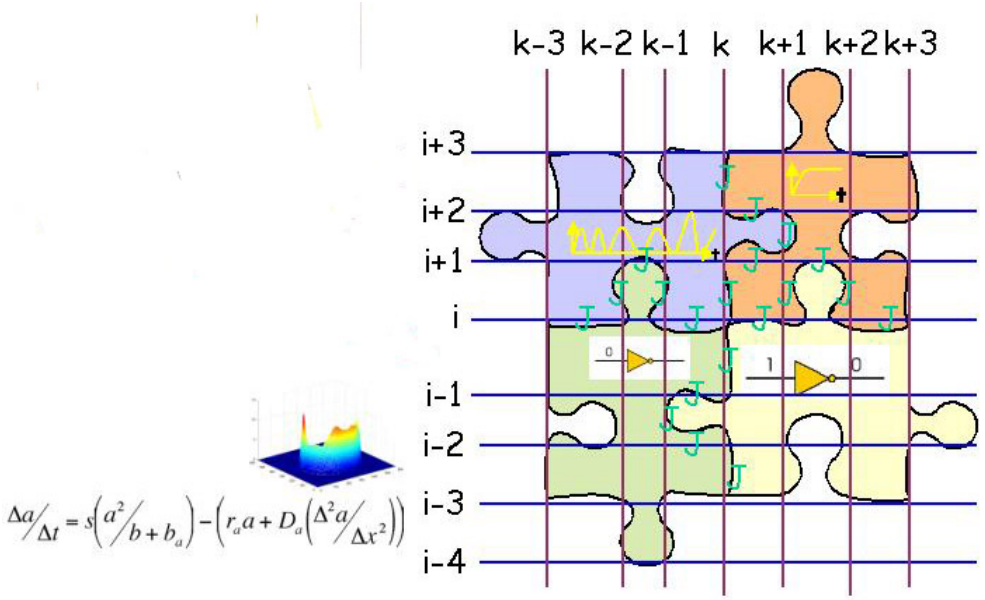

Figure 9. Illustration of my computational method. I simulate biological cells using a discrete CA model by imposing a lattice on the cells and simplifying the intracellular genetic circuits to pre-assigned cell-state diagrams or digital gates. Cells can deform by gaining or losing pixels driven by energy minimization on a spatial scale no smaller than the lattice mesh size. I model any chemical reactions and their kinetics using continuum partial-differential equations (*PDE*s) and then couple them to the discrete CA model.

Chapter Three treats chick limb development. Most previous explanations of biological patterning have invoked the Turing Mechanism, where biological patterns emerge from the diffusion and reaction of two chemical substances, the *activator* and the *inhibitor*. However, the inhibitor is often hard to identify experimentally. Therefore, I propose a novel, non-Turing, biological mechanism that forms stripes and spots, using only experimentally-observed phenomena, particularly cell-cell adhesion and cell-ECM adhesion, and implement two-dimensional and quasi-two-dimensional CPM simulations of chick limb precartilage mesenchymal condensation *in vitro*. The simulations successfully reproduce much of the density-dependent morphology of the experiment without requiring an inhibitor. This mechanism can explain cell clustering during mesenchymal morphogenesis where the classical Turing Mechanism does not apply.

Chapter Four treats the initiation of the primitive streak during early chick gastrulation. I describe an electroporation technique that I developed, which allows easy genetic manipulation of the chick embryo as early as the

pre-gastrulation stage. This technique is important because it costs much less than developing transgenic lines and enables study of pre-gastrulation morphogenesis, which is impossible using retroviral techniques. The transfection technique is also useful for studying later development, since the embryos remain alive for extended periods and the cells remain transformed as long as the embryos survive. Using this technique, I studied the initiation of the primitive streak before and during early chick gastrulation, by randomly labeling epiblast cells in Stage XI-XII chick blastoderm (before the germ layers form) using Green-Florescent-Protein (*GFP*) electroporation and monitoring the cell movements using time-lapse microscopy. The cell movement patterns strikingly resemble flow patterns in complex viscous fluids. To investigate the flow's regulation mechanisms, I analyzed the velocity field of the movements both in normal embryos and when I manipulated the *Fgf* and *Wnt* signaling pathways.

Chapter Five summarizes the thesis and suggests future experiments and simulations.

In an appendix, I simulate chick limb-bud outgrowth *in vivo* to study

epithelial-mesenchymal interactions. My model assumes that the ectodermal cells secret cues for the mesenchymal cells to proliferate, migrate and differentiate. The simulation reproduces the sequential shape changes of the early limb bud.

CHAPTER

TWO

COMPUTER-BASED MORPHOGENESIS

2.1 Overview

Results from biological experiments are rarely unambiguous; instead they usually suggest several possible underlying mechanisms. With the given experimental clues, we can formulate models with a minimal set of reasonable assumptions to study the biological problem theoretically. A good model can describe and reproduce the experimental observations and provide predictions to guide future experimental investigations to test itself and other models. Mathematical models can help us quantify conceptual models and identify their important parameters. Computer simulations provide numerical results when analytical solutions are unobtainable for a model's many evolving components and non-linear interactions, as is always the case in biology. Now, in a post-genomic era of ever-rising computing power, the development of computer-based morphogenesis helps us towards the goal of understanding the principles of biological morphogenesis.

In this chapter, I first review some of the most influential models proposed to explain biological patterning during morphogenesis. Some of the models originated as pure conceptual models, for instance the 'Gradient and Positional-Information' Model, some are mathematical models and some are

individual-based or agent-based models. The mathematical models usually treat chemical concentration, cell density and force as a continuous 'fields' and employ differential equations to describe their dynamics. Turing's Reaction-Diffusion Model falls into this category. The individual- or agent-based models usually are CA models, which treat cells as discrete units with pre-assigned rules for their interactions and signal processing. This class of models emphasizes local cell properties like cell adhesion and physical and geometrical concepts like energy. It predicts the global consequences of local interactions of members of a population. The Potts Model is a typical individual-based model, which I will discuss in detail.

A manageable and meaningful computational study of morphogenesis must balance simplification and the maintenance of important biological details. Though we are far from being able to model morphogenesis in vertebrate embryos, comprehensive multi-scale models of other organisms have been able to accommodate, combine and hybridize different mechanisms, classes of theories and models, and reproduce not only patterns, but also shapes, and in some cases also the kinetics, observed during development [16, 41-45], which no individual component can produce.

2.1.1 The Gradient and Positional-Information Model

The influential 'Gradient and Positional-Information' Model [46-48] demonstrates how the interplay between genetic mechanisms and generic mechanisms like diffusion instructs cells what to become. The model assumes that a soluble substance (*morphogen*) diffuses from a source of production to a sink of degradation, establishing a continuous range of concentrations within a region, with the highest concentrations being near the source of the morphogen. Theoretical considerations suggest that such gradients could only function over relatively small distances, less than 100 cell diameters [49]. The cells respond differentially to different concentrations of the gradient. The cellular response mechanisms can be spatially non-uniform and temporally evolving (Figure 10 adapted from [48]). This model does not account for cell movement and its effects on the establishment of the gradient or on the cells' response. Experimental evidence supporting the existence of morphogens and their effects on developmental patterning (reviewed in [50, 51]) comes from the measurement of the anterior-posterior Bicoid gradient during early *Drosophila* axis patterning [52], and in chick limb development, the anterior-posterior Sonic-Hedgehog gradient and skeletal-pattern duplication [28, 53] and the distal-proximal arrangement of skeletal components and overlapping *Homeobox* gene-expression gradients [54, 55].

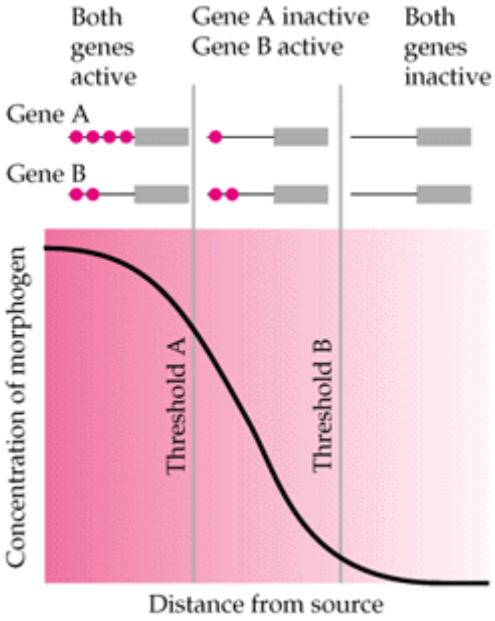

Figure 10. A hypothetical model for how gradients establish positional information. The concentration of a morphogen decreases with distance away from its source. In this diagram, the receptors for the morphogen are enhancer elements of two genes that control cell fate, but the receptors could also be cytoplasmic receptors or membrane receptors. One receptor (in this case, the enhancer on gene A) needs a high concentration of morphogen in order to act. At high concentrations of morphogen, both genes A and B are active. At moderate concentrations, only gene B is active. Where the morphogen concentration falls below another threshold, neither gene is active. Adapted from [48].

2.1.2 Turing's Reaction-Diffusion Model

In 1952, in one of the most important papers in theoretical biology, Turing postulated a chemical mechanism for generating coat patterns. He suggested that biological form follows a prepattern in the concentration of chemicals (morphogens). Turing began with the assumption that morphogens can react with one another and diffuse through cells. He then employed a mathematical model to show that if morphogens react and diffuse in an appropriate way, then spatial patterns of morphogen concentrations can arise from an initially uniform distribution. In the simplest example, he considered two morphogens *a* (*activator*) and *i* (*inhibitor*) such that 1) *a* catalyzes the production of both *a* and *i*; 2) *i* inhibits the production of both *a* and *i*; and 3) *i* diffuses faster than *a*.

Many chemistry and biology experiments seem to allow a Turing-Model explanation. Castets and colleagues observed Turing-type chemical patterns [56] and theory can indicate the correct parameter regime to produce chemical reactions showing Turing-type instability. In biology, researchers have found a growing number of developmental patterns that seem to fit Turing's scenario, such as butterfly wings [57] and animal and fish skins [58-60]. For example, Young applied a local Activator-Inhibitor Simulation to study animal skin patterning [61]. Gierer and Meinhardt reformulated and applied Turing's Reaction-Diffusion Model to study patterns on sea shells

and zebra skins and head formation in *Hydra* [62, 63]. Kondo and Asai simulated reaction-diffusion waves during pattern rearrangement in the skin of the marine angelfish, *Pomacanthus* [60].

One limitation of Turing Models is that they can explain the formation of patterns during morphogenesis, but not the evolution of the shapes of the domains where the chemical reaction and diffusion take place. Some biological Turing Patterns like stripes on zebra skin, form and lock-in during early development. The length-scales of the patterns simply expand as the animals grow. Other biological Turing Patterns, like stripes on angelfish [60] develop continuously and are sensitive to the geometry of domain boundaries, so the patterns evolve as the animal grows, keeping the pattern length-scale constant. Reference [64] studies the stability of Turing Patterns under domain shape changes.

Turing Models have other limitations. The existence and identity of morphogens, especially the inhibitors, is often speculative [65]. Also, morphogens may not diffuse freely across a cell population as the model assumes. In the well-connected cells in an epithelial sheet, the diffusion of certain chemicals is receptor-based. Also, the interactions of regulatory molecules usually form a complex network, whose description requires more than the two components of the original Turing Model. Last, how the

chemical prepattern produces the actual biological pattern is not straightforward, due to cell movement and differentiation more complex than simply following the chemical prepattern [66, 67].

Despite its limitations, 50 years after its birth, the Turing Model remains attractive, since it explains many experiments in chemistry and biology using very simple ideas. The original Turing Model has developed into a more complete mathematical theory with entire classes of Reaction-Diffusion Models [68]. These models apply if the characteristic wavelength of the pattern is large compared to the diameter of individual cells, for instance a leopard's coat, where the number of cells in a leopard spot at the time the pattern is laid down is on the order of 100 [68].

2.1.3 The Mechano-Chemical Model

In this section, I discuss one typical individual-based model of morphogenesis: the Mechano-Chemical Model, which focuses on physical forces. Parameters and factors in the model are experimentally measurable quantities such as cell and ECM densities, traction forces, tissue deformations, *etc.*. Odell and coworkers used such a model to explain the folding of embryonic epithelia [69, 70]. If one cell in a layer contracts, it stretches other cells. If many cells pull on each other, they reduce their apical surface and invaginate. The mechanism could apply to sea-urchin

gastrulation, *Drosophila* ventral-furrow formation and amphibian neurulation.

Such a population effect is more robust and realistic than assigning each cell a unique genetic program coding for its detailed shape and position within the tissue. As Wolpert points out: "It is clear that the egg contains not a description of the adult, but a program for making it, and this program may be simpler than the description. Relatively simple cellular forces can give rise to complex changes in form. It seems simpler to specify how to make complex shapes than to describe them."

The Mechano-Chemical approach neglects chemical diffusion, reaction and signaling. Combining Mechano-Chemical Models with Reaction-Diffusion Models overcomes this limitation. When the cell population is large and the interaction forces complex, the Mechano-Chemical approach becomes computationally expensive. In this case, the Cellular Potts Model (*CPM*) provides a solution: Since the embryonic tissue is viscous, force is no longer proportional to the acceleration of cells, but their speed. Thus, we can consider the cells' effective energy instead of forces. I discuss the CPM in detail in the next section.

2.2 Biological Modeling Using the Cellular Potts Model

The Ising Model is a statistical model of ferromagnetic phase transitions, which allows the interacting spins to be either parallel or antiparallel. In 1952, Potts introduced his model [71], which his supervisor Domb had proposed for the topic of Potts' Ph.D. thesis, to generalize the Ising Model to more than two spin directions. The spin interaction energies are highly degenerate, with one interaction energy for any pair of like spins and another for any pair of unlike spins. Before Potts' endeavor, Ashkin and Teller had considered a two-dimensional square lattice consisting of four kinds of 'atoms' with nearest neighbors interacting and two distinct interaction energies, one between like and one between unlike atoms [72]. The Ashkin-Teller Model corresponds to the four-state Potts Model, so the Potts Model is also known as the Ashkin-Teller-Potts Model. The Potts Model has a rich phase structure and critical behavior [73, 74].

Later researchers extended and modified the original Potts Model to study different problems, for instance Weaire and Kermode [75-77] used it to model soap bubbles. In the early 80s Anderson, Grest, Sahni and Srolovitz applied the Q-state Potts Model to study coarsening or annealing of metallic polycrystals [78]. This application has several attractive features. First, imagining that the interior of a grain at the microscopic level consists of a lattice of atoms corresponding to the spins in the original Potts Model, with

the grain boundaries as the interfaces between different groups of atoms or crystal orientations is natural. Second, the driving force during metallic coarsening is grain-boundary energy and in the Potts Model the energy is proportional to the total grain-boundary area.

The Large-*Q* Potts Model has the potential to elegantly handle cellular pattern formation resulting from local interactions like differential surface adhesivity. Its successful application to coarsening in soap froth [79] and the analogy between soap froth and cells make it a good candidate for biological modeling. A two-dimensional hexagonal array of soap bubbles of equal area resembles a cell sheet morphologically [80]. Cells intercalate to change the tissue shape, *e.g.* in the *Drosophila* embryo, in a manner similar to the rearrangement of bubbles [81]. Though cells have a characteristic length-scale or size, while bubbles change in volume, pattern formation in both media involves boundary-length and free-energy minimization resulting from surface tension. Cell surfaces have elasticity and bulk compressibility like bubbles, but the membranes of different cells maintain separate identities. In most cases, the cytoskeleton regulates membrane rigidity and cell shape. Cells also exhibit different viscosity and elasticity under forces acting at different time-scales [82].

The original Large-*Q* Potts Model represented the spatial distribution of

cells, indexed by σ, by superimposing a lattice onto the cells. The value at a lattice site (i, j) is σ if the site lies in cell σ. Each cell occupies multiple lattice sites and the possibly disconnected set of lattice sites with the same index represents one cell. The interaction energy is zero between like spins and one between unlike spins. The Hamiltonian (the total effective free energy) is:

$$H_0 = \sum_{(i,j),(i',j')} (1 - \delta_{\sigma(i,j),\sigma'(i',j')}) \quad , \tag{2.1}$$

where (i, j) and (i', j') are neighboring lattice sites.

Glazier and Graner extended the Large-Q Potts Model to study cell sorting by adding two key mechanisms: variations in the spin-spin energy between cells to reflect differences in cell adhesion and a constraint to maintain the fixed volumes of cells [83, 84]. Since cell-cell adhesion is type-selective, Glazier and Graner [83, 84] introduced cell type as a new variable and thus cell-type-dependent spin-spin coupling into the Potts Model (Figure 11). An effective cell-type-dependent binding energy per unit area, $J_{\tau,\tau'}$, describes the net interaction between two cell membranes, where τ is the type of the cell on either side of the link, which incorporates both specific (*e.g.* integrins, cadherins) and nonspecific interactions (*e.g.* elastic effects due to cell deformations [85]). Accordingly, the Hamiltonian becomes:

$$H_1 = \sum_{(i,j),(i',j')} J_{\tau(\sigma(i,j)),\tau(\sigma'(i',j'))}(1-\delta_{\sigma(i,j),\sigma'(i',j')}) \quad , \qquad (2.2)$$

where $\tau(\sigma)$ denotes cell type.

Since during morphogenesis each cell retains its size without disappearing or growing, Glazier and Graner also introduced an area constraint term (or both volume and area constraints in three dimensions) into the Hamiltonian [83, 84]:

$$H_2 = H_1 + \sum_{\sigma} \lambda_A(\tau(\sigma))(A(\sigma) - A_t(\tau(\sigma)))^2 \quad . \qquad (2.7)$$

This new term stands for the cells' resistance to compression. The current cell area is $A(\sigma)$ and the type-dependent target cell area is $A_t(\tau(\sigma))$. $\lambda_A(\tau(\sigma))$ governs the compressibility of the cell. Deviation from the target area increases the total energy and therefore is unfavorable.

According to the DAH, in an aggregate of cells of two different types, the surface tensions at boundaries between like cells and unlike cells differ. The DAH [23] also proposes that the cells comprising an aggregate are motile, and the final organization of cells maximizes the strength of adhesive interactions summed over all the adhesive contacts in the aggregate. CPM simulation by Glazier and coworkers supported the DAH as the mechanism of tissue reorganization during cell sorting by quantitatively reproducing the kinetics of (i) clustering of cells and (ii) the reduction of heterotypic

boundary length in simple experimental cell aggregates [86]. Realistic values of the simulation parameters based on experimental measurements for *Hydra* cell aggregates produce a simulated diffusion constant agreeing with that in experiments [87]. In chick retina, the velocity distribution of a single pigmented cell in a neural-cell aggregate is identical to that of a simulated cell [88].

Jiang and coworkers introduced spin-external-field coupling to the CPM, in this case cells' chemotaxis to chemical signals, to simulate cell sorting during the mound stage of the life cycle of *Dictyostelium discoideum* [79, 89]. Their result supported the hypothesis that the cooperation of chemotaxis and differential cell adhesion leads to tip formation [79].

When an external field acts on cells, or some subset of cell types, the spins

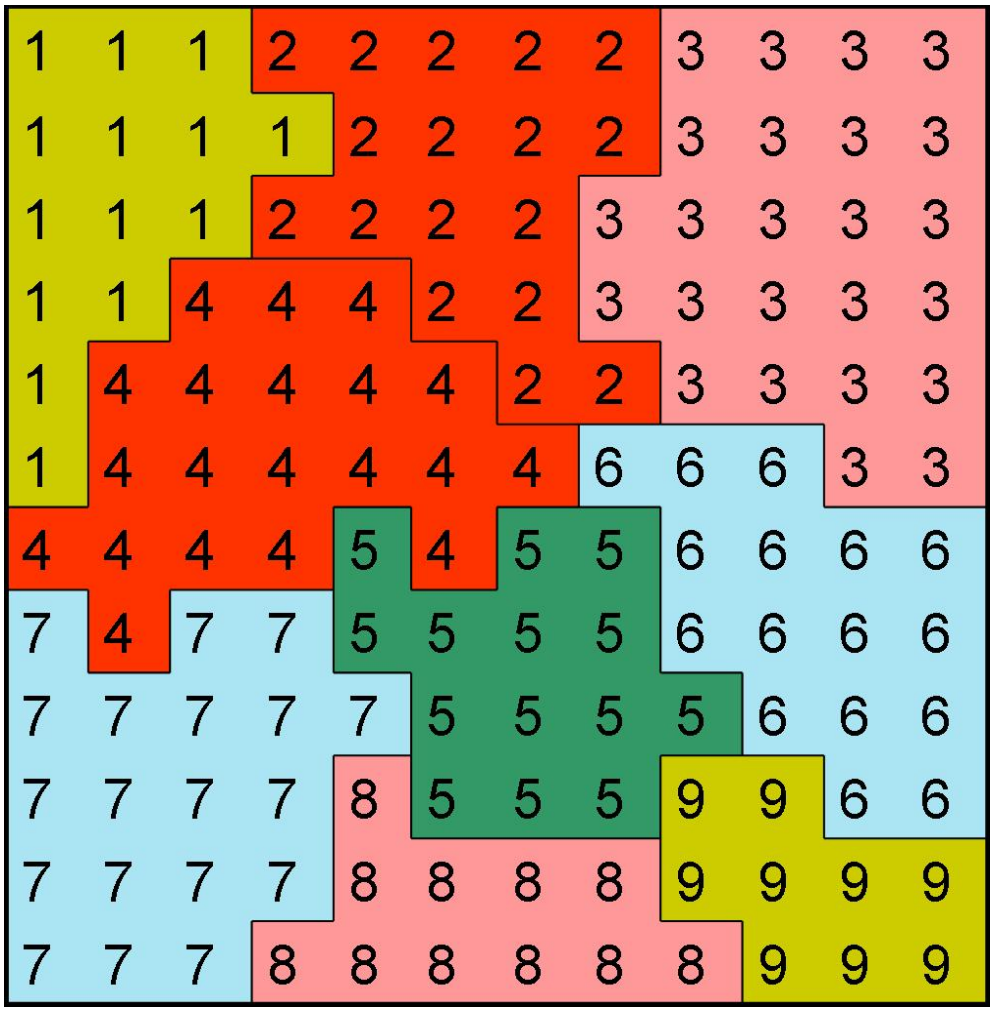

Figure 11. Schematic of a two-dimensional square lattice in the Large-*Q* Cellular Potts Model. Numbers are the cell indices and black lines indicate cell boundaries. The nine cells have five different types. Each color defines a unique cell type. The strength of the cell-cell surface adhesion is type-dependent.

within these cells need to couple to the external field through a term in the Hamiltonian. The force resulting from this coupling acts at cell boundaries. Unlike other soft condensed materials, *e.g.* bubbles, which respond mainly to fields like gravity [79], biological cells respond mainly to chemical fields within their environment. A new term describing cell-chemical-field coupling extends the Hamiltonian to:

$$H_3 = H_2 + \mu \sum_{i,j} C_{i,j} \,, \tag{2.8}$$

where μ is the chemical potential, $C_{i,j}$ is the chemical concentration at site (i, j), and the summation is over all the lattice sites 'seeing' the chemical field. By changing the sign of μ, cells can move up or down the chemical gradient, since cell boundaries move more often into sites with higher or lower chemical concentrations.

The evolution of the CPM is Monte-Carlo-Maxwell-Boltzmann. Assuming that cell boundary motion is thermally activated, Glazier and Graner used a modified Metropolis dynamics [90], which attempts to flip only boundary pixels, and prohibits heterogeneous nucleation to reduce the total number of flip attempts. This algorithm differs from the standard Metropolis algorithm, which allows arbitrary spin flips. The modified algorithm is more appropriate for my purposes since the probability of a flip creating a completely mismatched spin or a disconnected patch is low and biologically

unrealistic. The modification does not greatly affect the statistics of the patterns [84, 91, 92]. During one Monte Carlo Step (*MCS*), every boundary pixel tries to flip its spin to that of one of its neighboring pixels. Cells rearrange diffusively to minimize the total effective free energy of the pattern. At each step we select a lattice site (i, j) at random on the boundaries only and propose to change its index from σ to σ', where σ' is the index of an arbitrary neighboring lattice site different from σ. We accept the change with Boltzmann probability:

$$P(\sigma(i,j) \rightarrow \sigma'(i,j)) = \begin{cases} \{exp(-\Delta H/kt), & \Delta H > 0, T > 0 \\ 1, & \Delta H \leq 0, T > 0 \\ 0, & \Delta H > 0, T = 0 \\ 0.5, & \Delta H = 0, T = 0 \\ 1, & \Delta H < 0, T = 0 \end{cases} \quad . \quad (2.9)$$

$\Delta H = H_{after} - H_{before}$ is the energy gain the spin flip produced. T is the temperature used in the simulation, which corresponds to the amplitude of the membrane fluctuations, not of the thermal fluctuations, which are much smaller. Each such move corresponds to cell σ' displacing cell σ by one lattice site. The $T > 0$ flip rule applies to metallic materials and biological cells where fluctuations are significant [88, 93]. The $T = 0$ rule applies to soap foams, which are fluctuation free. Since I usually simulate at temperatures comparable to the free-energy differences, I anneal for a few MCS at T=0 at the end of the simulation to eliminate disconnected domains and crumpled cell boundaries. Usually, on a square lattice, I include up to

fourth-nearest neighbors when calculating the interaction energy (Figure 12) to balance computation time and lattice anisotropy [79], while on a hexagonal lattice I include up to second- or third-nearest neighbors [94].

The CPM describes biological cells as geometric domains with finite size and curvature and physical properties like adhesion. This representation is realistic, in the sense that the formation and deformation of cell boundaries drives the pattern, just as biological cells rearrange by making and breaking adhesive bonds. The CPM is flexible because its modular Hamiltonian consists of explicitly independent terms describing interactions. It is able to accommodate additional terms describing a variety of cell behaviors including cell growth, cell differentiation, mitosis and apoptosis [16]; cell-cell and cell-ECM adhesion [95, 96]; and cell polarity (as in convergent extension) [97, 98]. All of these mechanisms play essential roles during morphogenesis. Additionally, as new experimental results become available, we can add more terms to the Hamiltonian to describe new mechanisms.

Like every model, the CPM has limitations, some of which are intrinsic and some of which suggest further improvements and extensions. The CPM does not reproduce the realistic kinetics of energy dissipation as do Molecular-Dynamics (*MD*) Models, which calculate the actual forces acting on their components. Instead, it is a quasi-equilibrium model. In the CPM

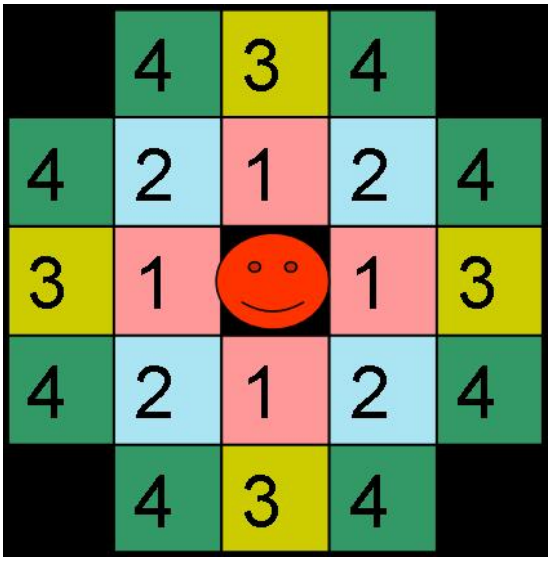

Figure 12. Schematic of the first-, second-, third- and fourth-nearest neighbors on a two-dimensional square lattice, indicated by numbers and different colors. The total number of neighbor pixels for a fourth-neighbor interaction is 20.

the lattice mediates force transduction, so cells can move by pulling on the lattice, which is biologically unrealistic. A possible solution is to use a quasi-finite-element method to discretize cells and solve for rigid body motion (Turner, *unpublished*). The current CPM model framework does not include many important biological features. For instance, the expression of adhesion molecules can be uneven across the membrane and can change over time, and cytoskeletal fluctuations and rearrangements can lead to cell polarity. We need to introduce new parameters to describe such cell anisotropy.

Several groups have hybridized the CPM with continuum models. Hogeweg and Marée combined *Partial Differential Equations* (*PDEs*) with the CPM to simulate the slug and culmination stages of *Dictyostelium* morphogenesis. The PDEs describe the subcellular relaying and oscillations of cAMP as excitable media and the CPM describes cellular differential adhesion and chemotaxis. These simulations helped to elucidate the roles of interacting genetic and environmental factors [41-43]. Applying such an approach to the study of morphogenesis requires building a standard, large-scale, biological simulation environment to replace variant 'home-made code.' CompuCell3D (*http://www.nd.edu/~lcls/compucell/*), which standardizes the CPM simulation environment and combines it with a PDE solver, serves this purpose [99].

CHAPTER THREE

CHICK LIMB DEVELOPMENT

3.1 Introduction

The developing limb has served as a classical model of morphogenesis for at least half a century. Since Zwilling and Saunders's pioneering work in the 1950s [100], new discoveries and theories have continually reformed this field [101-105]. For example, the Positional-Information Model, the Progress-Zone Model and the Early-Determination Model are major models proposed to explain patterning during limb development. Limbs permit molecular and surgical manipulations with dramatic results, but without fatal damage to the embryo. The underlying genetic regulation is conserved across vertebrates and is similar to that in other tissues [102]. In this chapter, after a concise introduction to our current understanding of limb development, I propose a novel mechanism explaining cell clustering during mesenchymal condensation and chondrogenesis, based only on experimentally-observed phenomena, particularly cell-cell adhesion and cell-ECM adhesion. I implemented a CPM simulation to study chick limb precartilage mesenchymal condensation *in vitro*, and the simulations successfully reproduced much of the density-dependent morphology of the experiment.

We describe the structure of limbs in terms of three axes: a proximo-distal (*PD*) axis that extends between the shoulder and the tips of the digits; an anterior-posterior (*AP*) axis that extends, *e.g.*, in the hand, between thumb and little finger; and a dorsal-ventral (*DV*) axis that runs from the back of the hand to the palm.

The basic structures of the limb bud and the adult limb are conserved among vertebrates (Figure 13 adapted from [101]). They consist of a proximal part (*Stylopod*) with a single skeletal element, a medial part (*Zeugopod*) with two elements, and a distal part (*Autopod*) composed of carpals or tarsals and a variable number of radiating digits. Morphological and functional diversity most likely derives from variations in the molecular mechanisms that sculpt the limb. Some of these molecular bases of this patterning are already known [101].

Vertebrate limbs originate as two pairs of limb buds that appear at specific levels of the embryonic flank. The limb bud contains mesenchymal cells encased in an ectodermal jacket. Some specific regions of the buds are signaling centers that pattern the bud along the AP, DV and PD axes. For example, the zone of polarizing activity (*ZPA*) patterns the AP axis; the apical ectodermal ridge (*AER*) maintains the outgrowth of the limb bud along the PD axis; and the dorsal and ventral ectoderm determine the DV

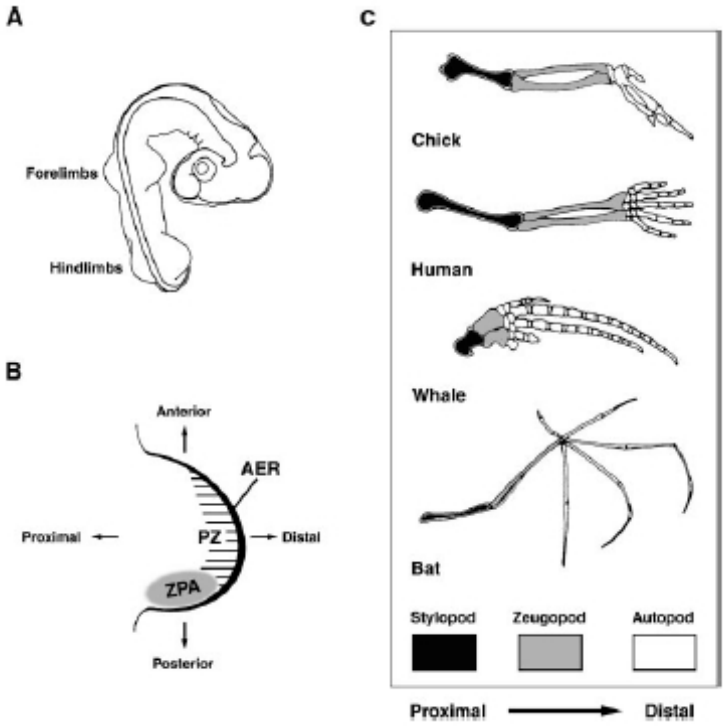

Figure 13. The basic structures of the limb. (A) Two pairs of limb buds (forelimb and hindlimb) appear at specific levels of the chick embryonic flank. (B) Dorsal view of the limb bud. The Zone of Polarizing Activity (*ZPA*) patterns the AP axis, and the Apical Ectodermal Ridge (*AER*) maintains the outgrowth of the limb bud. Not shown, the dorsal and ventral ectoderm determines the DV polarity of the distal part of the limb. (C) Schematic representations of the skeletal structure of forelimbs of several vertebrates. Generally they consist of a proximal part (*Stylopod*, in black) with a single skeletal element, a medial part (*Zeugopod*, in gray) with two elements, and a distal part (*Autopod*, in white) composed of carpals or tarsals and a variable number of radiating digits. Adapted from [101].

polarity of the distal part of the limb. These signaling centers create the sets of interlocking patterns which regulate cell proliferation, death, movement and differentiation during limb development. Some typical diffusible signaling molecules and the genes they activate include *Hox,* Sonic Hedgehog (*Shh), Wnt,* Fibroblast Growth Factors (*Fgf*s) and Bone Morphogenetic Proteins (*Bmp*s). Reference [102] summarizes the phenotypes experimental manipulation of these signaling centers and pathways produces.

The limb's shape and skeletal pattern vary along all three axes. The proximal skeletal pattern differs from the distal in the number and size of skeletal elements. The bud flattens in the DV direction and expands in the AP direction at its distal end before the digit skeletal pattern appears. The AP polarity also appears in the finger identity. The dorsal and ventral sides of the limb have different musculature and ectoderm morphology (like feathers).

3.2 Limb Skeletal Pattern — Precartilage Mensenchymal Condensation

3.2.1 Biological Background

The chick limb's skeletal elements begin as cartilage. The separate cartilage elements include the *humerus* (upper arm), *radius* and *ulna* (lower arm), and wrist and digits (hand). Each digit consists of a series of separate cartilage elements. Alcian-Blue staining reveals cartilage differentiation, showing that proximal skeletal elements, such as the humerus in the forelimb and the femur in the hindlimb, emerge first, and distal ones, such as the digits, emerge later. As the bud elongates, more distal skeletal elements differentiate progressively, until the complete skeletal plan is laid down in cartilage (Figure 14 adapted from [106]).

Mesenchymal condensation, in which *mesenchymal* cells (*i.e.*, cells that form part of bulk tissue rather than epithelial surfaces) *condense* (*i.e.*, coalesce into compact clusters), is the earliest stage of organogenesis and is crucial to the development of skeletal and other mesenchymal tissues (*e.g.* cartilage, kidney, lung, *etc.*). The morphology of the condensations lays down the shape of future organs (Figure 15 adapted from [107]). Precartilage mesenchymal cells are swarming cells that secrete a variety of complex molecules which form the extracellular matrix (*ECM*), the loosely-structured non-cellular scaffolding which surrounds and supports the cells, forming a porous environment which is largely responsible for the mechanical integrity of connective tissues and which provides a substrate for cell migration [108]. Recent experiments show that ECM molecules and

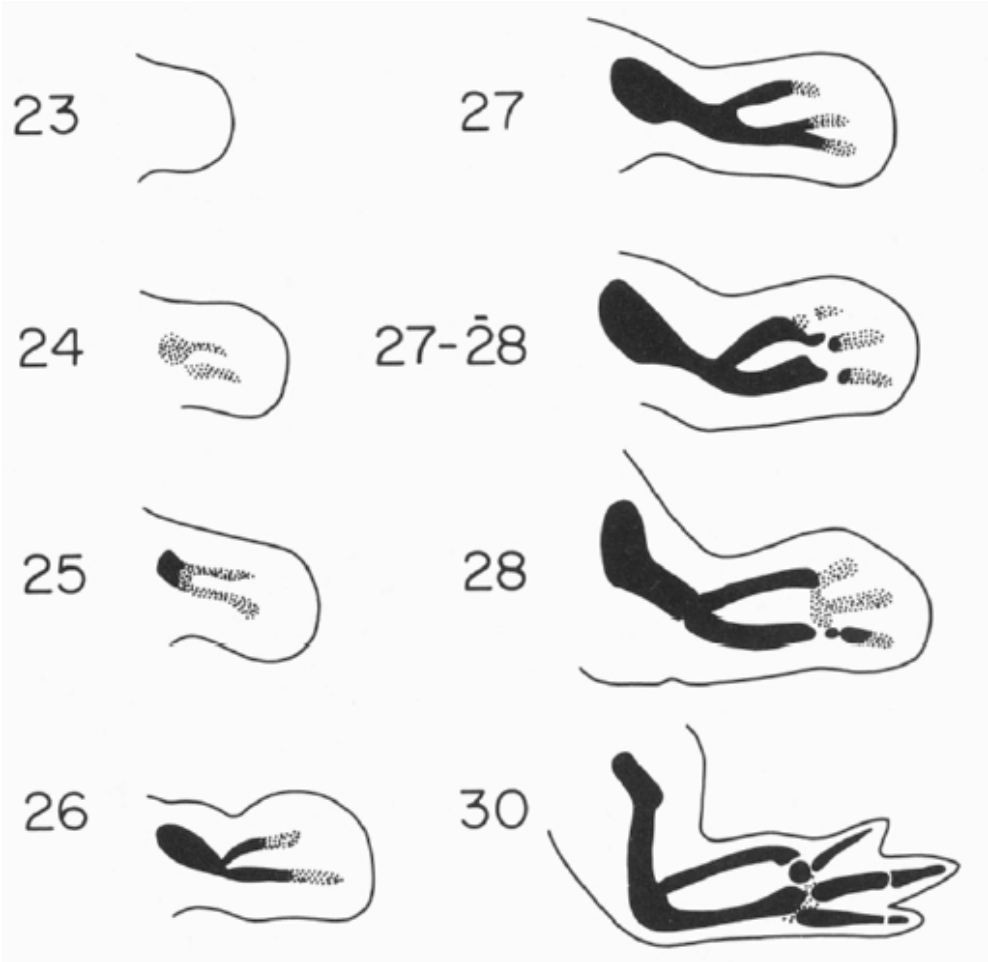

Figure 14. Progress of chondrogenesis in the chick wing bud between 4 and 7 days of development. Solid Black regions represent definitive cartilage; stippled areas represent early cartilage. Stages are those of Hamburger and Hamilton. The width of the limb bud is approximately 2mm. Copyright 1979 by the AAAS. Adapted from [106].

membrane-bound cell-adhesion molecules play an important role in initiating cell clustering during precartilage mesenchymal condensation [107].

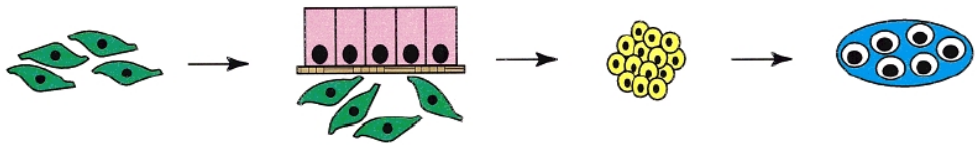

Figure 15. The four phases of the development of a skeletal element are (from left to right): migration of preskeletal cells (green) to the site of future skeletogenesis, which is always associated with an epithelium (purple) and epithelial basement membrane (brown); interactions of those cells with epithelial-cell products initiate condensation (yellow); and overt differentiation of chondroblasts or osteoblasts (blue). Adapted from [107].

Accumulated experimental evidence shows that the adhesive, non-diffusing molecule fibronectin play an important role in mesenchymal condensation, since its expression increases as condensation begins, and the expression peaks overlap with the condensation sites [109, 110]. Mesenchymal cells prefer to attach to fibronectin and can move up gradients of fibronectin concentration, a phenomenon called *haptotaxis*. Besides guiding cell migration, fibronectin also interacts with integrins on the cell surface and triggers intracellular signaling cascades which affect cell properties and gene expression [110]. Fibronectin expression and synthesis increase four-to-five-fold at the onset of condensation in precartilage mesenchymal-condensation sites both *in vivo* and *in vitro* [109, 111]. TGF-β

regulates fibronectin production [109, 112]. Condensing precartilage mesenchymal cells can also adhere to each other directly through transmembrane adhesion molecules, such as N-cadherins. Condensing cells express N-cadherin in the developing limb bud *in vivo* and in limb-bud micromass culture *in vitro* and the time of maximal expression of N-cadherin corresponds to the period of active precartilage mesenchymal condensation [113, 114]. Integrins, another class of cell-adhesion molecule, attach primarily to proteins bound to the ECM [115, 116]. Binding of fibronectin to integrin can promote cadherin-mediated cell-cell adhesion by upregulating cadherin production [117]. Changing the extracellular environment [118] and changing cell adhesiveness can influence the pattern of condensation *in vitro* [119]. Together, the above experiments suggest that attachment of mesenchymal cells to ECM and thus enhanced, local, cell-cell adhesion suffices to initiate and maintain cell clustering during precartilage mesenchymal condensation.

I tested this hypothesis (that cell-cell and cell-ECM adhesion could lead to the clustering and differentiation of a previously dispersed population of mesenchymal cells during precartilage mesenchymal condensation) experimentally and using a CPM simulation. To avoid the complications of three-dimensionality and multiple signaling pathways *in vivo*, I performed quasi-two-dimensional, *in-vitro*, micromass experiments, where precartilage

mesenchymal condensation is qualitatively similar to that *in vivo* [109].

3.2.2 Methods

In my chick-limb micromass culture experiments, I plated out in a petri dish a 10 µl DMEM culture-medium suspension of single cells from the distal 0.3mm of HH stage 24-26 chick wing or leg buds [120]. After 45 minutes, some of the cells settled and attached to the bottom of the dish, creating a 3mm circle of cells. I then used 1ml of DMEM culture medium to flush away any unattached cells. Condensation took place 18 to 36 hours after plating. I changed the medium once every 2 days. Five days after plating, I fixed the culture and stained it with Alcian Blue to visualize the differentiated cartilage [120]. Depending on the initial cell density, the cartilage pattern varied from a mixture of stripes and spots (medium density – 1.75 x 10^7 cells/ml) to spots only (low density -1.5 x 10^7 cells/ml) [95].

I also implemented a two-dimensional CPM simulation (Chapter Two) of micromass condensation. I used a 600x600 pixel square lattice and restricted the initial cell distribution to a circle in the middle. 600 pixels represent 3 mm in the experiment, setting the spatial scale to 5 μm/pixel. A typical limb-bud mesenchymal cell is approximately 15 μm in diameter when viewed as a flat two-dimensional disc. Therefore each cell occupies

approximately 7 pixels. I checked that making the cells larger or smaller (in lattice sites) changed the length and timescales (and the time to run the simulation) but did not change the qualitative behavior of the pattern.

My CPM Hamiltonian includes three terms:

$$H = \sum_{(i,j),(i',j')} J_{\tau,\tau'}(\sigma(i,j),\sigma'(i',j'))(1-\delta_{\sigma(i,j),\sigma'(i',j')}) + \sum_{\sigma} \lambda_A(\tau)(A(\sigma)-A_t(\tau))^2 + \sum_{(i,j)} \mu(\tau)C_f(i,j). \quad (3.1)$$

The first term describes the surface adhesion energy between cells and between cells and their environment. The sum is over (i, j) and (i', j') neighbors. τ denotes the cell type. I treat the environment, including the culture solution and substrate as a single cell with τ = 0, while all the biological cells are of type τ = 1. I make each cell's surface energy $J_{\tau,\tau'}(\sigma(i, j), \sigma(i', j'))$ a variable to reflect the increase in membrane-bound adhesion molecules in response to fibronectin. If $J_{11}(\sigma, \sigma') \neq J_{11}(\sigma', \sigma)$, I set $J_{11}(\sigma, \sigma') = J_{11}(\sigma', \sigma) = \min(J_{11}(\sigma, \sigma'), J_{11}(\sigma', \sigma))$. I also checked that setting $J_{11}(\sigma, \sigma') = J_{11}(\sigma', \sigma) = \max(J_{11}(\sigma, \sigma'), J_{11}(\sigma', \sigma))$, did not critically affect the final configuration of the simulation.

The second term stands for the cells' resistance to compression (as discussed in Chapter Two). Current cell area is $A(\sigma)$ and the type-dependent target cell area is $A_t(\tau(\sigma))$. $\lambda_A(\tau(\sigma))$ governs the compressibility of the cell.

Deviation from the target area increases the total energy and therefore is not favored.

The third term describes the preferential attachment of cells to fibronectin and the sum includes only the sites that lie within cells. $C_f(i, j)$ is the concentration of fibronectin at lattice site (i, j) and $\mu(\tau)$ is the unit strength of the fibronectin binding. I make the simplest assumption, that all cells have the same value of μ. When a cell occupies a pixel (i, j) previously occupied by medium, the energy decreases by $\mu C_f(i, j)$. In the reverse process, the energy increases by $\mu C_f(i, j)$, implying that cells prefer to bind to fibronectin rather than to the medium.

3.2.3 Conceptual Model and Computer Simulation

Based on the experimental results I described in the above section, I developed the following model for precartilage mesenchymal condensation in limb chondrogenesis: mesenchymal cells produce non-diffusing fibronectin and deposit it onto the substrate. Cells execute a random walk biased by their binding more strongly to fibronectin than to the substrate (haptotaxis). Fibronectin-cell-surface binding upregulates the production of cell-cell adhesion molecules such as N-cadherin, increasing cells' adhesiveness to each other. The pattern continues to evolve until the cell-cell and cell-ECM binding is so strong that the cells 'freeze' (*i.e.* attach

irreversibly to the substrate or fibronectin). The properties of the cells change during the experiment (Figure 16). According to experimental measurements, the fibronectin production rate increases five-fold six hours after plating [109]. In order to represent a simplified model of the genetic regulation within a cell, I assign each cell an internal phase parameter, with cells producing fibronectin during half of their 24-hour phase cycle, randomly initialized. The phase parameter distinguishes intracellular from intercellular and extracellular regulation of cell behavior. The actual fibronectin production is the product of the fibronectin production rate and the cell's internal phase parameter. N-cadherin expression increases 12 hours after plating [114]. Figure 16 (B) describes the changes of cell adhesiveness during condensation. $J_{11}(\sigma)$ represents the cell adhesiveness, which depends on the number of adhesion molecules on the cell membrane. The more adhesion molecules, the more adhesive the cell is and the smaller $J_{11}(\sigma)$. I made the simplest assumption for the upregulation of cell adhesion by cell-fibronectin binding: the increase of each cell's number of adhesion molecules is proportional to the fibronectin the cell has seen, reflected in a decreasing $J_{11}(\sigma)$. Visible condensation occurs 18 to 36 hours after plating [109] (the shaded area in Figure 16 (B)).

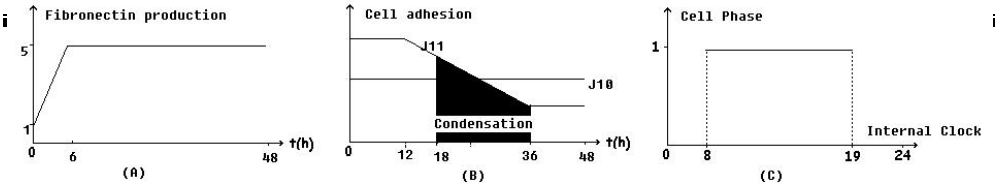

Figure 16. Micromass Condensation Model. (A) The fibronectin production of each cell. (B) The dependence of each cell's adhesiveness on the amount of fibronectin it has contacted. The shading shows the period of condensation. In the simulation I varies the slope by varying the initial J_{11} while fixing the final J_{11}. (C) Example of the fibronectin-producing phase of a cell: the sample cell produces fibronectin between 8 and 19 hours.

3.2.4 Results

Precartilage mesenchymal condensations at medium and low culture densities show very different morphologies (Figure 17). When the density is relatively high (Figure 17 (A)), the condensations consist of both spots and finger-like stripes, while spots form in low-density condensations (Figure 17 (B)). In Figure 17 (C), the cell concentration is 35%, while in Figure 17 (D), the concentration is about 15%. Figures 17 (D, E) show the fibronectin distribution underneath the cells. The key simulation parameters are: J_{11}=6.5 and μ=0.25.

If I consider the cells to be two-dimensional discs, the simulated densities seem much lower than in the experiments (effectively confluent for 10^7 cells/ml as determined from the initial cell-suspension cell counts). However, three arguments suggest that the experimental cell density on the bottom of the dish is much lower than the number counted in suspension

would suggest. In the micromass experiment, massive cell death occurs among cells not in condensations [121], which decreases the effective cell density. Adding and changing the medium also causes cell loss. Real cells can stretch vertically and crawl over each other. Three-dimensional simulations show that a stripe-and-spot pattern develops for initial densities between 50% and 100% (Figure 18). These densities agree with the experimental densities, confirming the sufficiency of the mechanisms in the simulation.

The pattern is robust: For each density, the same type of patterns occurs with minor modifications, even for different values of μ and J_{11} (Figure 19). μ represents the strength of the cell-ECM binding. The smaller μ, the coarser the pattern. The bigger μ, the smaller the clusters and the shorter the wavelength. μ's effect on the pattern is the same as changing the fibronectin production rate. Faster fibronectin production corresponds to bigger μ. J_{11} represents the strength of cell-cell adhesion. As the final J_{11} is fixed, the bigger the initial J_{11}, the stronger the upregulation of expression of cell-adhesion molecules and the coarser the pattern.

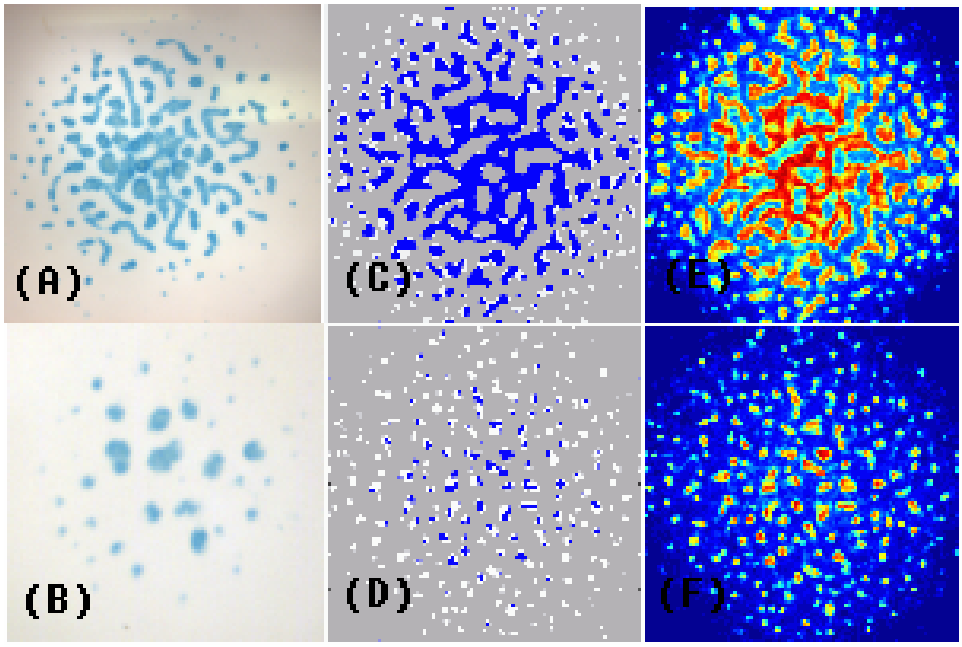

Figure 17. Comparison of Experimental and 2D Simulated Micromass Cell Culture. Experimental images of (A) medium (1.75×10^7 cells/ml) and (B) low (1.5×10^7 cells/ml) density condensations. The white background represents both low levels of fibronectin and empty space. In agreement with the experiment, (C) the simulated cells form stripes and spots at medium densities (35%) and (D) only spots at low densities (15%). (E), (F) The distribution of fibronectin in the simulation: the red fibronectin peaks co-localize with the cell clusters. Parameters: J_{11}=6.5 and μ=0.25.

The cell density is the most significant parameter controlling the pattern. At low density, spots always form, while at high and medium densities, a mixture of spots and stripes forms, usually with stripes in the middle surrounded by spots. Usually the experimental protocol produces an initial distribution of cells with higher density in the middle. I simulated this nonuniform case using a Gaussian distribution of cells with maximum density at the center. This nonuniform distribution produced bigger and more continuous condensations in the middle, because the higher local density reduced the cell motility. Since the culture medium is serum free, cells do not divide; thus the model does not include cell division.

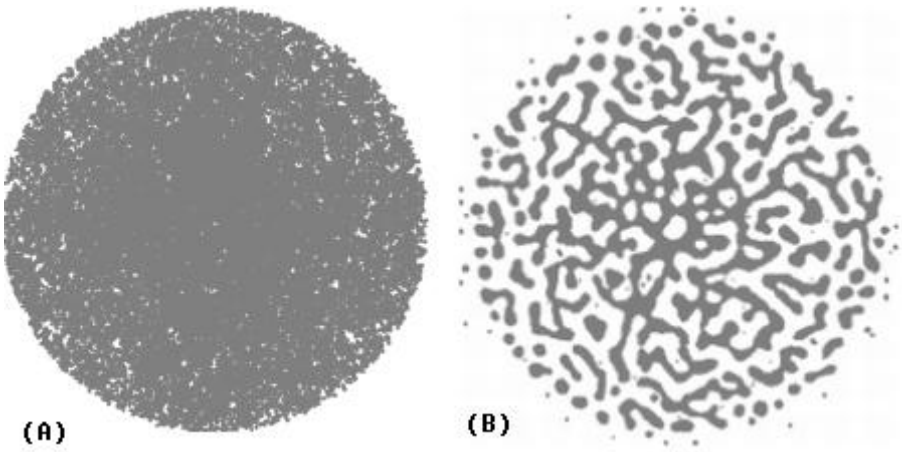

Figure 18. 3D simulation of micromass condensation. (A) Initial distribution of 19000 cells, equal to 90% spatial occupancy. (B) Configuration after 2400 MCS. The 3D simulation has room for two to three cell layers in the vertical dimension, allowing cells to crawl on top of each other during patterning.

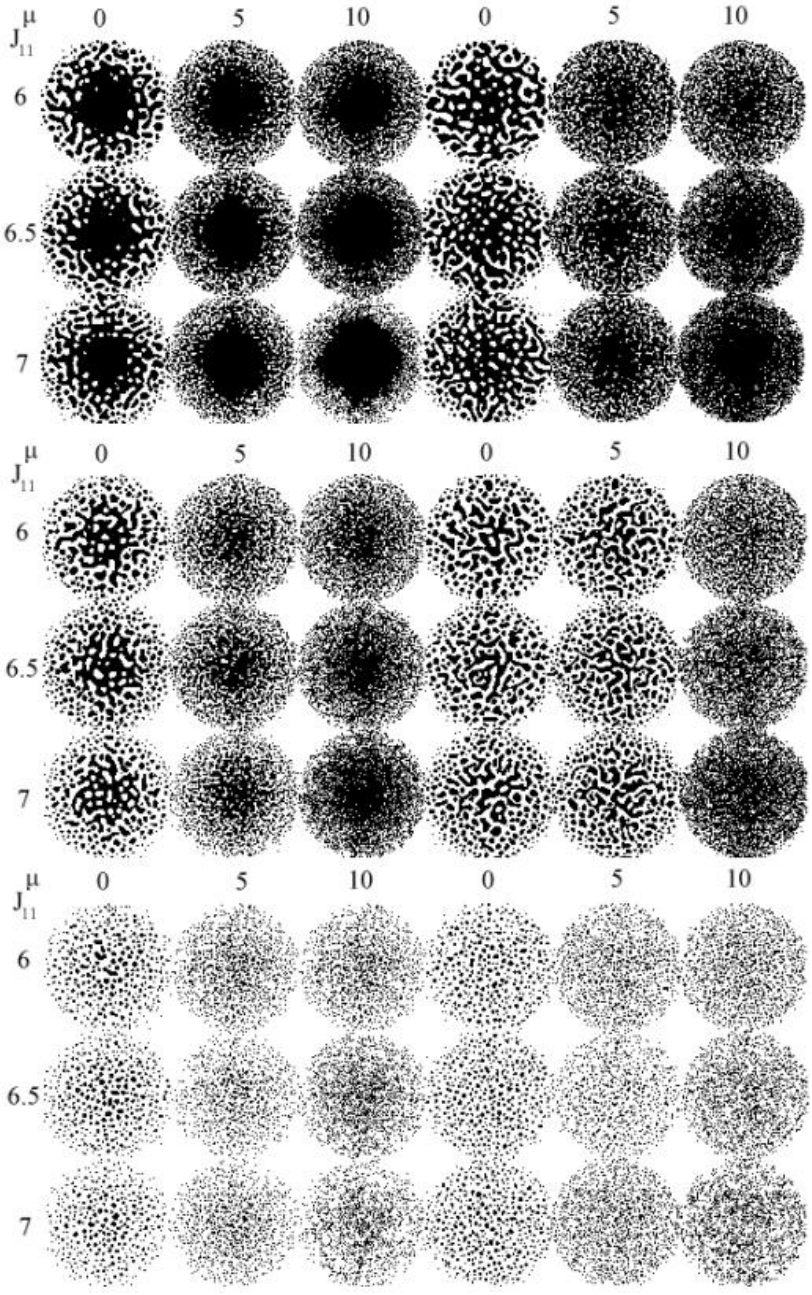

Figure 19. 2D Simulations of micromass condensation with different combinations of parameters: high cell density (upper), medium cell density (center) and low cell density (lower). The first three columns on the left show simulations with a linear radial gradient in the initial cell distribution, and the last three columns on the right show simulations with a uniform initial cell distribution. The rows group simulations with the same initial J_{11}, and the columns group those with the same μ.

Spot-stripe selection depends on the relative rates of cluster coalescence and rounding and the total time before the pattern freezes. Coalescence tends to produce elongated stripe-like clusters, while rounding produces spot-like clusters. The higher the cell density, the higher the rate of cluster coalescence. High density also lowers the cell mobility, slowing rounding, and reduces the time before cells bind irreversibly to the substrate, reducing the total amount of rounding. Thus high densities form stripes. When the cell density is low, coalescence is less frequent and cells have higher mobility and more time to diffuse before freezing, resulting in spots.

The choice of period and duration of fibronectin production does not have a critical effect on the final pattern (Figure 20). Initially unsynchronized clocks and equal production and non-production phases are the simplest assumptions, but are not essential. Linking the phase parameter to the cell cycle is an interesting topic for further investigation [122].

I also tested the temperature dependence of my model (Figure 21). Lower temperatures correspond to lower cell motility and lead to finer-textured patterns at all cell densities.

I restricted my study to qualitative descriptions of the parameter dependence

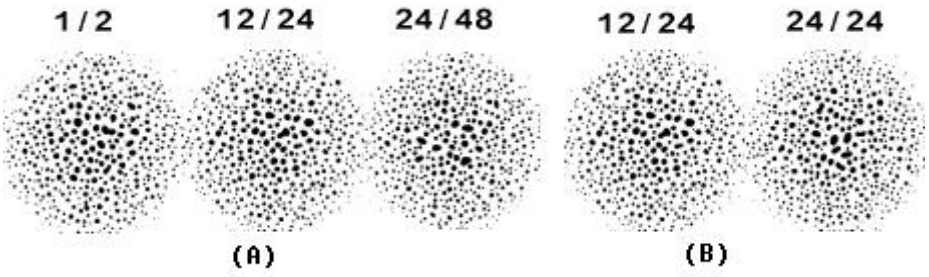

Figure 20. 2D simulated micromass condensation. (A) Comparison of final condensation patterns with different fibronectin production-cycle lengths after 24000 MCS: 2, 24 and 48 hours. In each case, the cells produce fibronectin 50% of the time. The middle image in (A) and the left image in (B) are identical. (B) Comparison of final condensation patterns with different periods of fibronectin production during a cycle: 12 hours out of a 24-hour cycle and 24 hours out of a 24-hour cycle.

of the patterns for a number of reasons. I had a limited number of experimental patterns for comparison and in these patterns I knew whether the parameters increased or decreased, but not their exact values. Thus a detailed quantitative comparison will require further, more accurate experiments. Second, characterizing inhomogeneous spot-stripe patterns mathematically is notoriously difficult. While the human eye and brain immediately pick out features like mean spot size, spotness *vs.* stripeness, tortuosity and degree of cluster overlap, standard pattern-analysis techniques like Fourier transforms, periodograms, particle-size distributions and wavelets cannot do so reliably. None of these methods works well for both spots and stripes and all require manual identification of the spot-stripe boundary. For example, Miura *et al.* [123] proposed a metric using the mean distance between stripes to characterize patterns, but the metric does not give consistent results for patterns containing both stripes and spots.

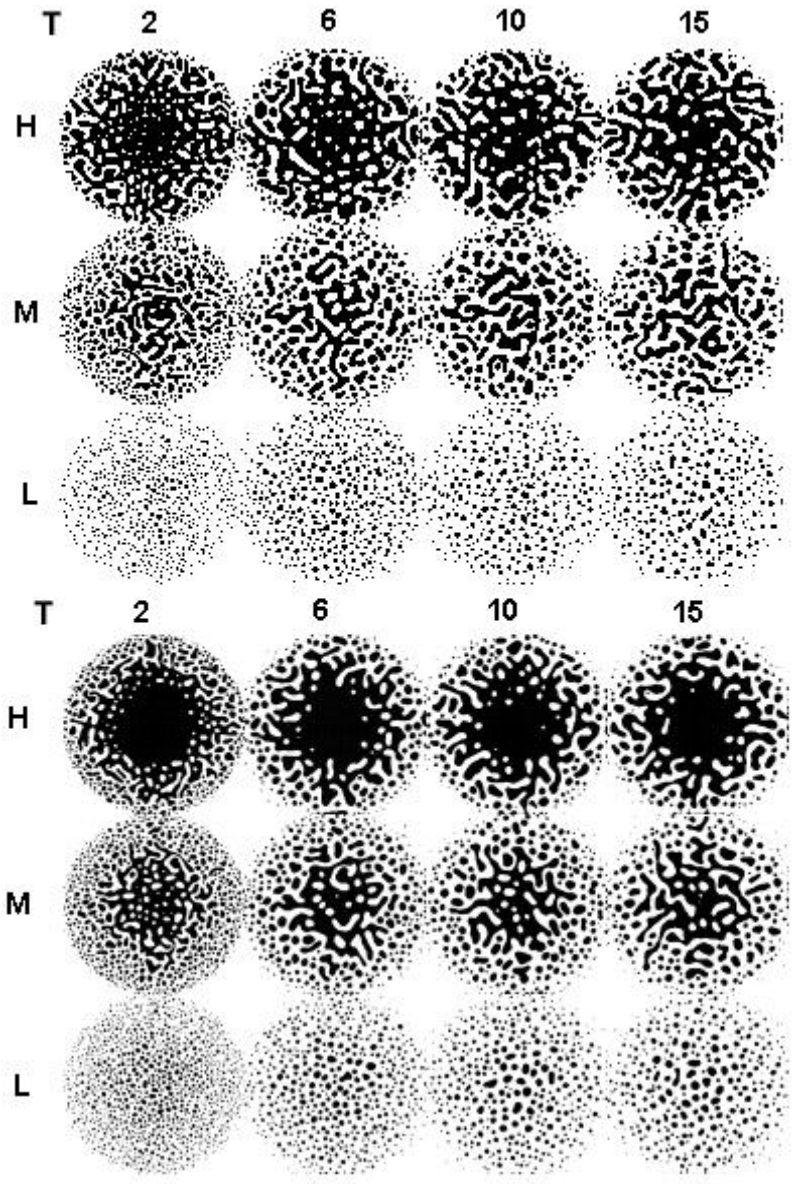

Figure 21. 2D simulated micromass condensation. The temperature dependence of the simulated condensation patterns. The top three rows show simulations with uniform initial cell distributions. The bottom three rows show simulations with a gradient in the initial cell distribution with highest density at the center. H: High density=$2.0x10^7$cells/ml, M: Medium density=$1.75x10^7$cells/ml, L: Low density=$1.5x10^7$cells/ml, T: Temperature=2, 6, 10, 15

3.2.5 Discussion

My investigation of generic mechanisms in limb chondrogenesis has revealed a novel mechanism for pattern formation. My simulations show that spot and stripe patterns similar to those observed experimentally can result from a density-dependent mechanism, different from known pattern-forming mechanisms like the Turing Mechanism where patterns emerge as a result of the diffusion and reaction of two chemicals [124]. In my model, the instability arises from positive feedback in fibronectin production and accumulation. Cells tend to stay longer in regions with more fibronectin, and hence become both more adhesive to each other and deposit even more fibronectin in those regions, further increasing the time the cells spend there. The wavelength grows continuously until cells stick and clusters cannot coalesce any more. Thus, my mechanism has no intrinsic wavelength. The duration and rate of coarsening together determine the final wavelength. Surface tension rounds clusters to reduce surface area while coalescence tends to elongate them. High densities of cells lower the cells' motility, leading to more stripe-like patterns, while at low densities cells move fast enough for the surface-energy-driven rounding of clusters to dominate. Higher temperatures lead to longer coarsening and hence coarser and smoother patterns. The instability has four time scales: the time till freezing, the rate of cluster coalescence, the rate of cluster rounding and the

rate of cluster growth. In contrast, the wavelength of a Turing Pattern depends on the diffusion constants of the morphogens and is independent of the cell density. My simulation involves surface-adhesion molecules and extracellular matrix, about which I know a fair amount. Most of the simulation parameters are experimentally measurable. For instance, Atomic Force Microscopy can directly measure the cell adhesiveness and cell-ECM binding strength. The cell size sets the spatial scale, while measuring the diffusion constant establishes the time scale. I can also refine the parameter diagrams as additional data become available.

So what makes the shape of a humerus different from the shape of a digit? My simulation demonstrates that the interplay between generic properties like cell density (number), cell-cell adhesion and cell-ECM binding, all of which are genetically regulated, can give rise to condensations of different sizes and shapes. How applicable is this result to condensation *in vivo*? Cell-sorting experiments suggest the presence of a gradient of N-cadherin expression along the PD axis of the limb, with more N-cadherin at the distal end [125, 126]. My model predicts that the increased N-cadherin distally should result in smaller, rounder condensations, as experiments indeed observe. This gradient overlaps with the gradient of *Hox* gene expression [54, 55, 127-129]. Manipulation of *Hoxa* genes [119] alters both cell adhesiveness and bone shape, again, agreeing with my model. *In vitro*

experiments have shown that the ECM environment also influences chondrogenic pattern formation [118].

Micromass condensation is much simpler than skeletal patterning *in vivo*. To study limb chondrogenesis *in vivo*, I need to account for cell proliferation and cell movement. For example, limb mesenchymal cells chemotax to FGFs which the AER secrets in intact limb [130]. Different models make different assumptions concerning the cell proliferation pattern, which affects both the skeletal pattern and the shape of the limb bud (as I will discuss in the Appendix). I could simulate these mechanisms by letting cells divide and execute random walks biased not only by local cell-ECM binding, but also by chemotaxis in the PD direction to diffusing FGFs from the AER.

CHAPTER

FOUR

EARLY CHICK GASTRULATION

4.1 Overview: Gastrulation—From Cells to Embryo

"It is not birth, marriage, or death, but gastrulation, which is truly the most important time in your life."

Lewis Wolpert (1986)

I now turn to a very different type of morphogenesis, the formation of the primitive streak during chick gastrulation. Unlike mesenchymal condensation, primitive-streak formation involves large-scale, coordinated movements throughout the embryo. To study cell movement during chick primitive-streak initiation, I randomly labeled epiblast cells in Stage XI-XII chick blastoderm using Green-Florescent-Protein (*GFP*) electroporation and tracked the cell movements. I also checked cell orientation and shape along the primitive streak. I observed no obvious, large-scale orientation, but a gradient of cell size along the streak, indicating that cells at the anterior tip of the streak may elongate in the DV direction and ingress earlier than cells at the posterior of the streak. To investigate regulation of cell movement, I

manipulated the *Fgf* and *Wnt* signaling pathways using dominant negative FGFR1 and Wnt11. The pathways play different roles during primitive-streak initiation. My electroporation technique costs much less than developing a transgenic line and enables study and manipulation of pre-gastrulation morphogenesis, which retroviral techniques do not. It is also useful for studying later developmental events like neural-crest cell differentiation and migration and nervous-system patterning, since the embryos survive for extended periods and the cells remain transformed as long as the embryos survive.

Gastrulation is marvelous. During gastrulation, cell movements massively reorganize the embryo from a simple hollow ball of cells in an epithelial monolayer, usually called the *blastula*, into a multi-layered organism. The primary germ layers (*endoderm*, *mesoderm*, and *ectoderm*) form and organize in their proper locations during gastrulation. Endoderm, the most internal germ layer, forms the lining of the gut and other internal organs. Ectoderm, the most exterior germ layer, forms skin, the brain, the nervous system, and other external tissues. Mesoderm, the middle germ layer, forms muscle, the skeleton, and the vasculature. Although the details of gastrulation differ between various groups of animals, the cellular mechanisms involved in gastrulation are common to all animals and each type of gastrulation needs to coordinate these mechanisms. See [131] for a

recent and comprehensive review of gastrulation.

Gastrulation involves changes in cell motility, cell shape, and cell adhesion. Many of the cells at or near the surface of the embryo move to new, more interior locations. The major types of cell movement during gastrulation are *invagination* and *evagination*, *ingression*, *involution*, *epiboly*, *intercalation* and *convergent extension* (Figure 22). The dramatic shape changes of the embryo during gastrulation result from a combination of these different types of cell movement.

Invagination and Evagination: an epithelial sheet of cells bends inward to form a pocket. If the apical side of the epithelium forms the *lumen* (central empty space) of the groove, then the movement is *invagination*. If the basal surface forms the lumen then the movement is *evagination*. An example is sea-urchin gastrulation.

Ingression: individual cells leave an epithelial sheet to become freely migrating mesenchyme cells, *e.g.*, neural-crest cells. During ingression, when cells receive certain extracellular cues, they alter their cellular architecture, subcellular control of motility, and relative adhesiveness to their neighbors. An example is early chick gastrulation.

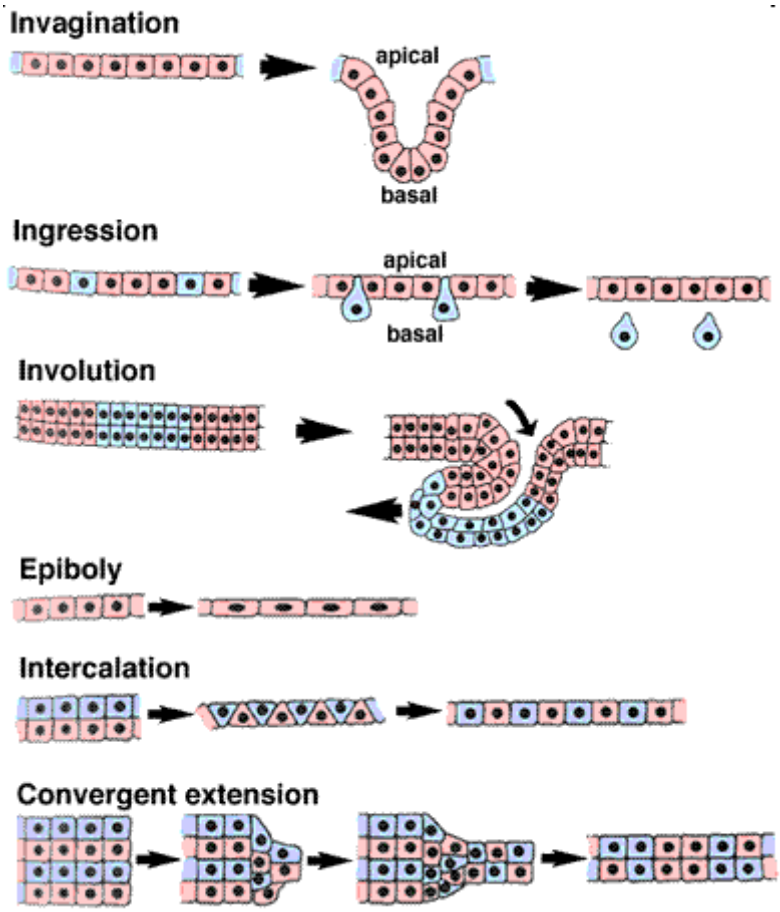

Figure 22. Six types of epithelial morphogenesis. Invagination: an epithelial sheet of cells bends inward. Ingression: individual cells leave an epithelial sheet and become freely-migrating mesenchyme cells. Involution: an epithelial sheet rolls inward to form an underlying layer. Epiboly: a sheet of cells spreads by thinning. Intercalation: rows of cells move between one another, creating an array of cells that is longer (in one or two dimensions) but thinner. Convergent Extension: rows of cells intercalate, but the intercalation is highly directional. The direction of cell elongation is often perpendicular to the direction of tissue elongation, the opposite of normal epiboly. From http://worms.zoology.wisc.edu/frogs/gast/gast_morph.html.

Involution: an epithelial sheet rolls inward to form an underlying layer via bulk movement of tissue. As material moves in from the edges of the sheet, material originally at the sites of ingression moves transversely underneath the exterior tissue.

Epiboly: a sheet of cells spreads by thinning in the apical-basal direction while its surface area increases in the other two directions.

Intercalation: rows of cells move between one another, creating an array of cells that is longer (in one or two dimensions) but thinner. The overall change in shape of the tissue results from cell rearrangement. Intercalation is a powerful way for a tissue sheet to expand. A specific form of intercalation, **Convergent Extension**, plays a key role during the formation of the primary body axis in amphibians, where convergent extension of the marginal zone creates the AP axis.

4.2 Early Chick Gastrulation: Primitive-Streak Initiation

4.2.1 Introduction

The pre-gastrulation chick embryo is a disk of cells (*blastoderm*) riding over the yolk, containing about 20,000 cells within the *epiblast* (Figure 23). The *subgerminal* space opens under the blastoderm. The blastula forms as

intercellular junctions break down and some cells ingress from the lower surface of the blastoderm to form the *hypoblast* (Figure 24). Cells in both the hypoblast and the epiblast continue to divide. *Endoblast* cells then replace the hypoblast, beginning at the posterior end of the embryo and proceeding in the anterior direction. In the epiblast, after 3-4 hours of incubation, a sickle-shaped group of cells at the posterior margin of the *area pellucida* (the clear and pale-staining center area of the blastoderm) and *area opaca* (a deeper-staining area peripheral to the *area pellucida*) thickens in the DV direction. They push anteriorly at the midline, and cells from the margins of the embryo move towards the center posteriorly. This cell 'circulation' creates an elongating thickening of cells along the AP midline. After 12 hours of incubation, this *primitive streak* structure is visible and has sharp boundaries. Gastrulation generates the three germ layers. The definitive endoderm and the mesoderm migrate from the epiblast to the interior of the embryo. These cells originate at the margins of the primitive streak. As cells move into the primitive streak, they break away from their neighbors and migrate as individual cells inside the embryo (Figure 25 adapted from [28]). For Scanning Electron Microscopy pictures of the detailed morphology of early chick gastrulation, see [132].

During early chick gastrulation, mesoderm and endoderm cells ingress at the primitive streak. The streak initiates between Eyal-Giladi & Kochav Stage X

and HH stage 2 (Figure 26 adapted from [135]). At stage X the embryo is essentially one layer thick and contains only epiblast, except for small islands of hypoblast at its ventral surface. At stage XII, the hypoblast has formed a sheet that covers half of the *area pellucida* and, by stage XIII, covers the entire lower surface of the blastocoel. The primitive streak appears at HH stage 2, when the endoblast starts to displace the hypoblast anteriorly [133, 134].

Fate mapping shows that the initial primitive streak mainly draws cells from the epiblast cells overlaying *Koller's Sickle* (*KS*), a sickle-shaped domain of multiple layers of cells in the Posterior Marginal Zone (*PMZ*) [135]. These cells express many genes important for later development, *e.g.*, signaling molecules of the FGF and Transforming Growth Factor β (*TGF-β*) families as well as cell-type-specific transcription factors [136-138]. The expression domains of most of these genes transform from a sickle via an intermediate triangle into an elongated streak stretching along the posterior-anterior midline, coincident with the formation of the primitive streak. The cells change their gene expression, as they move in response to signals from elsewhere in the embryo [139]. Early time-lapse observations and analysis suggested that primitive-streak initiation involves large-scale cell movement [140]. Recent DiI labeling experiments have shown that cells at different positions in the sickle transform into cells at different AP positions along the

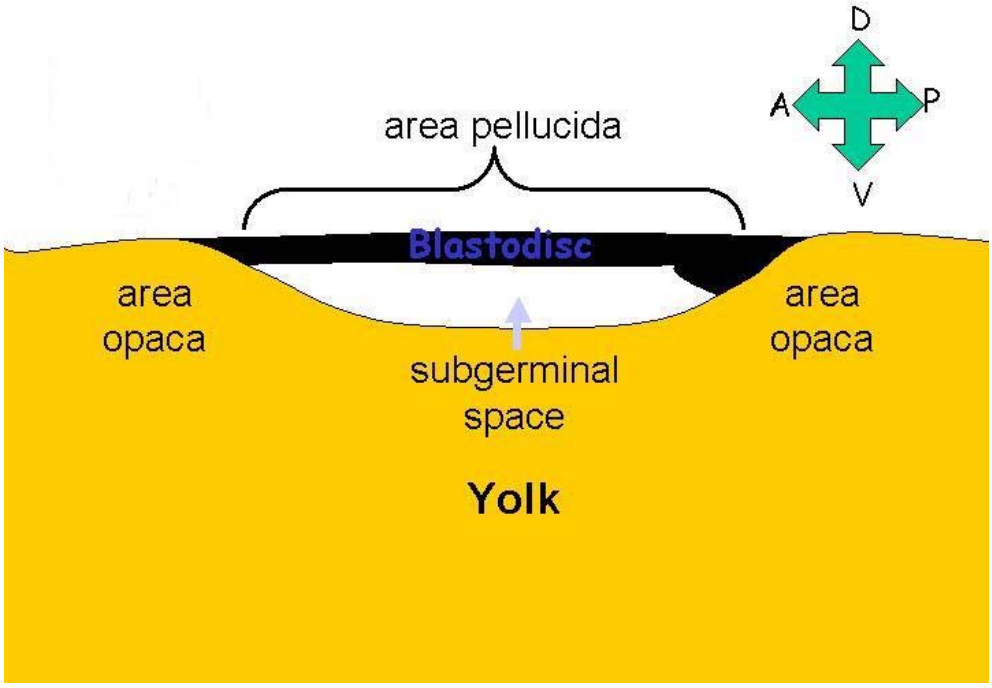

Figure 23. Relative positions of the *area pellucida*, *area opaca*, blastodisc and subgerminal space before chick gastrulation starts. The thickened posterior end of the *area pellucida* is known as *Koller's Sickle* (*KS*) or the *Posterior Marginal Zone* (*PMZ*). Adapted from http:// www.academic.regis.edu/mghedott/BL412/devel10.ppt.

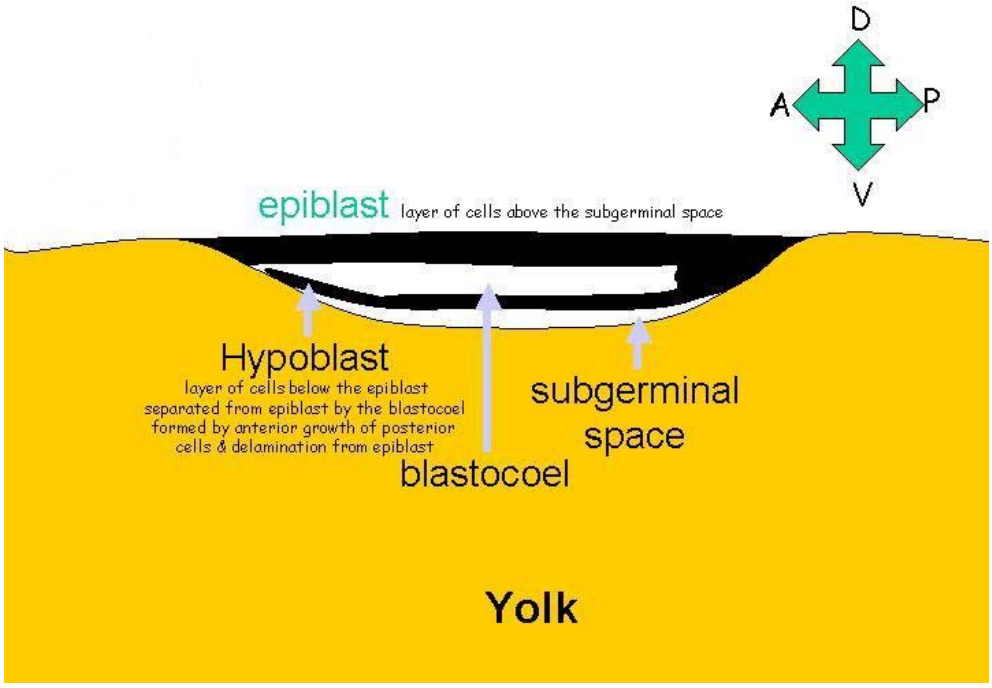

Figure 24. Relative positions of epiblast, hypoblast, blastocoel and subgerminal space during early chick gastrulation. Adapted from http:// www.academic.regis.edu/mghedott/BL412/devel10.ppt.

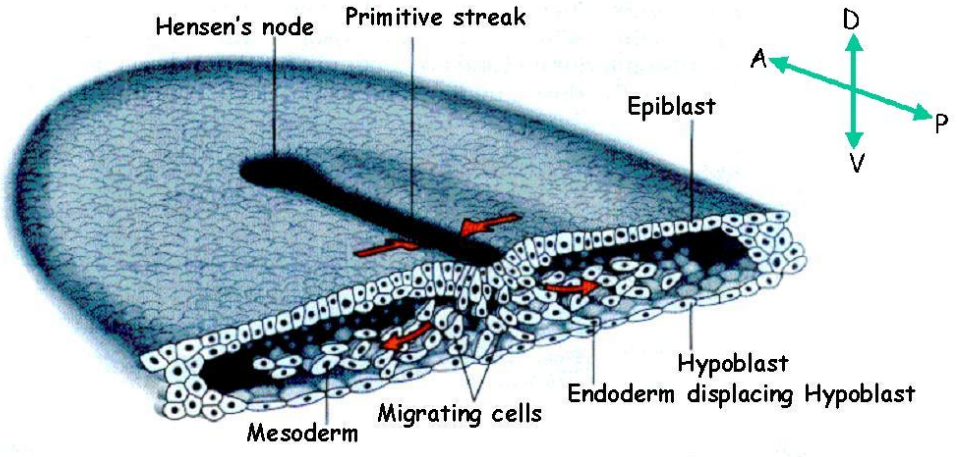

Figure 25. Formation of the primitive streak, the mesoderm and the endoderm. Adapted from [28].

streak [141]. Primitive-streak initiation requires nodal signaling, and experiments have shown that the hypoblast may secrete a nodal antagonist to prevent ectopic streak formation [142]. Mis-expression of the TGF-β family member Vg1, which the PMZ normally expresses, leads to ectopic streak formation through the *Wnt* pathway [143-145].

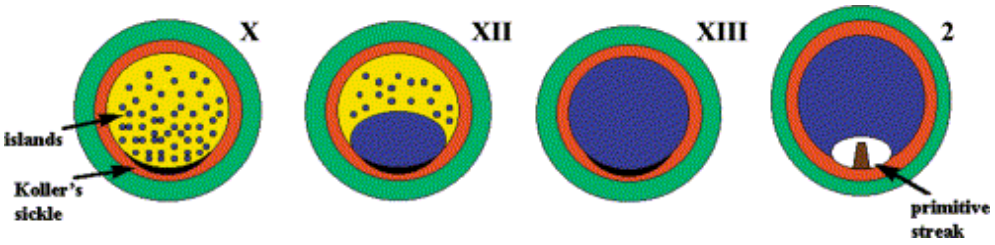

Figure 26. Hypoblast and endoblast in early chick embryos. Schematic of early stages of development. At stage X the embryo is essentially a monolayer, except for small islands of hypoblast (blue) on its ventral surface. At stage XII, the hypoblast has formed a sheet that covers half of the *area pellucida* and, by stage XIII, covers the entire lower surface of the blastocoel. The primitive streak (brown) appears at stage 2, when the endoblast (white) has started to displace the hypoblast anteriorly. Green, *area opaca*; red, marginal zone; yellow, *area pellucida* epiblast. Adapted from [135].

Cells divide rapidly during primitive-streak initiation [146]. LacZ-expressing-retrovirus transfection experiments suggested that successive oriented cell divisions drive primitive-streak initiation and extension (Figure 27 adapted from [147]). In this scenario, cells in the center of the sickle repeatedly divide with their mitotic spindles aligned along the AP axis of the embryo, forming strings of cells aligned in the AP direction. At least three other models attempt to explain primitive-streak initiation. The first model hypothesizes that epiblast cells migrate from

lateral regions towards the midline during ingression. The second model assumes that HNK-1-positive cells, which are dispersed within the epiblast, individually ingress into the blastocoel and migrate to the posterior midline to form the initial primitive streak. The third model assumes that posterior-lateral epiblast cells sequentially migrate to the midline and then move anteriorly along the midline. I could test these models by comparing the cell movement observed in experiments to the cell movement the three models predict (See Section 4.2.4).

Cui *et al*. (to appear, *Developmental Biology*) analyzed the velocity fields of cell movement in the epiblast during primitive-streak initiation, using time-lapse bright-field microscopy. They labeled several groups of cells in the epiblast with DiI and tracked their movements and fates. The cells moved in two counter-rotating vortices meeting at the future site of the primitive streak, with the movement along the midline in the posterior-anterior direction. The pattern resembles stirred viscous flow. Cycling/dividing cells initially distribute randomly in the epiblast but later confine to the boundary between the *area pellucida* and the *area opaca*. Culturing the embryos in the DNA-polymerase-inhibitor aphidicolin to block cells in their S phase during streak progression caused severe defects in later gastrulation but did not inhibit primitive-streak initiation, indicating that cell division is necessary for primitive-streak extension, but not for

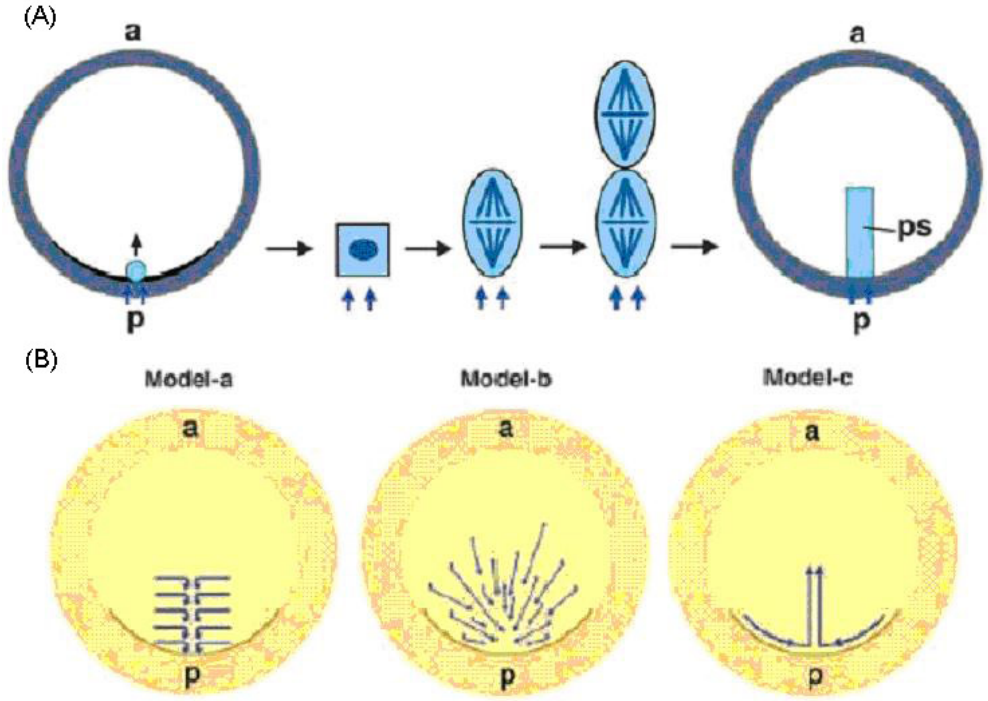

Figure 27. Schematic of different models of primitive-streak initiation. (A) How directed cell division could drive primitive-streak initiation along the AP axis. The blue spot in the left diagram marks the primitive-streak precursor area at prestreak stages (XXII), while the blue bar in the right diagram represents the HH-stage-3 primitive streak. In between, cell division of precursor cells is polarized. Blue arrows, inductive signal; PS: primitive streak; AP: anterior-posterior axis. (B) Three distinct models of primitive-streak initiation. Blue lines indicate migration or movement of primitive-streak precursors. (a) Epiblast cells migrate from lateral regions towards the midline during ingression. (b) HNK-1-positive cells, which are dispersed within the epiblast, individually ingress into the blastocoel and migrate to the posterior midline to form the initial primitive streak. (c) Posterior-lateral epiblast cells sequentially migrate to the midline and then move anteriorly along the midline. Adapted from [147].

primitive-streak initiation. This observation seems to rule out the oriented-cell-division model of streak formation.

To study more cell movement during chick primitive-streak initiation in more detail, I randomly labeled epiblast cells in Stage XI-XII chick blastoderm using GFP electroporation and monitored cell movements by time-lapse microscopy. I also fixed HH stage 3 embryos and stained for F-actin to check cell orientation and shape along the primitive streak. To investigate regulation of cell movement, I interfered with the *Fgf* and *Wnt* signaling pathways using dominant negative FGFR1 and dominant negative Wnt11 electroporation.

4.2.2 Materials and Methods

4.2.2.1 Embryo Culturing and Electroporation

I incubated fertilized white leghorn eggs (Rhode Island Red, Winter Farm, Thirplow, Herts, UK) for 1-6 hours at 38^{o}C in a humid incubator before culturing. I cultured embryos using the EC culture technique [148]. I dropped a total of 0.5µl DNA (from Midi Prep) plasmid from Clonetech dissolved in simple saline onto each embryo's ventral side, then removed the embryos from their agar plates and put them with their ventral sides

down between two electrodes 2 mm apart and pre-wetted with simple saline solution. I used a home-made "electroporator" [149] to apply a single square pulse of 10-15 V and 50 ms duration (with the field pointing from dorsal to ventral) to the embryos, then put them back onto the agar plates and incubated them at 37^{o}C. After 3 to 5 hours, cells started displaying strong florescence, while the vectors with inserted exotic DNA fragments took as long as 9 hours to express. I transferred the embryos to a custom-made, air-heated microscope incubation chamber, kept at 38^{o}C and 90% humidity, and imaged for the next 20 hours.

4.2.2.2 Constructs

Reference [150] describes the dnFGFR1-GFP construct in detail. I constructed a dnWnt11 insert from Xenopus Wnt11 (deleting the c-terminal tail according to the scheme described for Wnt8) [151, 152] and cloned it into the pcDNA 3.1 expression vector. The cells failed to secrete a GFP-tagged Wnt11 protein, though they expressed the plasmid at high levels. Therefore, I mixed the dnWnt11 plasmid with the pEGFP-N1 expression vector and transfected the cells with the mixture so that cells picked up and expressed both plasmids.

4.2.2.3 Imaging and Analysis

I took bright-field and fluorescence images every 2 or 3 minutes with a

Hamamatsu cooled CCD camera, as in reference [150]. I calculated cell movements by accumulating information in successive time-lapse images using routines Dr. Cornelis Weijer's group wrote in the Optimas VI (Media Cybernetics) macro language.

4.2.2.4 Embryo Fixation and Staining

I fixed embryos at HH stage 2-3 in formaldehyde-triton containing rhodamine phalloidin, then gave them two extended washes with PBS before examining them with a Leica confocal microscope. I took optical sections at approximately 4μm vertical intervals and displayed them in a maximum-intensity projection.

4.2.3 Results

4.2.3.1 Cell Movement during Primitive-Streak Initiation

Early cinematographic experiments described a "Doppelwirbel" or "polonaise" movement accompanying streak formation [140]: cells from both sides of the PMZ moved towards the center of the marginal zone where they joined up to extend anteriorly. Extensive fate mapping clarified the fate of the cells in the epiblast [153].

I labeled a mosaic of epiblast cells in the blastoderm of HH stage XI-XII

chick by GFP electroporation. I incubated the transfected embryos using the EC culture method [154] and recorded their time-lapse development on an inverted Zeiss microscope during the following 20 hours. I collected both bright-field (Figure 28) and fluorescence images (Figure 29) at 3 minute intervals. The experiments showed primitive-streak initiation and the two counter-rotating vortices of cell movement in the epiblast, which merged at the site of the future streak (Figure 30). Two areas of relatively little movement that did not coincide with any particular morphological structures formed the centers of both vortices. Speeds of cell movement varied between 0μm/minute and 10μm/minute, with the highest speeds at the outer periphery of the vortices. The flows began before the streak appeared as an optically dense structure. Initially the cells displaced outward, more or less isotropically in all directions, due to cell division, which increased the surface area of the epiblast. However, within an hour the movement of the labeled cells suddenly changed to produce the counter-rotating flows. Tracking the cells over longer periods of time revealed relatively little displacement or mixing between adjacent cells. Cells tend to stay together during migration. Cells did not appear to speed up or slow down (Figure 31).

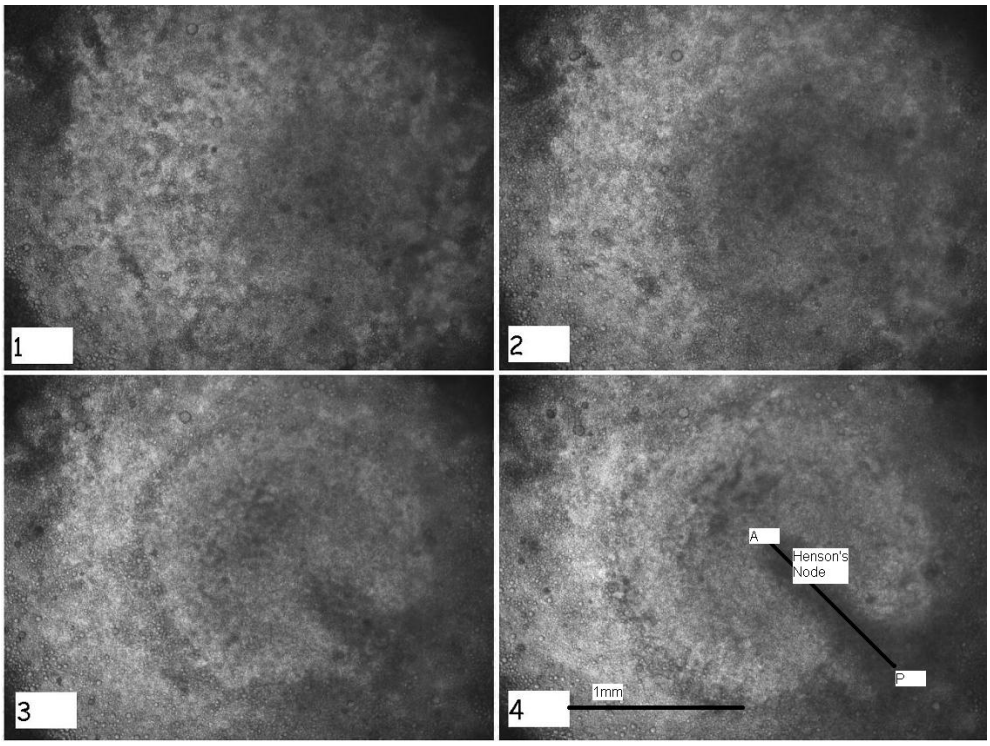

Figure 28. Time-lapse bright-field images of chick embryos in EC culture. The interval between frames is about 5 hrs. Bar=1mm. A: Anterior. P: Posterior.

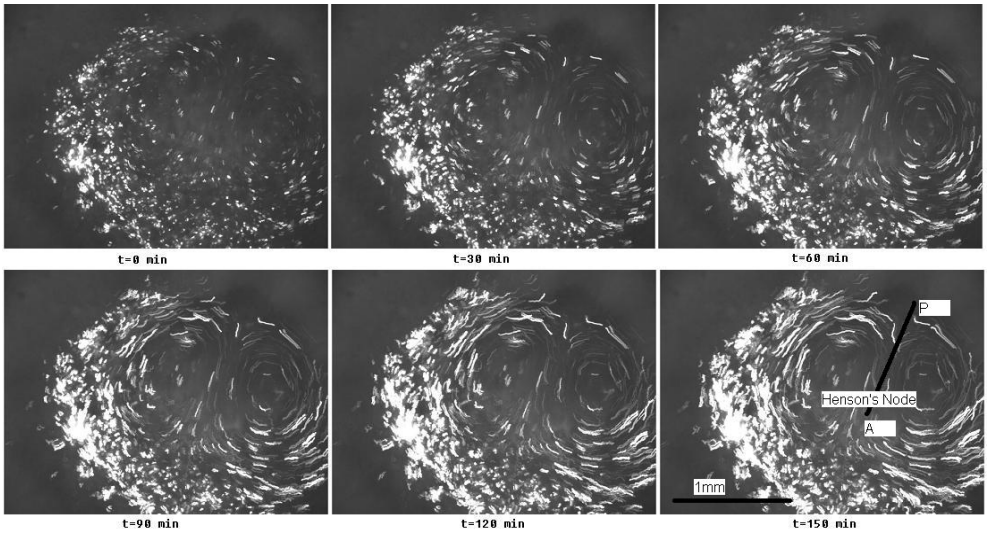

Figure 29. Time-lapse fluorescent images of GFP-transfected chick embryos in EC culture. I randomly labeled cells in the chick blastoderm with GFP. Each dot in the picture represents 1-10 cells. I calculated the tracks by processing successive images using Optimas. Bar=1mm. A: Anterior. P: Posterior.

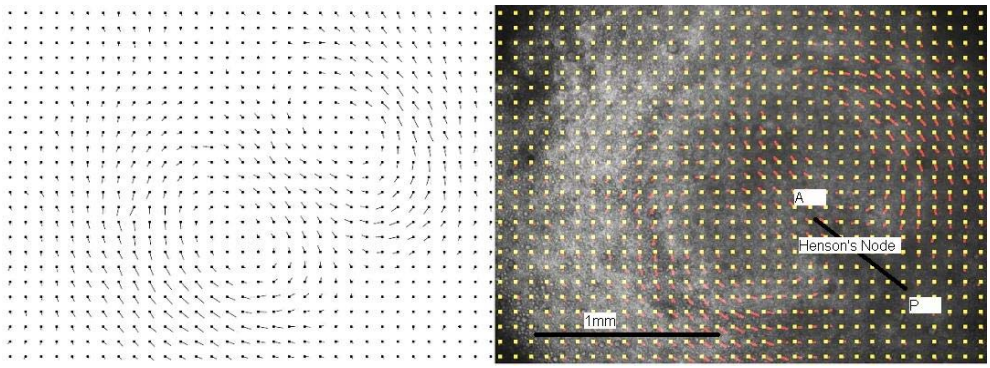

Figure 30. Vector field of cell velocities during primitive-streak formation calculated from the bright-field images. Left: vector field only. Right: the merged image of the vector field and the brightfield image. Yellow dots indicate the origin of the vector and the red bar indicates the direction of the flow. Vector length is proportional to the speed. Bar=1mm. A: Anterior. P: Posterior.

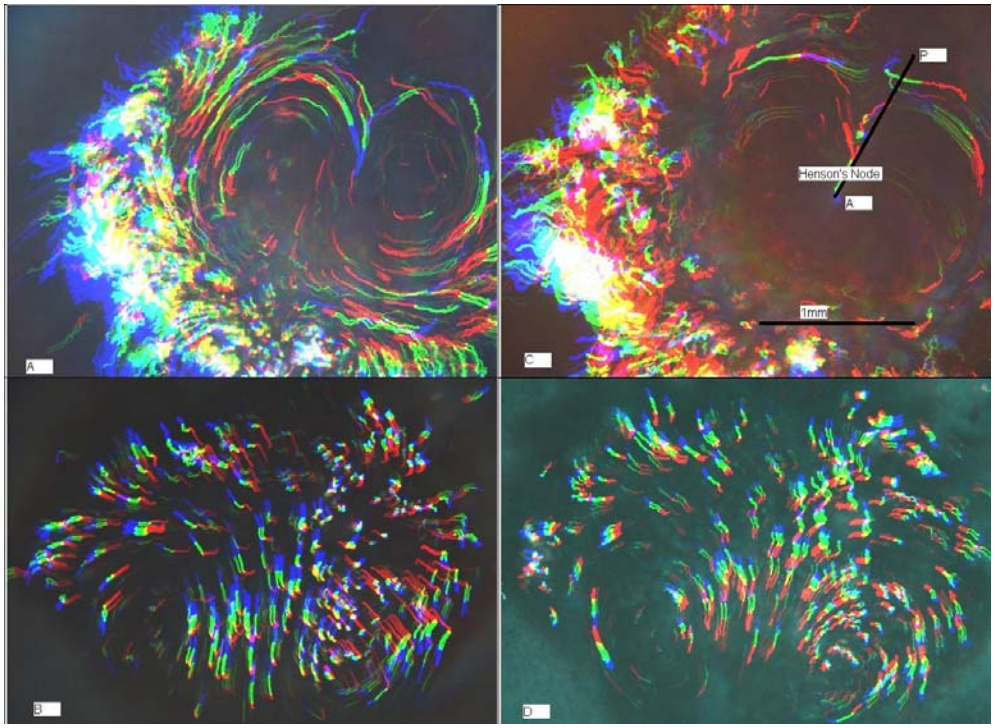

Figure 31. Tracks of GFP-labeled cells during streak formation. The movements over periods of three successive hours are colored red, green and blue respectively. (A) and (B) show the first 9 hours of the experiments and (C) and (D) the second 9 hours. (A) and (C) and (B) and (D) are two separate experiments. Scale bar is 1mm.

4.2.3.2 Cell Orientation and Shape Change during Primitive-Streak Initiation

As I mentioned, experiments which labeled posterior cells with lacZ-expressing virus particles suggested that oriented cell division drove primitive-streak initiation [147]. However, my observations of cell movements suggest an alternative explanation, *i.e.*, the mother and daughter

cells stay interconnected and line up as a result of the observed movements rather than driving them. Application of aphidicolin did not prevent primitive streak initiation, but did block the counter-rotational flows (Cui, *et. al.*, to appear, *Developmental Biology*).

Mosaic GFP labeling showed that the epiblast cells divided during their period of large-scale movement, with the cells in the outer periphery dividing two to three times during the 20 hours of observation. The time interval between divisions averaged 378± 30 minutes (*N*=20), which would result in a four-fold increase in the area of the epiblast in 12 hrs assuming that the epiblast is an essentially two-dimensional sheet. This predicted two-fold increase in embryo diameter is slightly less than, but not far from, the change observed experimentally.

I fixed HH stage 3 embryos and stained for F-actin to check for any oriented cell alignment and polarization along the primitive streak, which is a sign of cells going through convergent extension (Figure 32). I observed no alignment or polarization, but I did observe a gradient of cell size along the streak. Cells at the anterior tip appeared smaller than the cells at the posterior end of the streak. If I assume that cell volume is more or less constant, the cells at the tip of the streak could be elongating in the DV direction and ingressing earlier than the cells at the posterior end of the

streak. To further test this hypothesis, I would need to view the ingression from the side.

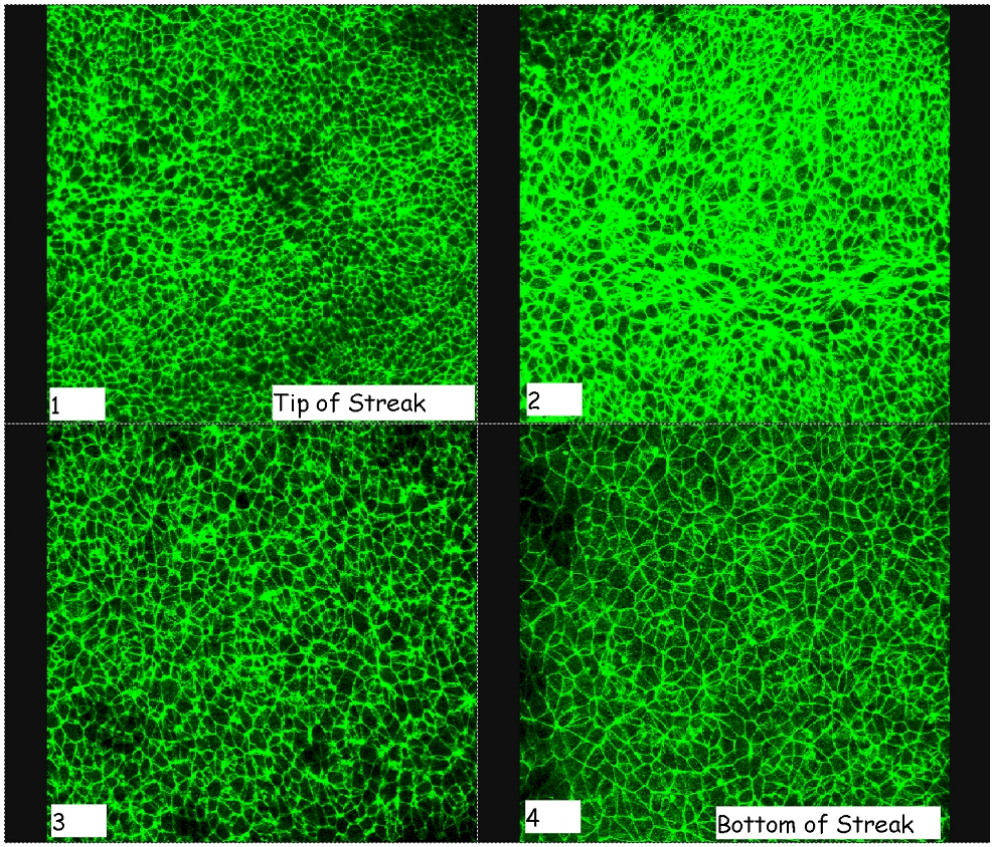

Figure 32. Fixed embryos at HH stage 3 stained with rhodamine phalloidin, imaged using a Leica confocal microscope, 40x optical zoom. Optical sections taken approximately 4μm apart vertically and shown in a maximum-intensity projection suggest a gradient of cell size along the AP axis, with the smaller cells at the anterior tip of the streak. The AP axis is from left to right. The field of view is approximately 375μm wide.

4.2.3.3 The Role of *Fgf* and *Wnt* Pathways during Primitive-Streak Initiation

The molecular basis of cell-movement regulation during primitive-streak initiation is unclear. GFP labeling showed very little relative displacement between adjacent cells during large-scale cell movement, which does not fit easily into the scenario of convergent extension as proposed for *Xenopus* gastrulation [155]. I could interfere with particular signaling pathways by transfection with dominant-negative or active signaling molecules. Candidate signaling molecules for movement regulation during gastrulation are members of the FGF family. The early epiblast expresses high levels of FGF receptors, especially FGFR1 and several FGFs [156, 157]. To investigate the role of FGF during primitive-streak initiation, I transfected the blastoderm with a dominant-negative FGFR1 construct [150]. Expression of this construct before primitive-streak initiation resulted in abnormal development or prevented the formation of a normal streak, depending on the expression level (Figure 33). In experiments where fewer cells expressed the construct, abnormally short streaks formed and the cell movement pattern was abnormal. Higher expression levels completely inhibited primitive-streak initiation. The typical counter-rotating vortices never developed, and I observed only a reduced amplitude of radial outward movement, probably due to decreased cell division in the epiblast, which I would expect because FGF signaling also helps regulate cell division and

fate determination [158].

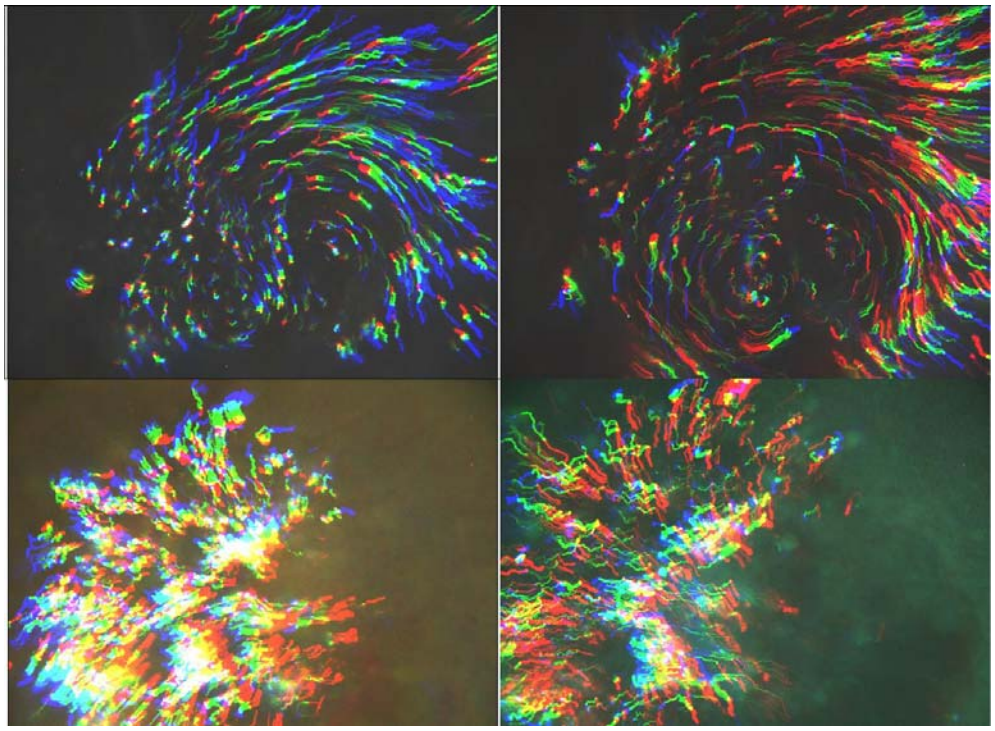

Figure 33. Expression of a dominant-negative FGF receptor inhibits primitive-streak formation in chick embryo. Upper: An embryo expressing a low level of a GFP-tagged FgfR1 receptor develops a recognizable but abnormal primitive streak. Lower: An embryo expressing a high level of a GFP-tagged FgfR1 receptor does not develop a recognizable primitive streak. The color coding of the tracks is the same as in Figure 32. The field of view is approximately 2.8mm wide.

The planar-polarity signaling pathway (Figure 34 adapted from [159]) is involved in convergent extension, where cells intercalate to change tissue shape [155, 159]. This pathway also involves signaling through the non-canonical *Wnt* pathway, possibly mediated by Wnt-5a and Wnt11. Downstream components of this pathway may include signaling though Dishevelled, and Rho-kinase, which possibly signals to the actin-myosin

cytoskeleton [81, 160, 161]. *Wnt11* expression occurs throughout the epiblast and hypoblast of the *area pellucida* during primitive-streak initiation [143].

To investigate the role of the non-canonical *Wnt* pathway, I transfected the blastoderm with a dominant-negative Wnt11 construct [152]. Primitive streaks initiated normally and the associated counter-rotating flows were normal (Figure 35). The streak still formed and elongated, but the extension was in the posterior direction only, failing to extend in the anterior direction, resulting in massive posterior cell movement. These data suggest that *Wnt11* signaling is not necessary for primitive-streak initiation, but is essential to the anterior extension of the streak. Anterior and posterior streak extensions are experimentally independent. Experiments with the Rho-kinase inhibitor Y27632 showed similar results: streaks formed without anterior extension, confirming previous findings that Y27632 resulted in minor defects in primitive streak progression and larger defects during primitive streak regression [162, 163].

4.2.4 Discussion

Chick primitive-streak initiation involves large-scale cell movement and tissue remodeling. The movement has characteristic counter-rotating flows that meet, merge and bifurcate towards either anterior or posterior at the

posterior pole of the embryo. These flows do not seem to result in large-scale cell-cell rearrangements. Instead, whether inside or outside the forming streak, cells tend to maintain their positions relative to their neighbors. Neither the qualitative flow pattern over long periods of time, nor quantitative velocity-field analysis at specific times immediately indicate whether some or all cells move actively or which cells move actively and which passively. I do not know much about the regulation of cell movements since the movements do not coincide with the expression of known growth factors, and cells' gene expression changes as cells move and integrate signals from their changing environment [139]. Neither do I know what controls cell proliferation in the embryo. Again, the pattern of cell division does not correspond to the expression pattern of any known growth factors.

Here I discuss four possible mechanisms for primitive-streak initiation. Do the cells inside the forming streak move actively from the posterior to the anterior and thus 'stir' the rest of the epiblast like a spoon stirring a cup of coffee? If so, two questions are critical: first, how does the 'spoon' form? Do the streak-cell precursors originally in the KS domain at the PMZ intercalate like a "zipper" at the midline? Second, what drives the 'spoon' to move anteriorly? Does the streak form by convergent extension of cells in the KS [159]? Cui *et al.*'s experiments with a cell-division inhibitor seem to

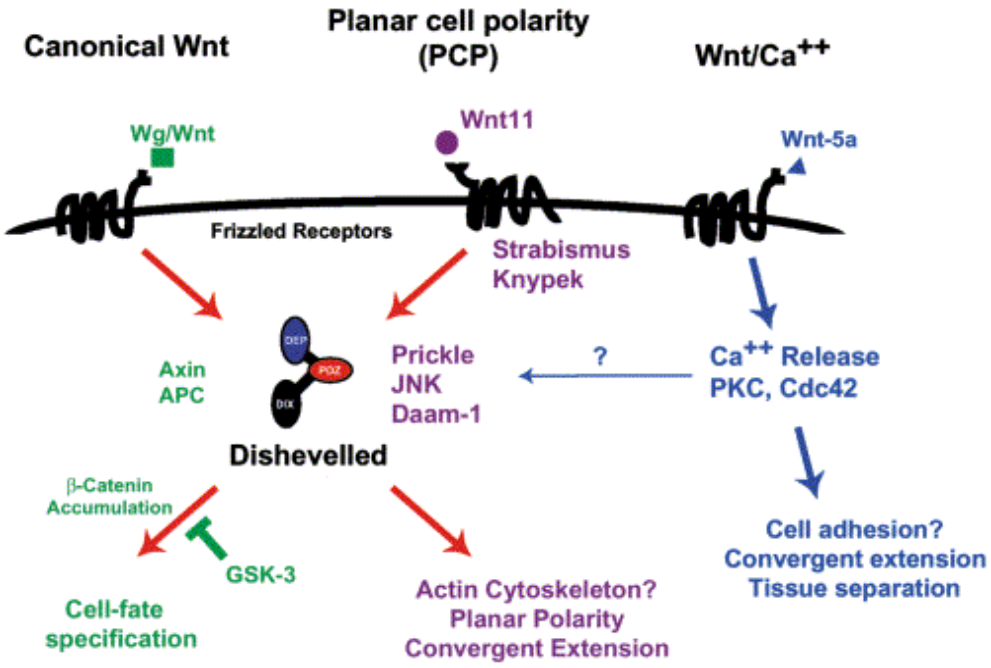

Figure 34. Canonical Wnt, PCP, and Wnt/Ca^{2+} signaling pathways. PCP pathway members are shown in purple, Wnt components in green, and Wnt/Ca^{2+} components in blue. Adapted from [161].

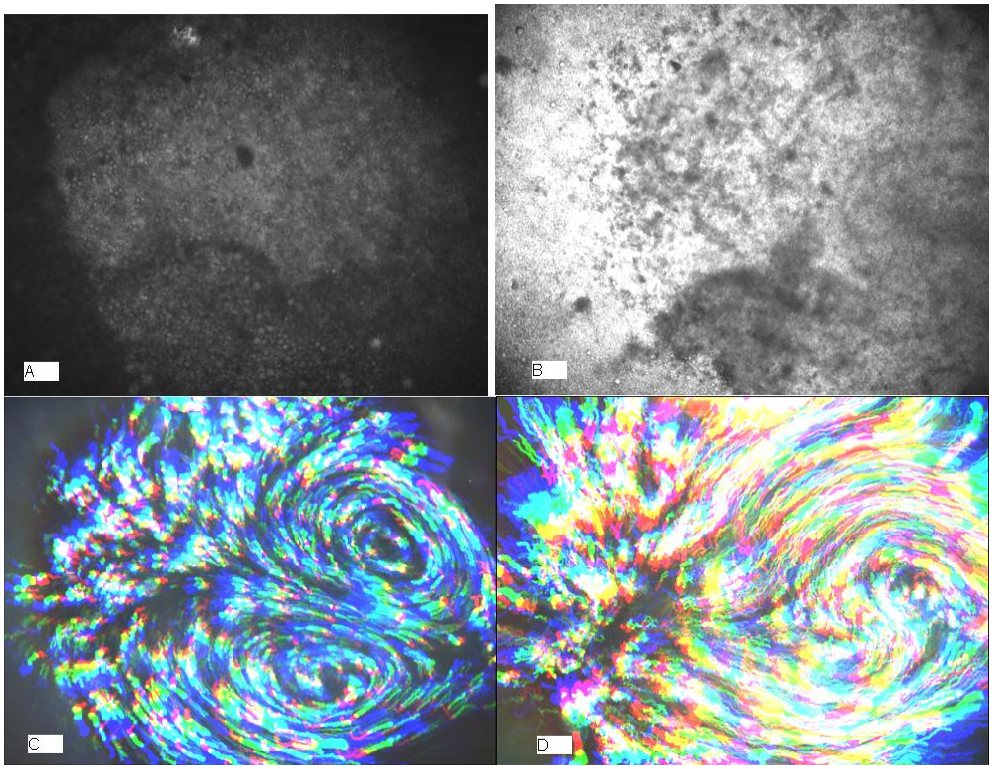

Figure 35. Expression of dominant-negative Wnt11 inhibits the anterior extension of the primitive streak in chick embryo. Bright-field image and cell tracks of GFP-expressing cells during the initial stages (A) and (C) and later stages (B) and (D) of streak formation in an embryo transfected with a dominant-negative Wnt 11 construct. A streak starts to form with the characteristic counter-rotating flows. However, once the tip of the streak has formed, it does not move in an anterior direction. Instead it remains fixed relative to the anterior margin of the embryo. The streak elongates by adding more cells to its posterior. This change in behavior makes the cell tracks point backwards towards the bottom of the streak. The field of view is approximately 2.8mm wide.

suggest that streak formation is autonomous and does not require cell division but that the circular movements do (Cui *et al.*, to appear, *Developmental Biology*) However, little experimental evidence suggests that cells in the streak intercalate in isolation as they do in *Xenopus* [164]. Such movements would require local rearrangements of cells, which would depend on cells making and breaking contacts dynamically, regulated by turnover of adhesion molecules as occurs during germ-band extension in the *Drosophila* embryo which I did not observe [81].

My experiments with the Rho-kinase inhibitor Y27632 and overexpression of the dominant-negative Wnt11, showed that the planar-polarity signaling pathway is not crucial to primitive-streak initiation. The failure of the streak to extend anteriorly suggests that Wnt11 plays a role in extension, possibly allowing the cells in the anterior part of the embryo to move relative to each other. Since Wnt8C and Vg1 can together introduce ectopic streak formation [143], I hypothesize that Vg1 defines the future mesoderm by facilitating the epithelial-mesenchymal-transition (*EMT*). Vg1 can change both cell adhesion and ECM composition and thus convert the confluent cell layer into a set of loosely-connected individual cells. Wnt8C might also regulate cell behaviors like convergent extension.

In the second scenario, do the non-streak epiblast cells move posteriorly and

'squeeze' the future streak cells anteriorly like 'toothpaste,' or a 'fountain' or a 'volcano?' Is this case analogous to the 'reverse fountain' mechanism Marée and Hogeweg have proposed to explain fruiting body formation in *Dictyostelium discoideum* (Figure 36 adapted from [42])? His simulation demonstrates that in both 2D and 3D chemotaxis can generate pressure waves, which push the stalk through the prespore cell population. However, I have no evidence of chemotactic behavior by epiblast cells nor of any chemo-attractant secreted by the posterior part of the chick embryo.

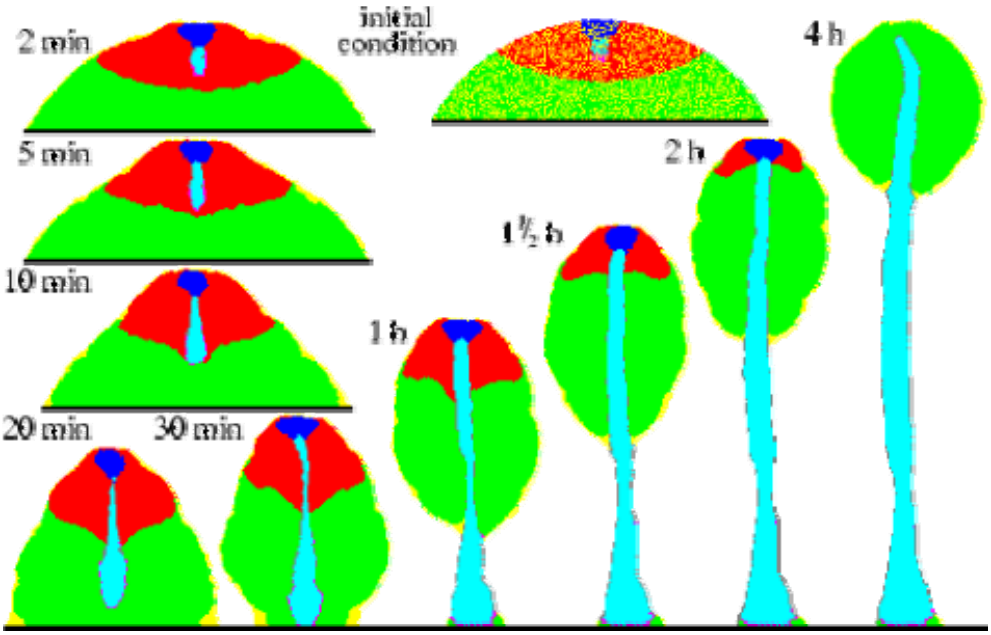

Figure 36. Time sequence of simulated *Dictyostelium* culmination. Green represents Prespore cells. Red represents PrestalkO cells. Blue represents PrestalkA cells. Cyan represents stalk cells. Notice that the downwards growth of the stalk is analogous to primitive-streak progression. The simulation demonstrates that chemotaxis by prespore cells can generate pressure waves, which push the stalk through the prespore-cell population. Adapted from [42].

The third scenario is rather physical, assuming that all the cells in the epiblast try to move anteriorly in response to some perturbation. Since in the middle, more cells sit at the mid-point of the AP axis than anywhere else, the net force is the biggest there and these cells move forward. Since all cells connect to each other via cell-cell contacts, the adhesion transfers the shear, as in a viscous fluid. Thus cells at the periphery have to move posteriorly, resulting in the observed tissue-flow circulation, which resembles the vortices that form in a cup of coffee when I blow across it [165]. The *area opaca* serves as a rigid boundary.

The fourth scenario hypothesizes chemo-attractant and chemo-repellent fields to which the streak cells respond by progressing anteriorly. Xuesong *et al.* have recently shown that mesoderm cells respond chemotactically to FGFs [150], and that cells in the epiblast express FGF receptors from an early stage [166]. In my experiments using a dominant-negative FGFR1 receptor, high expression levels inhibited streak formation. Thus, FGF signaling is necessary for streak formation. However, the dominant negative could block either cell differentiation, especially the EMT in the forming mesoderm, or the chemotaxis machinery, or both. Clarification will require local activation or inhibition of FGF signaling. Does FGF signaling control cell differentiation and motility by regulating cadherin expression and/or turnover? Applying an FGF soaked bead (50 ng/ml) had no major effect on

streak initiation or cell movement (Figure 37). Another drawback of the chemotaxis hypothesis is that individual mesoderm cells can chemotax towards FGFs, but the sheet of epiblast cells deforms globally, which does not fit the classical scenario of chemotaxis.

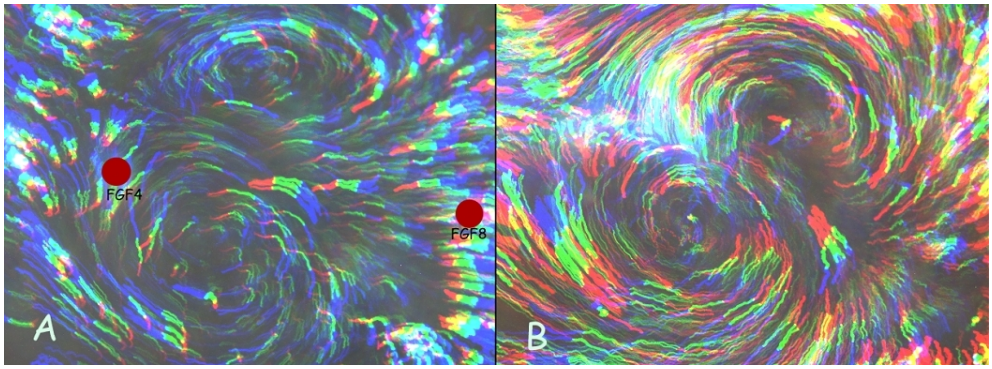

Figure 37. Cell movement after applying two beads soaked with 50ng/ml of (A) FGF4 and (B) FGF8. The patterns seem normal. The color coding is the same as in Figure 32. The field of view is approximately 2.8mm wide.

My work did not explore the role of the hypoblast in primitive-streak initiation, although previous studies hypothesized that the hypoblast helps to localize the primitive streak through antagonistic *Nodal* signaling [142]. Since the hypoblast and epiblast are very close to each other, and the composition of the intermediate ECM changes during primitive-streak initiation [138], the posterior-to-anterior replacement of hypoblast by endoblast could generate mechanical forces, which the ECM would transduce to the epiblast, producing the vortices. Thus, the hypoblast-epiblast interaction could be mechanical rather than, or in

addition to, chemical.

In conclusion, by tracking the cell movement during primitive-streak initiation, I observed vortex-like cell movement, similar to that in model C in Figure 27. The cell movement described in model A in Figure 27 seems to take place when the primitive streak extends, following its initiation. I found no direct evidence of cell movement as described in model B. Experimental work in my group (Cui *et al.*, to appear, *Developmental Biology*) and theoretical work by other groups [167] oppose the hypothesis that oriented cell division drives primitive-streak initiation. Thus the induction and regulation mechanism of primitive-streak initiation is still unknown. All the four hypotheses I listed need further investigation.

CHAPTER FIVE

CONCLUSION AND OUTLOOK

I have studied generic mechanisms in embryonic tissue morphogenesis both theoretically and experimentally, using chick limb and chick gastrulation as models. Their possible mechanisms differ since the mesenchymal cells in the limb and the epiblast cells in the blastoderm behave differently. The isolated limb mesenchymal cells originally dispersed in the ECM condense and go through a mesenchymal-to-epithelial transition (*MET*). In contrast, during primitive-streak formation, the epiblast cells originally form a confluent epithelial cell layer, and, at the site of the forming streak, go through an epithelial-to-mesenchymal transition (*EMT*) and start moving through the blastocoel as individual mesodermal cells.

I have proposed a novel non-Turning mechanism to explain stripe and spot formation via cell-cell adhesion and cell-ECM interactions. I contend that the Turing RD Mechanism only applies to epithelial morphogenesis, where cells form continuous sheets, but does not apply to mesenchymal morphogenesis, where cells embed individually in the ECM. My model provides a possible mechanism explaining cell clustering, not only during limb precartilage mesenchymal condensation in micromass experiments, but also during other mesenchymal morphogenesis where individual cells are

initially dispersed in ECM. My CPM simulations reproduce the density-dependent morphology of my micromass experiments.

I have developed an experimental electroporation protocol to label epiblast cells in chick EC culture *in vivo* with GFP. This protocol allowed me to show for the first time in detail that the cell movement during early chick gastrulation resembles vortices in viscous flow. In addition to allowing detailed morphological studies, the electroporation protocol is also valuable for molecular manipulations and pathway mapping. Through the ectopic expression of dnFGFR1 and Xenopus dnWnt11, I showed that the *Fgf* and *Wnt* pathways play different roles during chick primitive-streak initiation. The *Fgf* pathway seems to be involved in the EMT of the streak precursor cells, while *Wnt* helps regulate epiblast cell polarization and movement.

My general modeling strategy has been to simplify or ignore subcellular genetic regulatory machinery and treat cells as black boxes with simple rules for their reactions to extrinsic signals. In the future I must include genetic regulation, giving cells an intracellular genetic regulatory network so they can make their own decisions to divide, die, migrate, differentiate or change their properties and relations to their neighbors in response to external signals. The input genetic regulation can be as simple as a small-scale Boolean network, as messy as real gene-expression profiling

data from microarrays, or as complicated as a huge set of differential equations describing differential gene expression.

Limb development has long served as a paradigm for DV, AP and PD axis patterning. My research focused on PD patterning. Recent experiments have challenged the dominant Progress-Zone Model of PD patterning. The mesenchymal cells in the distal 0.3mm of the early limb bud seem to have determined fates rather than being undifferentiated as the Progress-Zone Model holds. The differentiated subgroups of cells then expand in a proximal-to-distal sequence [168]. I have separately simulated limb bud growth (Appendix) and mesenchymal condensation *in vitro* (Chapter Three). Now the question is how bud shape affects the condensation pattern *in vivo* and how to coordinate the two individual simulations to reproduce the evolution of both the skeletal pattern and tissue shape in developing chick limb. Some experiments suggest that *Tbx3* controls the width of the limb bud and thus the number of digits, [169] but the mechanism is not clear. I need to move my current simulations of limb-bud growth into 3D. Since my simulations suggest that cell density, cell division and chemotaxis are crucial factors determining the cell condensation pattern and tissue shape, I need quantitative data on mesenchymal-cell migration, division and differentiation *in vivo*. The recombinant limb-bud assay [170] is a good way to test the roles of different underlying molecular pathways.

Further understanding of chick gastrulation requires elucidation of the involvement and interactions of *Fgf*, *Wnt* and other pathways like *Nodal*, *Slug* and *Vg1*. The following experiments would address key areas of my ignorance:

- The *Wnt* pathway plays a key role in convergent extension during *Xenopus* gastrulation [171]. Does the *Wnt* pathway also play a role in early chick gastrulation and is convergent extension the mechanism of primitive-streak initiation? Disheveled is a downstream target of Wnt. Disheveled distributes uniformly in the cytoplasm when the *Wnt* pathway is not active but moves to the membrane when the *Wnt* pathway is active. Confocal microscopy would allow me to observe the intracellular transport of Disheveled (Figure 38) and thus monitor the activation of *Wnt*.
- Stern and coworkers have shown that placing a Vg1-expressing cell pellet on the marginal zone can lead to ectopic streak formation [172]. I could also observe the alteration of cell movements during ectopic streak formation by grafting a Vg1-expressing cell pellet (Figure 39) at the anterior PMZ and comparing these cell movements to the endogenous movements to determine whether the underlying mechanism is the same.

- Genes of the *Slug* super-family interact with the *Fgf* pathway and regulate the EMT [158]. Since my experimental studies did not reveal the role of cell differentiation and cell migration, I could transfect the blastoderm with *Slug/Snail* construct to see how the pattern changes when the transfected epiblast cells go through the EMT. I could then determine whether the normal cell-movement pattern results from epithelial-specific properties.
- PIP_3-kinase signaling is downstream of integrins, which may control the adhesion of moving cells to the ECM. I could transfect the blastoderm with the PIP_3-degrading enzymes Pten and CDC42 to elucidate the role of cell-ECM interactions during primitive streak initiation.

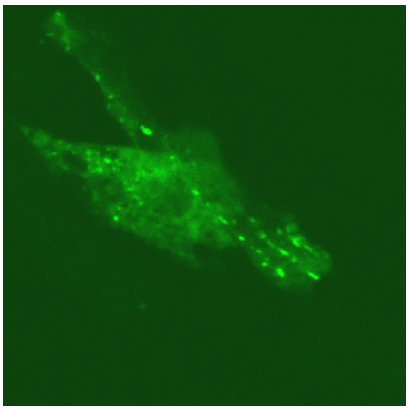

Figure 38. Confocal microscope image of a single cell in the chick blastoderm at approximately HH2. The bright spots show dishevelled protein during transport along microtubules. The cell is approximately 20 μm long.

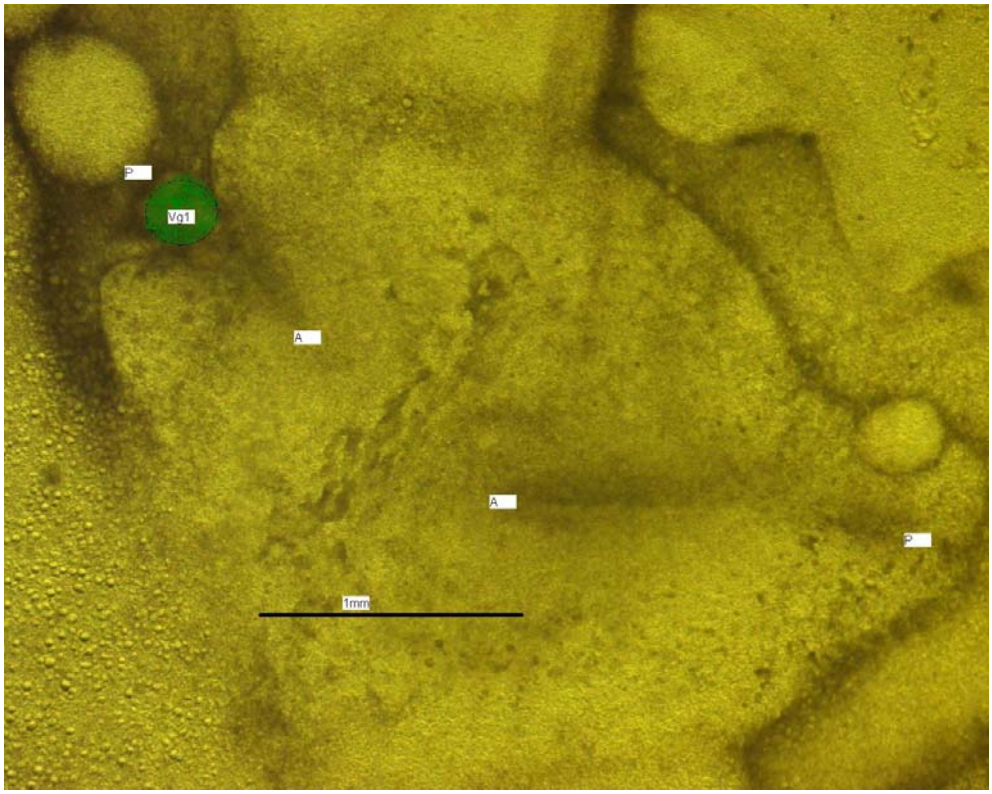

Figure 39. A Vg1-expressing cos-7 cell pellet placed on the marginal zone of a stage X chick embryo induces ectopic streak formation at the site of the pellet. In this case, the ectopic streak (upper left) is 150 degrees counter-clockwise from the endogenous streak. The green dot indicates the cell pellet. Bar=1mm. A: Anterior. P: Posterior.

Many theoretical models attempt to explain chick primitive-streak initiation. Page and co-workers developed an Activator-Inhibitor Model, assuming a traveling wave of inhibitor across the epiblast [173]. Painter and co-workers proposed a Chemotactic Model for the progression and regression of the primitive streak [174]. Most recently, Bodenstein and Stern used a new simulator 'Nudge++' to simulate the streak as a steady-state system continuously recruiting neighboring epiblast cells, with cells ingressing into deeper layers, and moving inside the streak [167]. They showed that polarized cell division was not necessary for primitive-streak initiation agreeing with the experimental observations [147]. However, their model used experimentally-measured cell movement as the input. Therefore this model does not have the emerging property that the interplay of genetic and generic mechanisms gives rise to the precise cell movement pattern I observed experimentally. To test the four hypothetical mechanisms for primitive-streak initiation and progression in Chapter Four, I need to implement a series of 3D CPM simulations of those mechanisms and try to reproduce the vortice

CHICK LIMB BUD OUTGROWTH

A.1 Progress-Zone Model *vs*. Early-Specification Model [102, 104]

In this appendix I discuss preliminary 2D CPM simulations which attempt to evaluate the validity of the Early-Specification Model.

In the 1970s Summerbell, Lewis and Wolpert proposed the Progress-Zone Model to explain patterning of the limb along the PD axis [100]. They defined the *progress zone* to be a region of mesenchymal cells from the AER to about ~300μm proximal. They proposed that the AER causes progressive changes in mesenchymal cell specification, from proximal to distal fates, though the influence of the AER keeps the cells undifferentiated. The longer the mesenchymal cells spend in the progress zone, the more distal their fate or *positional value*. As the limb grows, cells move out of the progress zone and differentiate according to the positional value that they acquired within it. The first cells to leave the progress zone generate proximal structures, while cells that leave later form distal elements, specifying PD fate progressively. The Progress-Zone Model has remained popular despite the lack of conclusive experiments to test it [103].

Recently *Dudley et al.* proposed the Early-Specification Model [168], which significantly extends our understanding of what happens after AER removal. They found that removal of the AER between stages 18 and 22 results in a relatively constant 200µm distal zone of cell death. After stage 24, AER removal does not affect cell survival, although it does significantly reduce cell proliferation. They proposed two new ideas: First, that cells that will contribute to all PD segments form in stratified domains within the early limb bud, with each domain corresponding to one segment, and second, that the size of the limb elements reflects the population of PD progenitors that lie outside of the zone of cell death in the experiments. Cells thus differentiate according to a PD fate, which they acquire early in limb-bud development, a mechanism quite different from the Progress-Zone Model. However, their experiments could not show the cells' state of specification to reveal when the cells 'learn' their future PD positions.

The main difference between the Progress-Zone Model and the Early-Specification Model is the timing of PD specification (Figure 40 adapted from [104]). The Progress-Zone Model suggests that cells acquire precise PD positional information, which tells them where they are with respect to certain boundaries. The mechanism to specify skeletal elements is not clear. The Early-Specification Model suggests that cells specify more broadly as progenitors of stylopod, zeugopod or autopod cells, and that,

over time, each cell population expands while cell-cell interactions and signaling determine which particular structures the cells will form.

A.2 Computer Simulation of the Early-Specification Model

Combining the Early-Specification Model [168] with the observation that AER-secreted FGF4 chemo-attracts limb mesenchymal cells [130], I implemented a 2D CPM version of the Early-Specification Model (Figure 41 partly adapted from [175]) to study the growth of the limb bud between HH stages 17 and 20. The generic mechanisms I included were mesenchymal cell division and chemotaxis to a diffusing growth factor, which the AER secretes. Cell division is spatially uniform [176]. I assumed that after HH stage 16, all cells in the AER secrete FGF8 uniformly. The FGF8 diffuses distally to proximally, creating a gradient along the PD axis with higher concentrations distally. The 'penetration length' defined by FGF8 diffusion is 300μm, to agree with the accepted Progress-Zone thickness. The concentration of FGF8 specifies the cell types via three thresholds, representing the progenitor cells for stylopod, zeugopod and autopod. The stylopod progenitors divide first. The posterior half of the AER secrets FGF4, a chemoattractant [130]. It diffuses proximally with a diffusion length longer than for FGF8. My preliminary results show morphology changes during limb outgrowth between HH stages 17 and 20 (Figure 42). The simulation qualitatively captured the characteristic

asymmetric growth of the limb, with more rapid distal growth at the posterior margin of the limb, though I still need to refine the parameters for a better fit (Figure 43).

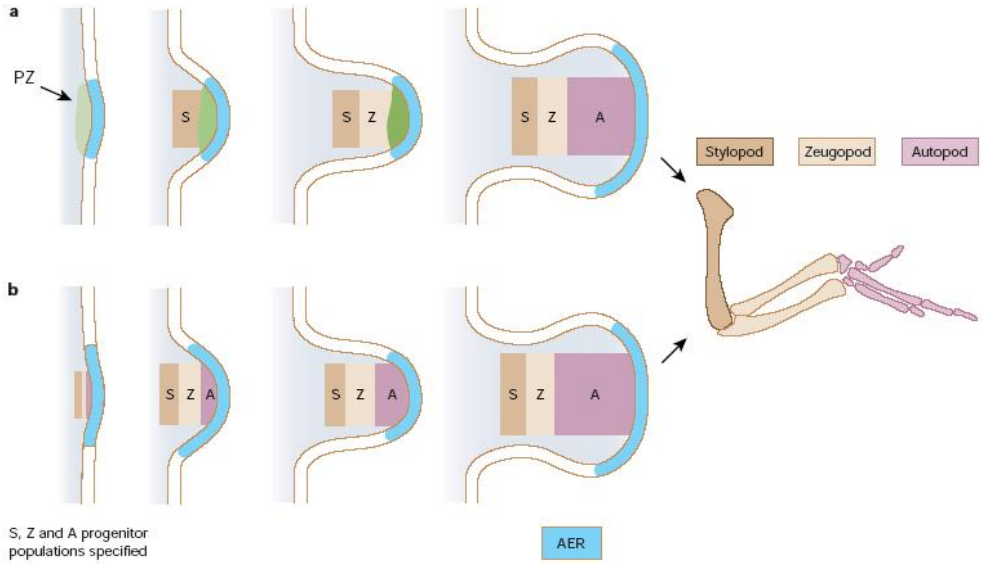

Figure 40. Two models for PD limb skeletal patterning. (a) The Progress-Zone Model proposes that the mesenchyme at the distal tip of the limb bud constitutes a Progress Zone (PZ, in green) of fixed dimensions, in which cells receive progressively more distal positional information over time (as indicated by the change in intensity of the green color from one stage to the next). When cells exit the Progress Zone they fix their determination, and no longer respond to signals from the AER (blue). Thus, the first cells to leave become stylopod (*S*) progenitors. Those that leave later become zeugopod (*Z*) progenitors and still later, autopod (A) progenitors. (b) The Early-Specification Model proposes that at an early limb-bud stage, cells determine to which of the three compartments of the limb they belong. The cell populations then expand through cell division. Adapted from [104].

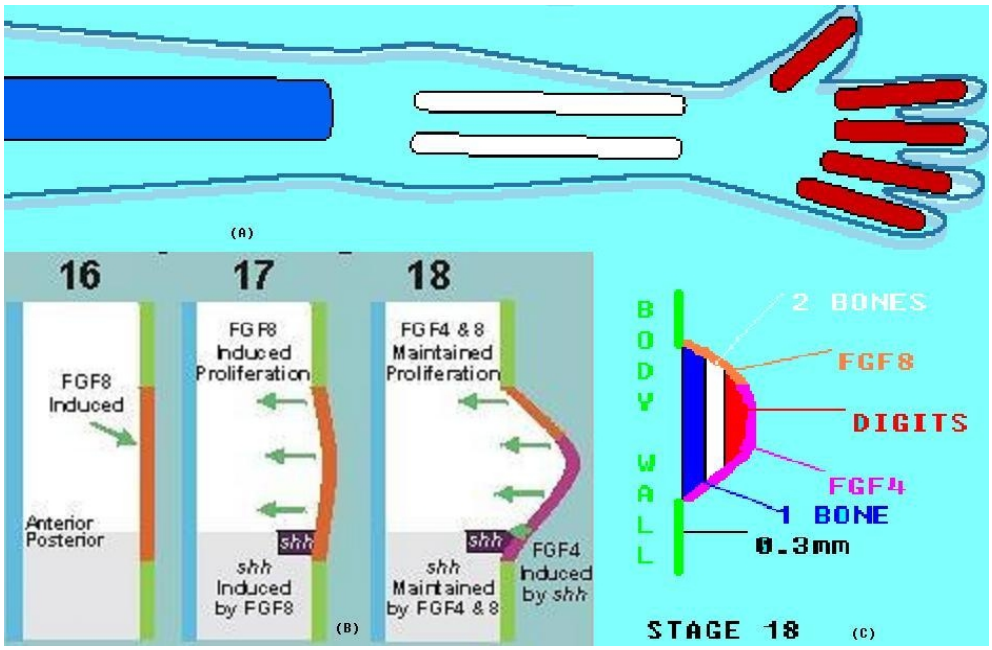

Figure 41. Schematic of limb bud outgrowth in the Early-Specification Model. (A) The skeletal pattern of a forlimb. Blue: Stylopod. White: Zeugopod. Red: Autopod. (B) Molecular mechanisms controlling limb skeletal patterning between embryonic stages 16 and 18: Green: Body wall. Orange: AER that secretes FGF8. Purple: Section of the AER that secrets FGF4. The arrows indicate the secretion of FGF from the AER into the mesenchyme cells underneath. (C) Combining (A) and (B) gives a model of early mesenchymal-identity determination at embryonic stage 18. Colors represent the same tissue identities as in (A) and (B). Adapted from [175].

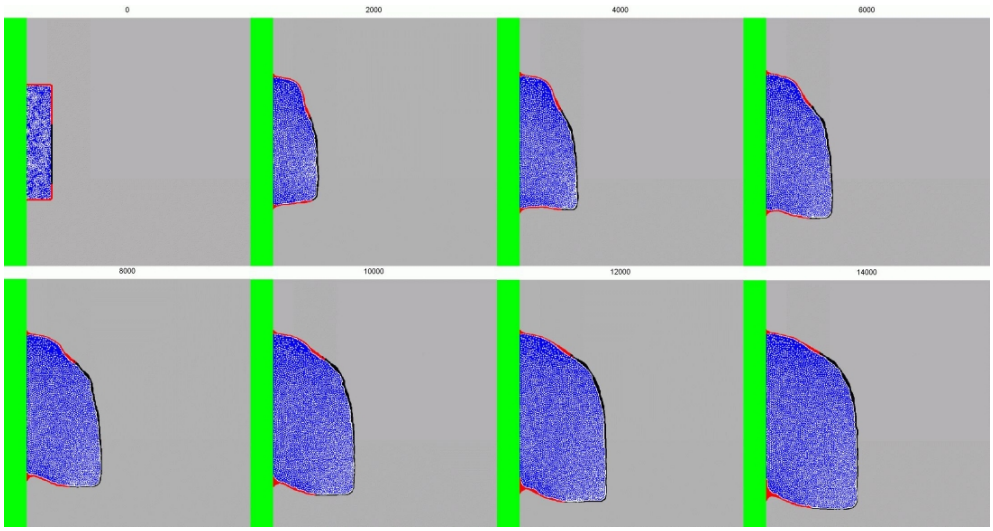

Figure 42. 2D CPM simulation of chick limb-bud outgrowth under the Early-Specification Model. Green: Body wall. Red: Ectodermal cell layer. Black: AER. Blue: Mesenchymal cell layer. White: ECM. The simulation shows that combining the Early-Specificaton Model and FGF4, a chemo-attractant, secreted from the AER asymmetrically along the AP axis, can reproduce the limb bud's outgrowth in the PD direction and its asymmetric growth in the AP direction.

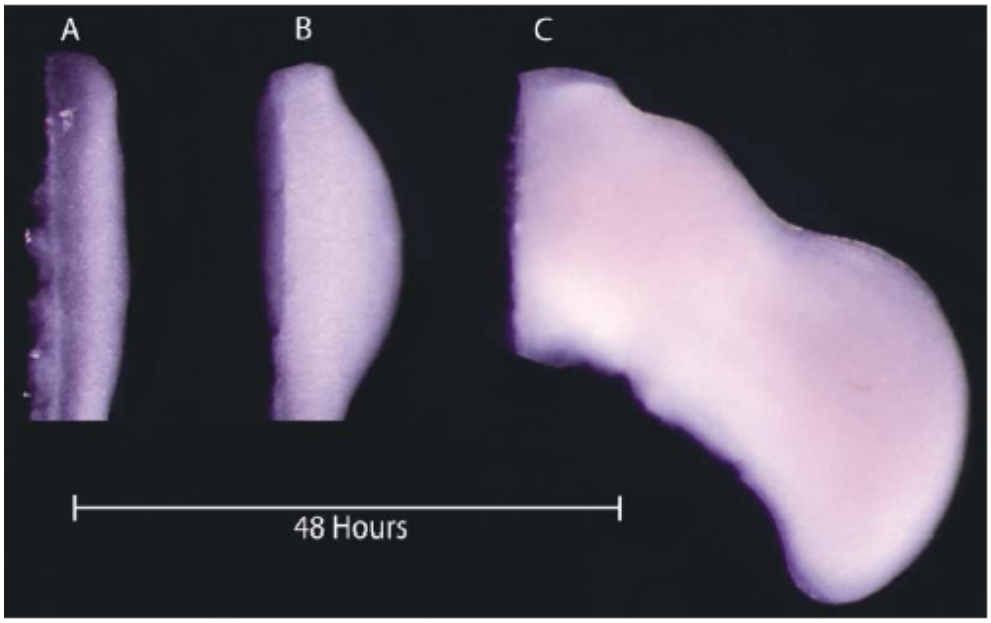

Figure 43. Chick wing development (A) Presumptive wing bud region marked by slight thickening of the lateral plate mesoderm. (B) Wing bud. (C) Elongated wing bud with a broad plate at tip in which primordia of digits are forming. All specimens at the same magnification. Development from (A) to (C) takes approximately 48 hours. The AP dimension is about 2mm.

REFERENCES

1. Fraser, S. E. and Harland, R. M., *The molecular metamorphosis of experimental embryology.* Cell **100**: p. 41-55 (2000).

2. Goodwin, B. C., Kauffman, S., and Murray, J. D., *Is morphogenesis an intrinsically robust process?* J Theor Biol **163**: p. 135-144 (1993).

3. Dawkins, R., *The Selfish Gene*: Oxford University Press (1990).

4. Lewontin, R., *The Triple Helix: Gene, Organism, and Environment*: Harvard University Press (2001).

5. Newman, S. A. and Comper, W. D., *'Generic' physical mechanisms of morphogenesis and pattern formation.* Development **110**: p. 1-18 (1990).

6. Steinberg, M. S., *Mechanism of tissue reconstruction by dissociated cells. II. Time-course of events.* Science **137**: p. 762-763 (1962).

7. Armstrong, P. B., *Cell sorting out: the self-assembly of tissues in vitro.* Crit Rev Biochem Mol Biol **24**: p. 119-149 (1989).

8. Heintzelman, K. F., Phillips, H. M., and Davis, G. S., *Liquid-tissue behavior and differential cohesiveness during chick limb budding.* J Embryol Exp Morphol **47**: p. 1-15 (1978).

9. Malacinski, G. M. and Neff, A. W., *The influence of gravity on the process of development of animal systems.* Adv Space Res **4**: p. 315-323 (1984).

10. Crick, F. H. C., *Diffusion in embryogenesis.* Nature **225**: p. 420-422 (1970).

11. Vale, R. D., *Intracellular transport using microtubule-based motors.* Annu Rev Cell Biol **3**: p. 347-378 (1987).

12. Goto, T., Macdonald, P., and Maniatis, T., *Early and late periodic*

patterns of even skipped expression are controlled by distinct regulatory elements that respond to different spatial cues. Cell **57**: p. 413-422 (1989).

13. Thompson, D. W., *On Growth and Form*: Cambridge University Press (1917).

14. Ball, P., *The Self-Made Tapestry*: Oxford University Press (1999).

15. Hogan, B. L., *Morphogenesis.* Cell **96**: p. 225-233 (1999).

16. Hogeweg, P., *Evolving mechanisms of morphogenesis: on the interplay between differential adhesion and cell differentiation.* J Theor Biol **203**: p. 317-333 (2000).

17. Richardson, M. K., Hanken, J., Selwood, L., Wright, G. M., Richards, R. J., Pieau, C., and Raynaud, A., *Haeckel, embryos, and evolution.* Science **280**: p. 984-986 (1998).

18. Beysens, D. A., Forgacs, G., and Glazier, J. A., *Cell sorting is analogous to phase ordering in fluids.* Proc Natl Acad Sci U S A **97**: p. 9467-9471 (2000).

19. Lenhoff, S. G., *Hydra and the Birth of Experimental Biology --1744*: The Boxwood Press (1986).

20. Wilson, H. V., *On some phenomena of coalescence and regeneration in sponges.* J Exp Zool **5**: p. 245-258 (1907).

21. Holtfreter, J., *Experimental studies on the development of the pronephros.* Rev Can Biol **3**: p. 307-343 (1944).

22. Townes, P.L. and Holtfreter, J., *Directed movements and selective adhesion of embryonic amphibian cells.* J Exp Zool **128**: p. 53-120 (1955).

23. Steinberg, M. S., *Reconstruction of tissues by dissociated cells. Some morphogenetic tissue movements and the sorting out of embryonic cells may have a common explanation.* Science **141**: p. 401-408 (1963).

24. Steinberg, M. S., *Does differential adhesion govern self-assembly processes in histogenesis? Equilibrium configurations and the emergence of a hierarchy among populations of embryonic cells.* J Exp Zool **173**: p. 395-433 (1970).

25. Foty, R. A., Pfleger, C. M., Forgacs, G., and Steinberg, M. S., *Surface tensions of embryonic tissues predict their mutual envelopment behavior.* Development **122**: p. 1611-1620 (1996).

26. Davis, G. S., Phillips, H. M., and Steinberg, M. S., *Germ-layer surface tensions and "tissue affinities" in Rana pipiens gastrulae: quantitative measurements.* Dev Biol **192**: p. 630-644 (1997).

27. Nicol, A., Rappel, W., Levine, H., and Loomis, W. F., *Cell-sorting in aggregates of Dictyostelium discoideum.* J Cell Sci **112**: p. 3923-3929 (1999).

28. Wolpert, L., Smith, J., Lawrence, P., Meyerowitz, E., Beddington, R., and Jessell, T., *Principles of Development*: Oxford University Press (2002).

29. Hynes, R. O., *Integrins: versatility, modulation, and signaling in cell adhesion.* Cell **69**: p. 11-25 (1992).

30. Hynes, R. O. and Lander, E. D., *Contact and adhesive specificities in the associations, migrations, and targeting of cells and axons.* Cell **68**: p. 303-322 (1992).

31. Juliano, R. L. and Haskill, S., *Signal transduction from the extracellular matrix.* J Cell Biol **120**: p. 577-585 (1993).

32. Rosales, C., O'Brien, V., Kornberg, L., and Juliano, R., *Signal transduction by cell adhesion receptors.* Biochim Biophys Acta **1242**: p. 77-98 (1995).

33. Shapiro, L., Kwong, P. D., Fannon, A. M., Colman, D. R., and Hendrickson, W. A., *Considerations on the folding topology and evolutionary origin of cadherin domains.* Proc Natl Acad Sci U S A **92**: p. 6793-6797 (1995).

34. Takeichi, M., *Cadherin cell adhesion receptors as a morphogenetic regulator.* Science **251**: p. 1451-1455 (1991).

35. Knust, E. and Leptin, M., *Adherens junctions in the Drosophila embryo: the role of E-cadherin in their establishment and morphogenetic function.* Bioessays **18**: p. 609-612 (1996).

36. Larue, L., Antos, C., Butz, S., Huber, O., Delmas, V., Dominis, M., and Kemler, R., *A role for cadherins in tissue formation.* Development **122**: p. 3185-3194 (1996).

37. Foty, R. A. and Steinberg, M. S., *The differential adhesion hypothesis: a direct evaluation.* Dev Biol **278**: p. 255-263 (2005).

38. Godt, D. and Tepass, U., *Drosophila oocyte localization is mediated by differential cadherin-based adhesion.* Nature **395**: p. 387-391 (1998).

39. Tepass, U., Godt, D., and Winklbauer, R., *Cell sorting in animal development: signalling and adhesive mechanisms in the formation of tissue boundaries.* Curr Opin Genet Dev **12**: p. 572-582 (2002).

40. Gumbiner, B. M., *Cell adhesion: the molecular basis of tissue architecture and morphogenesis.* Cell **84**: p. 345-357 (1996).

41. Marée, A. F., *From Pattern Formation to Morphogenesis*: MIT Press (2000).

42. Marée, A. F. and Hogeweg, P., *How amoeboids self-organize into a fruiting body: multicellular coordination in Dictyostelium discoideum.* Proc Natl Acad Sci U S A **98**: p. 3879-3883 (2001).

43. Marée, A. F. and Hogeweg, P., *Modelling Dictyostelium discoideum morphogenesis: the culmination.* Bull Math Biol **64**: p. 327-353 (2002).

44. Merks, R., *Branching Growth in Stony Corals*: Universiteit van Amsterdam (2003).

45. Merks, R., Hoekstra, A., Kaandorp, J., and Sloot, P., *Models of coral growth: spontaneous branching, compactification and the Laplacian growth assumption.* J Theor Biol **224**: p. 153-166 (2003).

46. Child, C. M., *Patterns and Problems of Development*: University of Chicago Press (1941).

47. Wolpert, L., *Positional information and the spatial pattern of cellular differentiation.* J Theor Biol **25**: p. 1-47 (1969).

48. Wolpert, L., *Positional information and pattern formation.* Curr Top Dev Biol **6**: p. 183-224 (1971).

49. Crick, F., *Diffusion in embryogenesis.* Nature **5231**: p. 420-422 (1970).

50. Gurdon, J. B. and Bourillot, P. Y., *Morphogen gradient interpretation.* Nature **413**: p. 797-803 (2001).

51. Teleman, A. A., Strigini, M., and Cohen, S. M., *Shaping morphogen gradients.* Cell **105**: p. 559-562 (2001).

52. Houchmandzadeh, B., Wieschaus, E., and Leibler, S., *Establishment of developmental precision and proportions in the early Drosophila embryo.* Nature **415**: p. 798-802 (2002).

53. Tickle, C., *Molecular basis of vertebrate limb patterning.* Am J Med Genet **112**: p. 250-255 (2002).

54. Nelson, C. E., Morgan, B. A., Burke, A. C., Laufer, E., DiMambro, E., Murtaugh, L. C., Gonzales, E., Tessarollo, L., Parada, L. F., and Tabin, C., *Analysis of Hox gene expression in the chick limb bud.* Development **122**: p. 1449-1466 (1996).

55. Izpisua-Belmonte, J. C. and Duboule, D., *Homeobox genes and pattern formation in the vertebrate limb.* Dev Biol **152**: p. 26-36 (1992).

56. Castets, V., Dulos, E., Boissonade, J., and Dekepper, P., *Experimental Evidence of a Sustained Standing Turing-Type Nonequilibrium Chemical Pattern.* Phys Rev Lett **64**: p. 2953-2956 (1990).

57. Sekimura, T., Madzvamuse, A., Wathen, A. J., and Maini, P. K., *A model for colour pattern formation in the butterfly wing of Papilio dardanus.* Proc R Soc Lond B Biol Sci **267**: p. 851-859 (2000).

58. Murray, J. D., *On pattern formation mechanisms for lepidopteran wing patterns and mammalian coat markings.* Philos Trans R Soc Lond B Biol Sci **295**: p. 473-496 (1981).

59. Aragon, J. L., Varea, C., Barrio, R. A., and Maini, P. K., *Spatial patterning in modified Turing systems: Application to pigmentation patterns on marine fish.* FORMA **13**: p. 213-221 (1998).

60. Kondo, S. and Asai, R., *A Reaction-Diffusion Wave on the Skin of the Marine Angelfish Pomacanthus.* Nature **376**: p. 765-768 (2002).

61. Young, D. A., *A Local Activator-Inhibitor Model of Vertebrate Skin Patterns.* Math Biosci **72**: p. 51-58 (1984).

62. Gierer, A. and Meinhardt, H., *A theory of biological pattern formation.* Kybernetik **12**: p. 30-39 (1972).

63. Meinhardt, H., *Models of biological pattern formation*: Academic Press (1982).

64. Barrio, R. A., Varea, C., Aragon, J. L., and Maini, P. K., *A two-dimensional numerical study of spatial pattern formation in interacting Turing systems.* Bull Math Biol **61**: p. 483-505 (1999).

65. Harrison, L. G., *What is the status of reaction-diffusion theory thirty-four years after Turing?* J Theor Biol **125**: p. 369-384 (1987).

66. Hirano, T., Sawai, S., Sawada, Y., and Maeda, Y., *Rapid patterning in 2-D cultures of Dictyostelium cells and its relationship to zonal differentiation.* Dev Growth Differ **42**: p. 551-560 (2000).

67. Sawai, S., Hirano, T., Maeda, Y., and Sawada, Y., *Rapid patterning and zonal differentiation in a two-dimensional Dictyostelium cell mass: the role of pH and ammonia.* J Exp Biol **205**: p. 2583-2590 (2002).

68. Murray, J.D., *Mathematical Biology*: Springer (2002).

69. Odell, G., Oster, G., Burnside, B., and Alberch, P., *A mechanical model for epithelial morphogenesis.* J Math Biol **9**: p. 291-295 (1980).

70. Odell, G. M., Oster, G., Alberch, P., and Burnside, B., *The mechanical basis of morphogenesis. I. Epithelial folding and invagination.* Dev Biol **85**: p. 446-462 (1981).

71. Potts, R. B., *Some generalized order-disorder transformations.* Proc Camb Phil Soc **48**: p. 106-109 (1952).

72. Ashkin, J. and Teller, E., *Statistics of Two-Dimensional Lattices with Four Components.* Phys Rev **64**: p. 178-184 (1943).

73. Wu, F. Y., *The Potts-Model.* Rev Mod Phy **54**: p. 235-268 (1982).

74. Manoj, G., *Persistence in q-state Potts model: A mean-field approach.* Physical Review E **67**: p. 026115-026119 (2003).

75. Weaire, D. and Kermode, J. P., *Computer-Simulation of a Two-Dimensional Soap Froth. 1. Method and Motivation.* Phil Mag B **48**: p. 245-259 (1983).

76. Weaire, D. and Kermode, J. P., *Computer-Simulation of a Two-Dimensional Soap Froth. 2. Analysis of Results.* Phil Mag B **50**: p. 379-395 (1984).

77. Weaire, D., Bolton, F., Molho, P., and Glazier, J. A., *Investigation of an Elementary Model for Magnetic Froth.* J Phys Cond Matt **3**: p. 2101-2114 (1991).

78. Sahni, P. S., Grest, G. S., Anderson, M. P., and Srolovitz, D. J., *Kinetics of the Q-State Potts-Model in 2 Dimensions.* Phys Rev Lett **50**: p. 263-266 (1983).

79. Jiang, Y., *Cellular Pattern Formation*: University of Notre Dame (1998).

80. Lewis, F. T., *The analogous shapes of cells and bubbles.* Proc AAAS **77**: p. 147-186 (1948).

81. Bertet, C., Sulak, L., and Lecuit, T., *Myosin-dependent junction remodelling controls planar cell intercalation and axis elongation.* Nature **429**: p. 667-671 (2004).

82. Phillips, H. M. and Steinberg, M. S., *Embryonic tissues as elasticoviscous liquids. I. Rapid and slow shape changes in centrifuged cell aggregates.* J Cell Sci **30**: p. 1-20 (1978).

83. Graner, F. and Glazier, J. A., *Simulation of Biological Cell Sorting Using a 2-Dimensional Extended Potts-Model.* Phys Rev Lett **69**: p. 2013-2016 (1992).

84. Glazier, J. A. and Graner, F., *Simulation of the differential adhesion driven rearrangement of biological cells.* Phys Rev E **47**: p. 2128-2154 (1993).

85. Drasdo, D. and Forgacs, G., *Modeling the interplay of generic and genetic mechanisms in cleavage, blastulation, and gastrulation.* Dev Dyn **219**: p. 182-191 (2000).

86. Upadhyaya, A., *Thermodynamic and Fluid Properties of Cells, Tissues and Membranes*: University of Notre Dame (2000).

87. Rieu, J. P., Upadhyaya, A., Glazier, J. A., Ouchi, N. B., and Sawada, Y., *Diffusion and deformations of single hydra cells in cellular aggregates.* Biophys J **79**: p. 1903-1914 (2000).

88. Mombach, J. C. and Glazier, J. A., *Single cell motion in aggregates of embryonic cells.* Phys Rev Lett **76**: p. 3032-3035 (1996).

89. Jiang, Y., Levine, H., and Glazier, J., *Possible cooperation of differential adhesion and chemotaxis in mound formation of Dictyostelium.* Biophysical Journal **75**: p. 2615-2625 (1998).

90. Metropolis, N., Rosenbluth, A., Rosenbluth, M., Teller, A., and Teller, E., *Equation of state calculations by fast computing machines*. J Chem Phys **21**: p. 1087-1092 (1953).

91. Graner, F. and Sawada, Y., *Can Surface-Adhesion Drive Cell Rearrangement. 2. A Geometrical Model.* J Theor Biol **164**: p. 477-506 (1993).

92. Graner, F., *Can Surface-Adhesion Drive Cell-Rearrangement .1. Biological Cell-Sorting.* J Theor Biol **164**: p. 455-476 (1993).

93. Mombach, J. C., Glazier, J. A., Raphael, R. C., and Zajac, M., *Quantitative comparison between differential adhesion models and cell sorting in the presence and absence of fluctuations.* Phys Rev Lett **75**: p. 2244-2247 (1995).

94. Holm, E. A., Glazier, J. A., Srolovitz, D. J., and Grest, G. S., *Effects of Lattice Anisotropy and Temperature on Domain Growth in the 2-Dimensional Potts-Model.* Phys Rev A **43**: p. 2662-2668 (1991).

95. Zeng, W., Thomas, G. L., Newman, S. A., and Glazier, J. A. *A novel mechanism for mesenchymal condensation during limb chondrogenesis in vitro.* in *Mathematical Modeling and Computing in Biology and Medicine: 5th Conference of the European Society of Mathematical and Theoretical Biology* p. 80-86 (2003).

96. Zeng, W., Thomas, G. L., and Glazier, J. A., *Non-Turing stripes and spots: a novel mechanism for biological cell clustering.* Physica A **341**: p. 482-494 (2004).

97. Zajac, M., Jones, G. L., and Glazier, J. A., *Simulating convergent extension by way of anisotropic differential adhesion.* J Theor Biol **222**: p. 247-259 (2003).

98. Zajac, M., Jones, G. L., and Glazier, J. A., *Model of convergent extension in animal morphogenesis.* Phys Rev Lett **85**: p. 2022-2025 (2000).

99. Izaguirre, J. A., Chaturvedi, R., Huang, C., Cickovski, T., Coffland, J., Thomas, G., Forgacs, G., Alber, M., Hentschel, G., Newman, S. A., and Glazier, J. A., *CompuCell, a multi-model framework for simulation of morphogenesis.* Bioinformatics **20**: p. 1129-1137 (2004).

100. Hinchliffe, J. R. and Johnson, D. R., *The Development of The Vertebrate Limb*: Clarendon Press (1980).

101. Capdevila, J. and Izpisua Belmonte, J. C., *Patterning mechanisms controlling vertebrate limb development.* Annu Rev Cell Dev Biol **17**: p. 87-132 (2001).

102. Niswander, L., *Pattern formation: old models out on a limb.* Nat Rev

Genet **4**: p. 133-143 (2003).

103. Tickle, C., *Patterning systems--from one end of the limb to the other.* Dev Cell **4**: p. 449-458 (2003).

104. Mariani, F. V. and Martin, G. R., *Deciphering skeletal patterning: clues from the limb.* Nature **423**: p. 319-325 (2003).

105. Duboule, D., *Making progress with limb models.* Nature **418**: p. 492-493 (2002).

106. Newman, S. A. and Frisch, H. L., *Dynamics of skeletal pattern formation in developing chick limb.* Science **205**: p. 662-668 (1979).

107. Hall, B. K. and Miyake, T., *All for one and one for all: condensations and the initiation of skeletal development.* Bioessays **22**: p. 138-147 (2000).

108. Comper, W. D., ed. *Extra Cellular matrix*. Vol. 2: *Molecular Components and Interactions*: Harwood Acdemic Publishers (1996).

109. Leonard, C. M., Fuld, H. M., Frenz, D. A., Downie, S. A., Massague, J., and Newman, S. A., *Role of transforming growth factor-beta in chondrogenic pattern formation in the embryonic limb: stimulation of mesenchymal condensation and fibronectin gene expression by exogenenous TGF-beta and evidence for endogenous TGF-beta-like activity.* Dev Biol **145**: p. 99-109 (1991).

110. Tomasek, J. J., Mazurkiewicz, J. E., and Newman, S. A., *Nonuniform distribution of fibronectin during avian limb development.* Dev Biol **90**: p. 118-126 (1982).

111. Kulyk, W. M., Upholt, W. B., and Kosher, R. A., *Fibronectin gene expression during limb cartilage differentiation.* Development **106**: p. 449-455 (1989).

112. Kulyk, W. M., Rodgers, B. J., Greer, K., and Kosher, R. A., *Promotion of embryonic chick limb cartilage differentiation by transforming growth factor-beta.* Dev Biol **135**: p. 424-430 (1989).

113. Oberlender, S. A. and Tuan, R. S., *Spatiotemporal profile of N-cadherin expression in the developing limb mesenchyme.* Cell Adhes Commun **2**: p. 521-537 (1994).

114. Oberlender, S. A. and Tuan, R. S., *Expression and functional involvement of N-cadherin in embryonic limb chondrogenesis.* Development **120**: p. 177-187 (1994).

115. Desban, N. and Duband, J. L., *Avian neural crest cell migration on laminin: interaction of the alpha1beta1 integrin with distinct laminin-1 domains mediates different adhesive responses.* J Cell Sci **110**: p. 2729-2744 (1997).

116. Monier-Gavelle, F. and Duband, J. L., *Cross talk between adhesion molecules: control of N-cadherin activity by intracellular signals elicited by beta1 and beta3 integrins in migrating neural crest cells.* J Cell Biol **137**: p. 1663-1681 (1997).

117. Dufour, S., Beauvais-Jouneau, A., Delouvee, A., and Thiery, J. P., *Differential function of N-cadherin and cadherin-7 in the control of embryonic cell motility.* J Cell Biol **146**: p. 501-516 (1999).

118. Miura, T. and Shiota, K., *Extracellular matrix environment influences chondrogenic pattern formation in limb bud micromass culture: experimental verification of theoretical models.* Anat Rec **258**: p. 100-107 (2000).

119. Yokouchi, Y., Nakazato, S., Yamamoto, M., Goto, Y., Kameda, T., Iba, H., and Kuroiwa, A., *Misexpression of Hoxa-13 induces cartilage homeotic transformation and changes cell adhesiveness in chick limb buds.* Genes Dev **9**: p. 2509-2522 (1995).

120. Downie, S. A. and Newman, S. A., *Morphogenetic differences between fore and hind limb precartilage mesenchyme: relation to mechanisms of skeletal pattern formation.* Dev Biol **162**: p. 195-208 (1994).

121. Omi, M., Sato-Maeda, M., and Ide, H., *Role of chondrogenic tissue in programmed cell death and BMP expression in chick limb buds.* Int J Dev Biol **44**: p. 381-388 (2000).

122. Ohsugi, K., Gardiner, D. M., and Bryant, S. V., *Cell cycle length affects gene expression and pattern formation in limbs.* Dev Biol **189**: p. 13-21 (1997).

123. Miura, T., Komori, M., and Shiota, K., *A novel method for analysis of the periodicity of chondrogenic patterns in limb bud cell culture: correlation of in vitro pattern formation with theoretical models.* Anat Embryol (Berl) **201**: p. 419-428 (2000).

124. Turing, A., *The chemical basis of morphogenesis.* Phil Trans Roy Soc B **237**: p. 37-72 (1952).

125. Mochizuki, A., Wada, N., Ide, H., and Iwasa, Y., *Cell-cell adhesion in limb-formation, estimated from photographs of cell sorting experiments based on a spatial stochastic model.* Dev Dyn **211**: p. 204-214 (1998).

126. Yajima, H., Hara, K., Ide, H., and Tamura, K., *Cell adhesiveness and affinity for limb pattern formation.* Int J Dev Biol **46**: p. 897-904 (2002).

127. Herault, Y., Kondo, T., Zakany, J., and Duboule, D., *Hox genes and genetic control of limb development.* Arch Pediatr **4**: p. 107s-111s (1997).

128. Burke, A. C., Nelson, C. E., Morgan, B. A., and Tabin, C., *Hox genes and the evolution of vertebrate axial morphology.* Development **121**: p. 333-346 (1995).

129. Dolle, P., Izpisua-Belmonte, J. C., Brown, J., Tickle, C., and Duboule, D., *Hox genes and the morphogenesis of the vertebrate limb.* Prog Clin Biol Res **383A**: p. 11-20 (1993).

130. Li, S. and Muneoka, K., *Cell migration and chick limb development: chemotactic action of FGF-4 and the AER.* Dev Biol **211**: p. 335-347 (1999).

131. Stern, C. D., *Gastrulation: From Cells to Embryo*: Cold Spring Harbor Laboratory Press (2004).

132. Lawson, A. and Schoenwolf, G. C., *New insights into critical events of avian gastrulation.* Anat Rec **262**: p. 238-252 (2001).

133. Eyal-Giladi, H. and Kochav, S., *From cleavage to primitive streak formation: a complementary normal table and a new look at the first stages of the development of the chick. I. General morphology.* Dev Biol **49**: p. 321-337 (1976).

134. Hamburger, V. and Hamilton, H. L., *A series of normal stages in the development of the chick embryo. 1951.* Dev Dyn **195**: p. 231-272 (1992).

135. Bachvarova, R. F., Skromne, I., and Stern, C. D., *Induction of primitive streak and Hensen's node by the posterior marginal zone in the early chick embryo.* Development **125**: p. 3521-3534. (1998).

136. Chapman, S. C., Schubert, F. R., Schoenwolf, G. C., and Lumsden, A., *Analysis of spatial and temporal gene expression patterns in blastula and gastrula stage chick embryos.* Dev Biol **245**: p. 187-199. (2002).

137. Chapman, S. C., Brown, R., Lees, L., Schoenwolf, G. C., and Lumsden, A., *Expression analysis of chick Wnt and frizzled genes and selected inhibitors in early chick patterning.* Dev Dyn **229**: p. 668-676 (2004).

138. Lawson, A., Colas, J. F., and Schoenwolf, G. C., *Classification scheme for genes expressed during formation and progression of the avian primitive streak.* Anat Rec **262**: p. 221-226. (2001).

139. Joubin, K. and Stern, C. D., *Molecular interactions continuously define the organizer during the cell movements of gastrulation.* Cell **98**: p. 559-571 (1999).

140. Vakaet, L., *Cinephotomicrographic investigations of gastrulation in the chick blastoderm.* Arch Biol (Liege) 387-426 (1970).

141. Lawson, A. and Schoenwolf, G. C., *Cell populations and morphogenetic movements underlying formation of the avian primitive streak and organizer.* Genesis **29**: p. 188-195. (2001).

142. Bertocchini, F. and Stern, C. D., *The hypoblast of the chick embryo*

positions the primitive streak by antagonizing nodal signaling. Dev Cell **3**: p. 735-744. (2002).

143. Skromne, I. and Stern, C. D., *Interactions between Wnt and Vg1 signalling pathways initiate primitive streak formation in the chick embryo.* Development **128**: p. 2915-2927. (2001).

144. Skromne, I. and Stern, C. D., *A hierarchy of gene expression accompanying induction of the primitive streak by Vg1 in the chick embryo.* Mech Dev **114**: p. 115-118 (2002).

145. Shah, S. B., Skromne, I., Hume, C. R., Kessler, D. S., Lee, K. J., Stern, C. D., and Dodd, J., *Misexpression of chick Vg1 in the marginal zone induces primitive streak formation.* Development **124**: p. 5127-5138. (1997).

146. Sanders, E. J., Varedi, M., and French, A. S., *Cell proliferation in the gastrulating chick embryo: a study using BrdU incorporation and PCNA localization.* Development **118**: p. 389-399. (1993).

147. Wei, Y. and Mikawa, T., *Formation of the avian primitive streak from spatially restricted blastoderm: evidence for polarized cell division in the elongating streak.* Development **127**: p. 87-96. (2000).

148. Chapman, S. C., Collignon, J., Schoenwolf, G. C., and Lumsden, A., *Improved method for chick whole-embryo culture using a filter paper carrier.* Dev Dyn **220**: p. 284-289. (2001).

149. Momose, T., Tonegawa, A., Takeuchi, J., Ogawa, H., Umesono, K., and Yasuda, K., *Efficient targeting of gene expression in chick embryos by microelectroporation.* Dev Growth Differ **41**: p. 335-344. (1999).

150. Yang, X., Dormann, D., Munsterberg, A. E., and Weijer, C. J., *Cell movement patterns during gastrulation in the chick are controlled by positive and negative chemotaxis mediated by FGF4 and FGF8.* Dev Cell **3**: p. 425-437. (2002).

151. Hoppler, S., Brown, J. D., and Moon, R. T., *Expression of a dominant-negative Wnt blocks induction of MyoD in Xenopus embryos.* Genes Dev **10**: p. 2805-2817 (1996).

152. Tada, M. and Smith, J. C., *Xwnt11 is a target of Xenopus Brachyury: regulation of gastrulation movements via Dishevelled, but not through the canonical Wnt pathway.* Development **127**: p. 2227-2238. (2000).

153. Hatada, Y. and Stern, C. D., *A fate map of the epiblast of the early chick embryo.* Development **120**: p. 2879-2889. (1994).

154. Chapman, S. C., Collignon, J., Schoenwolf, G. C., and Lumsden, A., *Improved method for chick whole-embryo culture using a filter paper carrier.* Dev Dyn **220**: p. 284-289 (2001).

155. Keller, R., Davidson, L. A., and Shook, D. R., *How we are shaped: the biomechanics of gastrulation.* Differentiation **71**: p. 171-205 (2003).

156. Karabagli, H., Karabagli, P., Ladher, R. K., and Schoenwolf, G. C., *Comparison of the expression patterns of several fibroblast growth factors during chick gastrulation and neurulation.* Anat Embryol (Berl) **205**: p. 365-370. (2002).

157. Walshe, J. and Mason, I., *Expression of FGFR1, FGFR2 and FGFR3 during early neural development in the chick embryo.* Mech Dev **90**: p. 103-110. (2000).

158. Ciruna, B. and Rossant, J., *FGF signaling regulates mesoderm cell fate specification and morphogenetic movement at the primitive streak.* Dev Cell **1**: p. 37-49 (2001).

159. Wallingford, J. B., Fraser, S. E., and Harland, R. M., *Convergent extension: the molecular control of polarized cell movement during embryonic development.* Dev Cell **2**: p. 695-706. (2002).

160. Habas, R., Dawid, I. B., and He, X., *Coactivation of Rac and Rho by Wnt/Frizzled signaling is required for vertebrate gastrulation.* Genes Dev **17**: p. 295-309 (2003).

161. Habas, R., Kato, Y., and He, X., *Wnt/Frizzled activation of Rho regulates vertebrate gastrulation and requires a novel Formin homology protein Daam1.* Cell **107**: p. 843-854 (2001).

162. Marlow, F., Topczewski, J., Sepich, D., and Solnica-Krezel, L.,

Zebrafish Rho kinase 2 acts downstream of Wnt11 to mediate cell polarity and effective convergence and extension movements. Curr Biol **12**: p. 876-884 (2002).

163. Wei, L., Roberts, W., Wang, L., Yamada, M., Zhang, S., Zhao, Z., Rivkees, S. A., Schwartz, R. J., and Imanaka-Yoshida, K., *Rho kinases play an obligatory role in vertebrate embryonic organogenesis.* Development **128**: p. 2953-2962. (2001).

164. Keller, R., Clark, W. H., and Griffin, F., eds. *Gastrulation: Movements, Patterns and Molecules*: Plenum Press (1991).

165. Vogel, S, *Life in Moving Fluids--the Physical Biology of Flow*: Princeton University Press (1994).

166. Chapman, S. C., Schubert, F. R., Schoenwolf, G. C., and Lumsden, A., *Analysis of spatial and temporal gene expression patterns in blastula and gastrula stage chick embryos.* Dev Biol **245**: p. 187-199 (2002).

167. Bodenstein, L. and Stern, C. D., *Formation of the chick primitive streak as studied in computer simulations.* J Theor Biol **233**: p. 253-269 (2005).

168. Dudley, A. T., Ros, M. A., and Tabin, C. J., *A re-examination of proximodistal patterning during vertebrate limb development.* Nature **418**: p. 539-544 (2002).

169. Tumpel, S., Sanz-Ezquerro, J. J., Isaac, A., Eblaghie, M. C., Dobson, J., and Tickle, C., *Regulation of Tbx3 expression by anteroposterior signalling in vertebrate limb development.* Dev Biol **250**: p. 251-262 (2002).

170. Fernandez-Teran, M., Piedra, M. E., Ros, M. A., and Fallon, J. F., *The recombinant limb as a model for the study of limb patterning, and its application to muscle development.* Cell Tissue Res **296**: p. 121-129 (1999).

171. Wallingford, J. B., Fraser, S. E., and Harland, R. M., *Convergent extension: the molecular control of polarized cell movement during embryonic development.* Dev Cell **2**: p. 695-706 (2002).

172. Shah, S. B., Skromne, I., Hume, C. R., Kessler, D. S., Lee, K. J., Stern, C. D., and Dodd, J., *Misexpression of chick Vg1 in the marginal zone induces primitive streak formation.* Development **124**: p. 5127-5138 (1997).

173. Page, K. M., Maini, P. K., Monk, N. A., and Stern, C. D., *A model of primitive streak initiation in the chick embryo.* J Theor Biol **208**: p. 419-438 (2001).

174. Painter, K. J., Maini, P. K., and Othmer, H. G., *A chemotactic model for the advance and retreat of the primitive streak in avian development.* Bull Math Biol **62**: p. 501-525 (2000).

175. Schwabe, J. W., Rodriguez-Esteban, C., De La Pena, J., Tavares, A. T., Ng, J. K., Banayo, E. M., Foys, B., Eshelman, B., Magallon, J., Tam, R., and Izpisua-Belmonte, J. C., *Outgrowth and patterning of the vertebrate limb.* Cold Spring Harb Symp Quant Biol **62**: p. 431-435 (1997).

176. Sun, X., Mariani, F. V., and Martin, G. R., *Functions of FGF signalling from the apical ectodermal ridge in limb development.* Nature **418**: p. 501-508 (2002).

VITA PAGE

Wei Zeng was born on January 2, 1977 in Tianjin, China. She graduated from Xin Hua High School, Tianjin in July 1995. She received a Bachelor of Science in physics with a minor in economics from Peking University, Beijing, China in June 1999. She received a Master of Science degree in physics from the University of Notre Dame in South Bend, Indiana in August, 2002. This dissertation was defended on Dec 15, 2004 at Indiana University, Bloomington, Indiana, USA.